

DOCTORAL THESIS

Combination of Advanced
Oxidation Methods for the
Energy-Efficient Abatement
of Aqueous and Gaseous
Hazardous Pollutants

Maarja Kask

TALLINN UNIVERSITY OF TECHNOLOGY
DOCTORAL THESIS
37/2021

**Combination of Advanced Oxidation
Methods for the Energy-Efficient
Abatement of Aqueous and Gaseous
Hazardous Pollutants**

MAARJA KASK



TALLINN UNIVERSITY OF TECHNOLOGY

School of Engineering

Department of Materials and Environmental Technology

This dissertation was accepted for the defence of the degree 30/06/2021

Supervisor:

Researcher Dr. Juri Bolobajev
Dept. of Materials and Environmental Technology
Tallinn University of Technology
Tallinn, Estonia

Co-supervisor:

Senior Lecturer Dr. Marina Krichevskaya
Dept. of Materials and Environmental Technology
Tallinn University of Technology
Tallinn, Estonia

Opponents:

Senior Researcher Dr. Monica Magureanu
Dept. of Plasma Physics and Nuclear Fusion
National Institute for Laser, Plasma and Radiation Physics
Bucharest, Romania

Professor Dr. Santiago Esplugas
Chemical Engineering and Analytical Chemistry Dept.
University of Barcelona
Barcelona, Spain

Defense of the thesis: 12/08/2021, Tallinn

Declaration:

Hereby I declare that this doctoral thesis, my original investigation and achievement, submitted for the doctoral degree at Tallinn University of Technology has not been submitted for doctoral or equivalent academic degree.

Maarja Kask

signature



European Union
European Regional
Development Fund



Investing
in your future

Copyright: Maarja Kask, 2021

ISSN 2585-6898 (publication)

ISBN 978-9949-83-724-3 (publication)

ISSN 2585-6901 (PDF)

ISBN 978-9949-83-725-0 (PDF)

Printed by Koopia Niini & Rauam

TALLINNA TEHNIKAÜLIKOO
DOKTORITÖÖ
37/2021

**Süvaoksüdatsiooniprotsesside
kombineerimine ohtlike saasteainete
energiatõhusaks lagundamiseks vees ja õhus**

MAARJA KASK



Contents

List of Publications	6
Author's Contribution to the Publications	7
Introduction	8
Abbreviations	10
1 Literature Overview	11
1.1 Ozonation	11
1.1.1 Enhanced Ozonation with Hydrogen Peroxide	14
1.2 Pulsed Corona Discharge Plasma Treatment.....	14
1.3 Photocatalytic Oxidation	17
1.4 Pollutants Under Consideration	19
1.5 Aim of the Study	20
2 Materials and Methods.....	22
2.1 Chemicals and Materials.....	22
2.2 Experimental Equipment and Procedure	22
2.2.1 Ozonation.....	22
2.2.2 Gas-Phase Pulsed Corona Discharge	23
2.2.3 Gas-Phase Photocatalytic Oxidation	25
2.2.4 Combination of Pulsed Corona Discharge with Photocatalytic Oxidation	26
2.3 Analytical Methods.....	27
2.3.1 Analysis of Aqueous Matrix.....	27
2.3.2 Analysis of Gaseous Matrix	28
3 Results and Discussion	29
3.1 Oxidation Energy Efficiency of Aqueous Pollutants by Ozonation and PCD Treatment. Content of Exhaust Air Originating from PCD Equipment	29
3.2 Photocatalytic Treatment of Gaseous Pollutants	33
Conclusions	40
References	41
Acknowledgements.....	47
Abstract.....	48
Lühikokkuvõte.....	50
Appendix 1	53
Appendix 2	63
Appendix 3	81
Curriculum Vitae	95
Elulookirjeldus.....	98

List of Publications

The list of author's publications, on the basis of which the thesis has been prepared:

- I **Kask, M.**; Krichevskaya, M.; Preis, S.; Bolobajev, J. (2021). Oxidation of Aqueous N-Nitrosodiethylamine: Experimental Comparison of Pulsed Corona Discharge with H₂O₂-Assisted Ozonation. Journal of Environmental Chemical Engineering, #105102. DOI: 10.1016/j.jece.2021.105102.
- II **Kask, M.**; Bolobajev, J.; Krichevskaya, M. (2020). Gas-Phase Photocatalytic Degradation of Acetone and Toluene, and their Mixture in the Presence of Ozone in Continuous Multi-Section Reactor as Possible Air Post-Treatment for Exhaust from Pulsed Corona Discharge. Chemical Engineering Journal, 399, #125815. DOI: 10.1016/j.cej.2020.125815.
- III **Kask, M.**; Krichevskaya, M.; Preis, S.; Bolobajev, J. (2021). Oxidation of Aqueous Toluene by Gas-Phase Pulsed Corona Discharge in Air-Water Mixtures Followed by Photocatalytic Exhaust Air Cleaning. Catalysts, 11 (5), #549. DOI: 10.3390/catal11050549.

Author's Contribution to the Publications

Contribution to the papers in this thesis are:

- I The author fulfilled majority of the experiments, supervised the experimental work of a MSc student, interpreted the obtained data, and wrote the paper with the help of co-authors.
- II The author carried out most of the experiments, supervised the experimental work of a MSc student, interpreted the obtained data, and wrote the paper with the help of co-authors. The results were presented by the author at conference "The 6th European Conference on Environmental Applications of Advanced Oxidation Processes"; Portorož, Slovenia, June 26–30, 2019, and at summer school "3rd European Summer School on Environmental Applications of Advanced Oxidation Processes"; Alcoy, Spain, June 3–7, 2019.
- III The author carried out a major part of the experiments, supervised the experimental work a MSc student, interpreted the obtained data, and wrote the paper with the help of co-authors. The author presented the results at the online conference "Athens Conference on Advances in Chemistry"; Athens, Greece, March 10–14, 2021.

Introduction

The presence of hazardous pollutants in the environment has become a great worldwide issue. The population growth has led to extensive production and consumption of goods accompanied by higher quantities of wastewater and air pollution as well as an increasing need for clean potable water. Contaminated water and air, in fact, are also the sources of mankind diseases. To deal with the pollution in water and air, several conventional technologies are in use. These, however, mainly comprise separation techniques like adsorption or membrane processes, e.g., nanofiltration, reverse osmosis, transferring the pollutant from one phase to another without its degradation. A variety of pollutants also demonstrate a refractory character towards bio-oxidation, bringing to front a highly promising application of advanced oxidation processes (AOPs) that are based on the generation and utilisation of reactive oxygen species, principally hydroxyl radicals (HO^\bullet), participating in the formation of harmless end products like H_2O and CO_2 in case of complete mineralisation. Advanced oxidation processes are also effective in disinfection of air and water. In given context, the development of AOP-based technologies deserves a significant attention.

Parameters, that are decisive for the applicability of environmental technologies are energy consumption, installation cost, and ease of operation and maintenance. Ozonation is one of the well-known and commercially available AOP for water treatment, where ozone is synthesised in dielectric barrier discharge (DBD). Though, ozonation has several drawbacks hindering the overall efficacy of the process. For instance, the treatment of water with ozone follows the gas-liquid mass transfer comprising therefore a certain limitation. In addition, *ex situ* synthesis of ozone requires its following transportation into the matrix to be treated and results in higher energy demand compared to electrical discharge process, where the generation of oxidative species occurs *in situ*.

A cost-effective alternative, pulsed corona discharge (PCD), has demonstrated its unequalled energy efficiency in oxidation of aqueous organics because of the more efficient utilisation of *in situ* generated various reactive species, predominantly HO^\bullet and O_3 . However, PCD treatment faces the problem of residual ozone in the exhaust air originating from the setup. Besides, low concentrations of fugitive compounds are also present in the outlet air if volatile organic compounds (VOCs) are treated, therefore requiring additional treatment. Photocatalytic oxidation successfully degrades low concentrations of airborne VOCs as well as ozone at ambient temperature. Photocatalytic reactors with commercial potential operating in continuous mode are under research and development. These reactors are characterised by a fixed area of the photocatalytic surface, while modular reactors allow to steadily increase the photocatalytic surface area by a certain increment and thus are useful for the testing and collection of essential data for the successful application of systems operating in continuous mode.

The thesis was aimed to provide necessary data for the development of cost-effective technologies for the abatement of hazardous organic compounds from water and air. The pollutants under consideration were N-nitrosodiethylamine (NDEA), a water disinfection by-product, known to possess carcinogenic properties, and acetone and toluene, that are VOCs widely used in numerous industries and known to negatively influence the central nervous and respiratory systems. The oxidation kinetics of NDEA as a single pollutant have not been investigated earlier. Toluene and acetone are widely used model water and air pollutants.

The PCD as chemical-free and cost-effective technology was studied for the degradation of NDEA and toluene. In the case of NDEA, the energy efficiency was studied in comparison to traditional ozonation and its combination with H_2O_2 . The control parameters were pH, temperature, pulse repetition frequency, the concentration of H_2O_2 , and in case of ozonation, O_3 concentration. For the abatement of VOCs and ozone in PCD exhaust air, a unique multi-section photocatalytic reactor, allowing a stepwise increase in the surface coated with a photocatalyst, was used. The reactor was applied for oxidation of toluene, acetone, and their mixture, and O_3 depletion under various operating conditions, including the presence or absence of ozone, variations in initial pollutant concentrations, specific residence time (SRT), and air humidity. The photocatalytic reactor was used in combination with PCD equipment for the post-treatment of the exhaust air containing residual O_3 and toluene at different residence time and SRT. The purpose was to evaluate the feasibility of the combination for the abatement of VOCs in both aqueous and gaseous phases together with O_3 comprising the novelty in research.

The findings made in the study contribute to the possible application of environmentally friendly and energy efficient PCD in water treatment in larger scale as a possible addition or alternative to conventional water treatment technologies, whereas multi-section photocatalytic reactor helps to obtain valuable data for the development of air purifiers working in continuous regime. The novel combination of these technologies contributes to a possible application of the studied approach in closed-loop energy-saving ventilation systems.

Abbreviations

AOP	Advanced oxidation process
DBD	Dielectric barrier discharge
E	Energy efficiency
FTIR	Fourier transform infrared spectroscopy
HPLC	High performance liquid chromatography
NDEA	N-nitrosodiethylamine
PCD	Pulsed corona discharge
PCO	Photocatalytic oxidation
ppm	Parts per million
pps	Pulses per second
RH	Relative humidity
SRT	Specific residence time
VOC	Volatile organic compound

1 Literature Overview

Nowadays, the occurrence of hazardous pollutants in the environment has become a great concern, presenting a detrimental effect on public health. A variety of environmental pollutants are known to be recalcitrant, being only transferred from one medium to another and thus requiring further handling. This concerns conventional treatment processes like bio-oxidation, membrane filtration, coagulation and, adsorption (Luo et al., 2014). To deal with this issue, advanced oxidation processes (AOPs) are considered as a viable solution (Gao et al., 2009; Padhye et al., 2010). The target of AOPs is to maximise the generation of one of the most reactive oxidants – hydroxyl radical (HO^\bullet) followed by its utilisation to degrade organic pollutants (Mo et al., 2009 (a)). Oxidation potentials of different oxidants associated with AOPs are depicted in Table 1.

Table 1. Oxidation potential of oxidants associated with AOPs (Wardman, 1989)

Oxidant	Oxidation potential, V
Positively charged hole, h^+ (TiO_2)	3.50
Hydroxyl radical, HO^\bullet	2.80
Atomic oxygen, O^\bullet	2.42
Ozone, O_3	2.07
Hydrogen peroxide, H_2O_2	1.78
Perhydroxyl radical, HO_2^\bullet	1.70

The following chapters 1.1–1.3 provide an overview of the studied AOPs, i.e., ozonation and pulsed corona discharge plasma (PCD) for water treatment, and photocatalytic oxidation (PCO) for air treatment. In chapter 1.4, the properties and occurrence of the studied hazardous pollutants under consideration are discussed.

1.1 Ozonation

Ozonation as a commercially available technology has been extensively studied for the abatement of organic pollutants in water and air (Bourgin et al., 2017; Ridgway et al., 2017; Wang et al., 2018; Kang et al., 2020; Restivo et al., 2021). It is commonly used in water treatment technologies as pre- or post-treatment, mainly to improve taste and odour, and to remove organic and inorganic matter from wastewater (Hoigné, 1998; Kasprzyk-Hordern et al., 2003; Gottschalk et al., 2010). However, due to its selectivity, it is an inefficient method for complete mineralisation of organic substances (Giri et al., 2007). Besides, the high reactivity of O_3 makes it a very unstable gas (Masschelein, 1992) with half-life values varying from seconds to hours dependent on several parameters, e.g., character of medium and temperature. The higher the temperature is, the faster the decomposition of ozone occurs (Ono and Oda, 2003).

For the generation of ozone, a dielectric barrier discharge (DBD) is usually applied. In traditional ozone generators, cylindrical Pyrex (Duran) glass tubes, sometimes also ceramic ones, are mounted inside stainless-steel tubes, high voltage and ground electrodes, with a diameter in the range of 20–50 mm in order to form annular discharge gaps 0.5–1 mm in width. Aluminium films, possessing conductive properties to avoid the creation of thermal plasmas like arc or spark, are connected along with a brush-shaped electrode inside the glass tubes to the high-voltage supply operating the standard

frequency in mains or deriving electricity from a generator. High-performance ozone generators nowadays employ non-glass dielectrics and the voltage derived from a high-frequency switch source (0.5–5 kHz) generating, for instance, a square-wave current. Higher operating frequencies deliver the desired density of power at much lower operating voltages, less than 5 kV in comparison to the typical 20 kV in the past, thus the discharge gap is narrower as a result of lower electrical stress on the dielectrics. Ozone production using DBD ranges from few mg·h⁻¹ to kg·h⁻¹. Several hundred discharge tubes are aggregated in large ozone generators (Kogelschatz, 2003; Chu and Lu, 2013). Figure 1 illustrates the ozone generation with DBD.

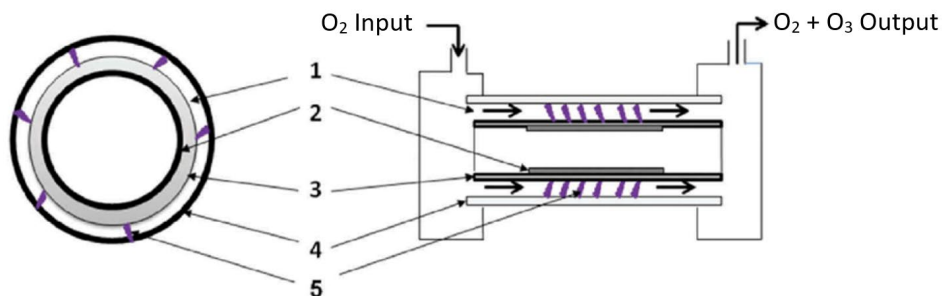


Figure 1. Ozone generation by means of DBD: 1 – discharge gap; 2 – high voltage electrode; 3 – glass tube; 4 – grounded electrode; 5 – plasma (Bechekir et al., 2019)

In DBD ozone generators, oxygen (O₂) is converted to O₃ via two-step reaction. The first step comprises the dissociation of O₂ by electron impact (Eqs. 1–3). If ozone is generated from air, reactions involving N[•] and N₂ occur (Eqs. 4–6). The second step is the reaction of atomic oxygen (O[•]) with molecular oxygen (Eq. 7) in the presence of a third body (M), i.e., O₂, N₂ (Magureanu et al., 2013; Magureanu et al., 2018).



High concentration of atomic nitrogen and nitrogen oxide, however, may quench oxygen atoms and assist ozone depletion, whereas O[•] high concentration results in dominating recombination into oxygen molecule (Lukes et al., 2005).

Ozonation itself is a pH-sensitive process that involves two types of oxidation reactions, direct and indirect (Gottschalk et al., 2010). Indirect reactions involve the utilisation of short-living HO[•] with a lifetime of ca. 0.02 μs in water (Ghanbari and Moradi, 2017) and ca. 200 μs in air (Magureanu et al., 2013) and proceed mainly at pH over 10 due to the abundance of hydroxide ions (HO⁻), which favour the formation of HO[•] from ozone. Direct reactions, on the contrary, occur in acidic media at pH lower than 3 by supporting the direct reactions between O₃ and the pollutant, whereas both pathways, direct and indirect, are present at pH range of 3–10 (Kasprzyk-Hordern, 2003). It is

noteworthy that ozonation is considered as AOP only when radical mechanism is dominating.

Molecular O₃ reacts readily via direct reactions with electron-rich moieties in aromatic and aliphatic compounds, i.e., unsaturated bonds, also amino and hydroxyl groups, whereas HO• are significantly less selective, and interact through indirect pathway with most of the organics, by attacking the pollutant normally by abstracting the hydrogen atom or, in the case of unsaturated molecules, by adding to the double bond (Hernandez et al., 2002). The rate constants for ozone and HO•-based reactions are typically in the range of 1.0–10⁶ M⁻¹ s⁻¹ and 10⁸–10¹⁰ M⁻¹ s⁻¹, respectively, thus, indicating that HO•-based reactions present a method of choice in the abatement of ozone-resistant compounds (Gottschalk et al., 2010).

The generation of non-selective HO• through the chain reaction of O₃, that is transported from the ozone generator into the treatment solution and is introduced to water, includes initiation, propagation, and termination reactions. The initiation comprises the reaction between ozone and HO⁻ leading to the formation of superoxide anion (O₂^{•-}) and hydroperoxyl radical (HO₂•) (Eq. 8), of which the latter is in acid-base equilibrium with the O₂^{•-} (Eq. 9) (Gottschalk et al., 2010).



In the propagation stage, the O₂^{•-} reacts with ozone forming an ozonide anion (O₃^{•-}), that promptly decomposes through hydrogen trioxide (HO₃•) to HO• (Eq. 10–12). HO• reacts with ozone by generating HO₄• (Eq. 13), which decay into HO₂• and O₂ (Eq. 14) may re-initiate the chain reactions (Eq. 9 and 10) (Gottschalk et al., 2010).



Although HO• possess a great effect on oxidation of pollutants, their overly high presence in the treated matrix may result in a termination reaction, caused by inefficient self-consumption of radical species (Eq. 15) (Gottschalk et al., 2010).



It is known that gaseous O₃ is sparingly soluble in water (Masschelein, 1992), therefore, its low transfer to aqueous phase clearly affects the oxidation efficiency of some refractory pollutants. To avoid mass transfer limitations and to amplify the mineralisation in ozonation, more extensive decomposition of O₃ with the generation of a vast number of radical species is a desired outcome (de Luis and Lombraña, 2018). As the increase in pH in the treatment solution for such purpose might be costly for radical scavenging by bicarbonates and carbonates accumulated in alkaline solutions (von Gunten, 2003), the addition of hydrogen peroxide serves as a cheaper alternative (de Luis and Lombraña, 2018).

1.1.1 Enhanced Ozonation with Hydrogen Peroxide

The abatement of refractory pollutants could be enhanced with the addition of H₂O₂ into O₃-treated solutions, commercially known as peroxone, for accelerated HO[•] production (von Gunten, 2003; Gottschalk et al., 2010). In addition to the lower cost mentioned above, the high solubility of H₂O₂ in aqueous phase guarantees its simple application (de Luis and Lombraña, 2018). Another advantage of H₂O₂/O₃ system is its non-dependence on the UV transmissivity as is O₃/UV combination, allowing its application also in turbid waters. The reaction of undissociated H₂O₂ with ozone (Eq. 16) is considered negligible, reacting with O₃ predominantly in the form of HO₂⁻ (Eq. 17 and 18) (Gottschalk et al., 2010).



Produced HO₂[•] enters the chain reaction (Eqs. 9–14) to generate HO[•]. Combining the Eqs. 9–14, 16, and 18 gives a net reaction (Eq. 19) as follows (Gottschalk et al., 2010):



The essential factors for the successful progression of the peroxone process are pH, temperature, and the addition of H₂O₂ in appropriate concentration at the right moment into the reactive system (Hernandez et al., 2002; de Luis and Lombraña, 2018). As could be seen from Eq. 19, the molar ratio between O₃ and H₂O₂ is 2:1, which is also considered as an optimum in many applications (Glaze et al., 1987). In fact, the suitable ratio is of particular importance, since H₂O₂ may also act as a scavenger at high concentrations resulting in utilisation of HO[•] (Eq. 20) (Hernandez et al., 2002).



The application of ozone in oxidation of organic pollutants, however, is generally costly due to its *ex situ* production that requires the transportation of relatively long-living ozone into the treatment solution as well as short-living HO[•], which survival is unlikely, thus resulting in higher demand for energy. Another feature that adds to the expenses is the necessity of using dry gases, air or oxygen, for the generation of ozone without a chance for, e.g., humid oxygen reuse. Costly synthesis and application of ozone hinder its implementation in water treatment, dictating the search for cost-effective alternatives (Krichevskaya et al., 2011). One of the promising AOPs, which provides efficient utilisation of various oxidants, for instance HO[•], O₃, H₂O₂, NO[•], atomic oxygen, superoxide anion, generated *in situ* in treatment devices is the application of nonthermal plasma of pulsed corona discharge.

1.2 Pulsed Corona Discharge Plasma Treatment

Corona discharge (CD) occurs near a pin or a thin wire, where an electric field is significantly enhanced, thus ionisation and emission are localised around the pin or wire. Corona discharge is also known as partial discharge since it normally does not extend up to the counter electrode. It can be operated with pulsed voltage or continuous voltage (direct current corona). Pulsed corona is produced by applying ultra-short, generally

sub-microsecond, voltage pulses to an electrode. Such short pulse duration avoids the transition to spark that may damage the electrodes and thus pulsed corona may be used at voltages and currents higher than that of continuous corona. Higher voltages magnify the electric field and cause the increased temperature of electrons resulting in accelerated ionisation and dissociation. From this, pulsed corona is favoured over continuous discharge in environmental applications (Chu and Lu, 2013; Magureanu et al., 2013).

Plasma consists of electrons or negative ions, positive ions, and neutral particles, and can be classified in several ways, for example, based on the thermodynamic equilibrium. Plasma generated in the gas-phase pulsed corona discharge is classified as nonthermal plasma. The main oxidative species formed in nonthermal plasma at atmospheric pressure are HO[•], O₃, H₂O₂, NO[•], atomic oxygen, superoxide anion, but also excited molecules and atoms, negative and positive ions, and free electrons, which formation and abundance depend on the type of plasma source (Schneider et al., 2020). Generally, the dominating ones in pulsed corona discharge are O₃ and HO[•]. All reactive species are mainly formed in the gas–liquid interface, where short-living oxidants generated in the discharge react with pollutants in the boundary layer of water or at close vicinity of gas–liquid interface (Ajo et al., 2017). From the mentioned oxidative species formed by electric discharge, the generation of O₃ and NO[•] was illustrated with Eqs. 1–7 in the previous chapter. Formation of hydroxyl radicals and atomic oxygen in plasma reactions mainly occur via water dissociation in gaseous phase caused by electron impact. The HO[•] recombination leads to the formation of H₂O₂ (Eqs. 21–23) (Lukes et al., 2005; Magureanu et al., 2013).



Electric discharge generation in air causes the formation of nitrogen-containing species, e.g., NO[•] and NO₂[•], which contribute to the decrease in pH while in contact with water, resulting in the formation of nitrous and nitric acids in plasma-treated solutions (Eqs. 24–26). In acidic environment, the peroxyxynitrous acid (O=N–OOH), and in alkaline and neutral media, the formation of peroxyxynitrite (O=N–OO[–]), are also present, of which the anionic and protonated forms of peroxyxynitrite could be directly or indirectly involved in oxidation of the pollutant (Kornev et al., 2013; Magureanu et al., 2013).



In addition to the production of highly reactive radical species and molecules, UV emission that can participate in oxygen, water, and H₂O₂ dissociation, or initiate reverse reactions of NO_x to produce O[•] and subsequently O₃ (Eqs. 27–31), is also generated in electric discharge plasma. Its intensity and wavelength range depend on various parameters, e.g., plasma type and gas composition (Magureanu et al., 2013).



Corona discharges are classified in several different forms depending on the field polarity and electrode configuration. Depending on the pin/wire electrode, either it is anode or cathode, corona is positive or negative. Regarding the electrode configuration, the commonly used design of laboratory scale CD setup is a pin-to-plate electrode pair (Figure 2a), where a needle is placed above the grounded plate and a high voltage pulse is applied to the needle electrode. Such design, however, is suitable only for laboratory studies since its industrial application is energy consuming as the discharge is not spread throughout the whole gaseous volume of the reactor. For the large-scale application in industry, wire-cylinder (Figure 2b) and wire-plate (Figure 2c), especially the first one, are used. Wire-cylinder provides rather homogenous discharge distribution and is simple to implement in a gas-flow system. To enable high gas throughput, multiple wire-cylinder reactors are positioned in parallel (Magureanu et al., 2013).

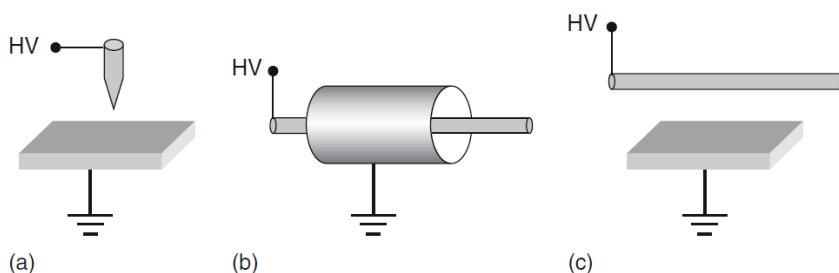


Figure 2. Geometries of corona discharges: a – pin-to-plate; b – wire-cylinder; c – wire-plate. HV – high voltage (Magureanu et al., 2013)

Among the advantages of PCD reactors, the simplicity in design and insensitivity towards gas humidity are important. Moreover, the reactor comprises a closed compartment where the oxidation of the pollutant occurs without a need for ozone synthesis and transport as in the case of ozonation (Preis et al., 2013 (a)). In addition, the system is operated at ambient temperature and pressure and does not need the addition of chemicals (Ajo et al., 2015). In gas-phase PCD, water is sprayed into plasma zone in water droplets and jets, thereby increasing the contact surface of plasma and water. This approach has demonstrated the highest efficiency in comparison to all nonthermal plasma types (Malik, 2010; Kornev et al., 2017).

However, one of the main limitations of PCD in the oxidation of aqueous pollutants is the lack of reliable pulse generators, thus also impeding the widespread use of PCD for commercial purposes since the uncertain operating of the pulse generator may cause the high-temperature spark in the setup (Preis et al., 2013 (b)). Energy transfer efficiency from pulse generator to the reactor is, additionally to the electrode configuration and droplet size, another important feature that affects the stability of the gas-phase PCD. An inappropriate inter-electrode distance may lead to decreasing discharge energy, poor matching of the PCD with generator, and higher residual voltage at the electrodes remaining for a longer time, therefore indicating the inter-electrode distance as a trade-off

between the energy transfer efficiency and spark formation in short inter-electrode gaps. To avoid the spark discharge in the reactor, the installation of a saturating inductor serves as a good solution, contributing to the decrease in voltage pulse duration (Kornev et al., 2017). Another drawback is that nonthermal PCD plasma technology for the treatment of both gaseous and aqueous pollutants may emit low concentrations of certain VOCs, including residual initial compounds, and certain amounts of ozone in the exhaust, therefore requiring post-treatment. However, a combination of PCD treatment with downstream photocatalytic utilization and destruction of ozone along with degradation of VOCs presents a method of choice.

1.3 Photocatalytic Oxidation

Photocatalytic oxidation (PCO) is an AOP in which pollutants react predominantly with reactive oxygen species formed through the activation of a semiconductor catalyst by light photons with appropriate wavelength with the subsequent conversion of organics into H_2O and CO_2 in the case of mineralisation. Photocatalytic oxidation is a promising technology to handle very low concentrations of pollutants at parts per billion (ppb) or parts per million (ppm) levels, which are representative loadings of pollutants in offices and buildings (Boyjoo et al., 2017). The process can be operated at room temperature and under atmospheric pressure, making it suitable for integration in existing heating, ventilation, and air conditioning (HVAC) (Costarramone et al., 2015; Boyjoo et al., 2017). It is a nonselective process with high activity towards various pollutants.

The photocatalytic mechanism on the surface of titanium dioxide (TiO_2), which is the most widely studied catalyst in PCO reactors, is illustrated in Figure 3.

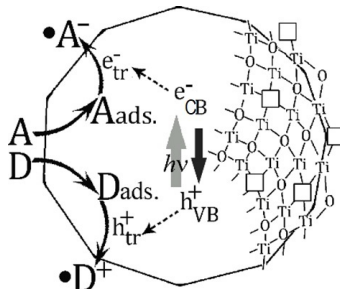
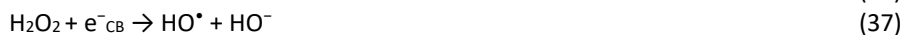
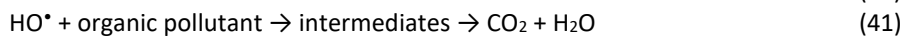
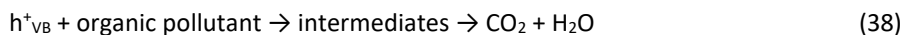


Figure 3. Mechanism of photocatalysis on the surface of TiO_2

The more precise explanation of the mechanism is that the photons reach the surface of the photocatalyst generating highly reactive electron/hole pairs (e^-/h^+) by moving the excited electrons from the valence band (h^+_{VB}) to conduction band (e^-_{CB}). For excitation, the photon energy ($h\nu$) must be equal to or exceeding the band gap energy (E_g) of semiconductor. In heterogeneous photocatalysis, oxygen generally serves as an electron acceptor (A) and H_2O as a donor (D). The photogenerated electrons are distributed on the surface of the catalyst, where they interact with adsorbed organic compounds and oxygen molecules ($A_{ads.}$). In the latter case, the electrons can generate a superoxide anion ($O_2^{\bullet-}$) in a reduction process with adsorbed O_2 , which can react with water ($D_{ads.}$) with subsequent generation of other reactive oxygen species (Eqs. 32–37) (Orellana-Garcia et al., 2016; Ren et al., 2017). It is documented that these trapping (tr) reactions occur in less than 30 ps (Quiroz et al., 2011).



Positive holes (h^+_{VB}) can either directly oxidise the adsorbed organic pollutant resulting in the formation of H_2O and CO_2 in mineralisation or react with water or HO^- by generating HO^{\bullet} . Hydroxyl radicals can non-selectively oxidise organics potentially also leading to mineralisation (Eqs. 38–41) (Orellana-García et al., 2016; Ren et al., 2017).



Concerning the properties of the catalyst, the specific surface area and the abundance of active sites are of high importance (Gogate and Pandit, 2004). In addition, the desirable photocatalyst should be chemically and biologically inert, photoactive and -stable, non-toxic, inexpensive, and applicable under visible and UV radiation (Fujishima et al., 2008). TiO_2 possesses many of the aforementioned characteristics (Gogate and Pandit, 2004; Orellana-García et al., 2016). A high photocatalytic activity is confirmed by wide band gap values of 3.23 and 3.02 eV for anatase and rutile, respectively (Mo et al., 2009 (b); Zhongbia et al., 2008; Irokawa et al., 2006).

For PCO of VOCs like benzene, toluene, acetone, ethanol, acetaldehyde, formaldehyde, and others, continuous reactors have often been used. The photocatalytic reactors for air treatment generally incorporate catalysts immobilised on solid support. Some configurations of simplified photocatalytic reactors are represented in Figure 4. Laboratory scale reactors are commonly coated plate (a) and annular (b) reactors with the catalyst immobilised on the reactor walls. Such reactors, however, are not intended for industrial applications since they are not designed to operate at high flow rates of air but are of utmost importance for kinetics studies. Other reactor configurations such as packed bed (c) and monolith (d) are designed with the purpose to have high catalyst-coated surface area to achieve better performance with the aim of possible commercialisation. Packed bed reactors are of simple construction and may provide high conversion per unit mass of catalyst, yet high radial radiation gradients can occur, and the unit can be difficult to maintain. Monolith reactors are compact and could be easily applied in HVAC systems allowing high throughput and low pressure drop. The main drawback is the quick reduction of light intensity through the monoliths, which could be eliminated, but in a rather challenging way given the small monolith channels' pore size, using individual optical fibres passing through each monolith. Other photocatalytic reactors comprise, for instance, honeycomb, multi-plate, corrugated plate and fluidized bed constructions (Ren et al., 2017; Boyjoo et al., 2017; Zazueta et al., 2013; Passalía et al., 2012).

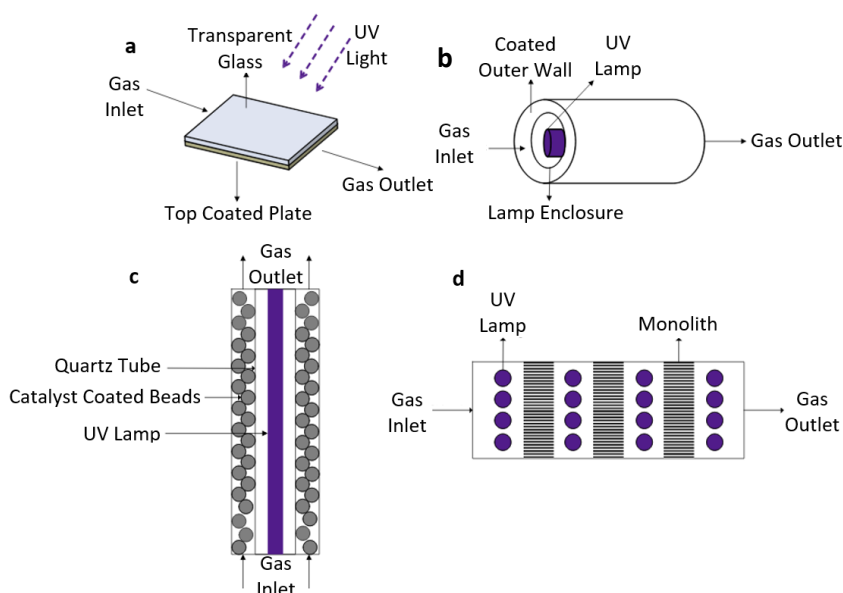


Figure 4. Configurations of gas-phase photocatalytic reactors: a – coated plate; b – annular; c – packed bed; d – monolith (top view) (Boyjoo et al., 2017)

Two main limitations in photocatalytic reactors are the mass and photon transfer. New photocatalytic materials for the absorption of visible light could increase the efficiency of photocatalytic oxidation. Another intensification technique includes a novel configuration of light source, reactor design, and optimal operating conditions. Parameters such as pollutant concentration, light intensity, air flow rate, and relative air humidity affect the rate of photocatalysis (Boyjoo et al., 2017). Photocatalytic decomposition of VOCs generally leads, however, to the formation of intermediates and by-products, which could be more toxic than the initial compound. Hence, the incomplete decomposition of VOCs in oxidation processes is one of the challenges to be faced. Besides, on some occasions, the by-products cause the poisoning of the catalyst requiring regeneration (Orellana-García et al., 2016). Application of ozone may serve as a solution to eliminate this problem, helping to avoid rapid blocking of active sites by degradation intermediates via their heterogeneous reactions with ozone.

1.4 Pollutants Under Consideration

N-nitrosodiethylamine (NDEA) is a water disinfection by-product formed in chlorination or chloramination of potable and waste waters. It is one out of about 300 existing nitrosamines, of which roughly 80-90% are known for their carcinogenic, mutagenic, and teratogenic properties (Xu et al., 2010; Zhou et al., 2012; Mazari et al., 2019). N-nitrosodiethylamine has been linked to the development of gastrointestinal tumours in humans (CSWRCB, 2021), thus having the allowable limit in water established in a few countries. For instance, State of California Department of Public Health and Australian Government have set the NDEA notification level in drinking water at $10 \text{ ng}\cdot\text{L}^{-1}$, and Norwegian Public Health Institute the acceptable limit of $4 \text{ ng}\cdot\text{L}^{-1}$ for NDEA in drinking water (Sørensen et al., 2015; CSWRCB, 2021). Since nitrosamines are known for their

recalcitrance towards conventional water treatment technologies, AOPs are considered as a viable solution (Gao et al., 2009; Padhye et al., 2010).

Toluene and **acetone** are hazardous VOCs present in the environment. Toluene is a hydrophobic aromatic hydrocarbon occurring in industrial wastewaters, originating from paint and coating production, oil refinery, and gas processing with reported concentrations ranging from 0.2 to 12,900 $\mu\text{g}\cdot\text{L}^{-1}$ (Mrowiec, 2014; Cseri et al., 2018; Anjum et al., 2019). Wastewaters subjected to the relevant treatment may still contain residual toluene (Mrowiec, 2014) that can be released to the ambient air, thereby possessing a harmful impact on ecosystems. In places with high traffic density, toluene concentration can reach 1,310 $\mu\text{g}\cdot\text{m}^{-3}$, and in urban air it can range from 5 to 150 $\mu\text{g}\cdot\text{m}^{-3}$ (Schneider et al., 2001; Batterman et al., 2007). Toluene along with acetone may also be detected in the indoor air. The main sources are paintings, tobacco smoke and several household products (Debono et al., 2009; Mo et al., 2009 (b)). Toluene being also a component of gasoline enters the indoor air with vehicle exhausts from outdoors (Batterman et al., 2007). For instance, the indoor concentrations of toluene in winter and summer in Windsor, Canada reached up to 12 and 30 $\mu\text{g}\cdot\text{m}^{-3}$, respectively, whereas in the case of acetone the reported concentrations were accordingly 32 and 137 $\mu\text{g}\cdot\text{m}^{-3}$ (Stocco et al., 2008). Human exposure to toluene and acetone has been reported to affect the central nervous and respiratory systems, also causing skin and eye irritation (Mo et al., 2009 (b); Debono et al., 2009). Toluene and acetone are both also known as model pollutants used to evaluate the efficiency of air purifiers (Costarramone et al., 2015), providing a reasonable basis for the comparison of their abatement with various methods in different matrices.

Ozone, widely used in environmental technologies due to its oxidative properties towards organic pollutants as discussed above, is also a toxic air pollutant. Although it occurs naturally in stratosphere forming a protective layer to avoid harmful effect of UV-light to living organisms, its presence at the ground level may damage respiratory system by aggravating lung diseases such as asthma, chronic bronchitis, and emphysema depending on the level of exposure. Ozone as a pollutant is not emitted directly into the atmosphere but is formed under sunlight via chemical reactions between VOCs and nitrogen oxides (NO_x), originating principally from industries and electric utilities, also from car exhaust. Ozone is also the main ingredient of the photolytic “smog”. Unhealthy levels of ozone are more likely reached on hot sunny days in urban areas; however, high levels can still be detected in colder climates. The existing ambient air quality standards established in 2015 require ozone concentrations to not exceed 0.070 ppm (0.14 $\text{ng}\cdot\text{m}^{-3}$) as averaged across three consecutive years as the fourth-highest daily maximum 8-hour concentration (EPA, 2021). From this, it is obvious that residual ozone originating from water treatment requires further handling and could be utilised as an oxidant in air photocatalytic post-treatment.

1.5 Aim of the Study

The development of novel energy efficient technologies as well as the subsequent improvement of the existing ones for efficient water and air treatment is one of the main goals in environmental technology. Commercially available ozonation is costly, whereas PCD, requiring additional studies and improvements for its large-scale application, is a promising method for the energy efficient oxidation of various hazardous organic compounds. Ozone, an oxidant, and toxic air pollutant present together with VOCs in PCD exhaust air requires post-treatment. Combination of electric discharge treatment

with downstream catalytic utilisation and destruction of ozone along with the degradation of VOCs presents a method of choice since photocatalytic oxidation successfully degrades low concentrations of airborne VOCs at ambient temperature. In addition to organic pollutants, both technologies are lethal to multiple microorganisms in water and air.

This thesis is aimed to provide data necessary for the development of cost-effective technologies for the abatement of hazardous organic compounds from water and air. The objectives of the study include:

- Clarify the PCD energy-efficiency of an unexampled PCD equipment in comparison to commercially used traditional ozonation and its combination with H_2O_2 in aqueous NDEA degradation, the oxidation kinetics of which as a single pollutant have not been studied earlier;
- studying the impact of process control parameters, i.e., initial pollutant concentration, residence time and specific residence time ($\text{s}\cdot\text{cm}^{-2}$), and humidity, on the degradation of acetone and toluene, and their mixture in the presence and absence of ozone using the unique continuous multi-section photocatalytic reactor with adjusting catalytic surface area for the development of air purification technologies; monitoring the depletion of ozone as toxic air pollutant throughout these experiments;
- evaluating the feasibility of the innovative combination of PCD equipment with photocatalytic reactor for the abatement of toluene in both aqueous and gaseous phases; this objective fills the gap in combined PCD-photocatalytic treatment for the elimination of the VOC in both phases.

The strategic structure of the study is illustrated in Figure 5.

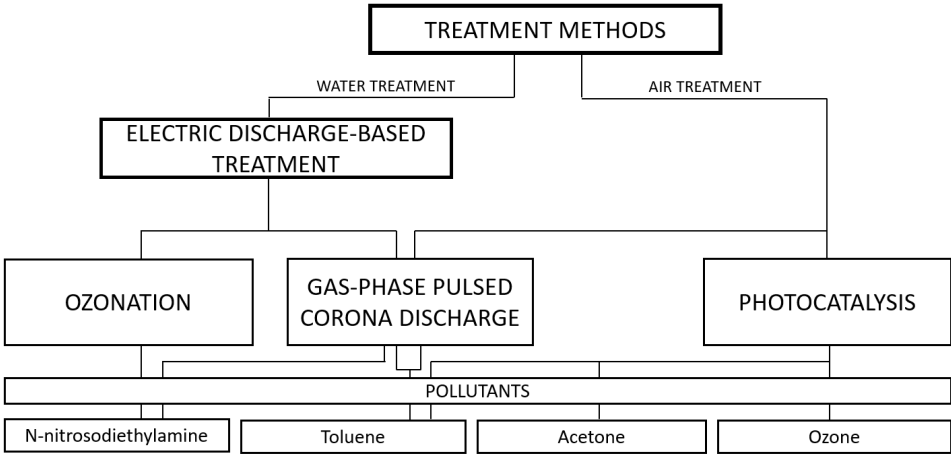


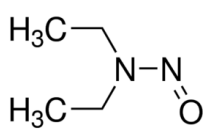
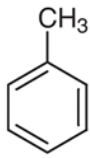
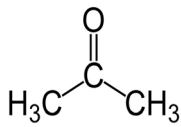
Figure 5. The strategic structure of the study

2 Materials and Methods

2.1 Chemicals and Materials

All used reagents were of analytical grade. Aqueous solutions were prepared using distilled water. Studied organic pollutants – N-nitrosodiethylamine, acetone, and toluene, were purchased from Sigma-Aldrich (Germany). Their chemical structure and physicochemical properties are depicted in Table 2.

Table 2. The properties of N-nitrosodiethylamine, acetone, and toluene

Properties	N-nitrosodiethylamine (NDEA)	Toluene	Acetone
Molecular structure			
Classification	Nitrosamine	Volatile organic compound	Volatile organic compound
CAS nr	55-18-5	108-88-3	67-64-1
Chemical formula	C ₄ H ₁₀ N ₂ O	C ₇ H ₈	C ₃ H ₆ O
Molecular mass, g mol ⁻¹	102.14	92.14	58.08
Solubility in water, g L ⁻¹	106.0 (24 °C)	0.526 (25 °C)	1.0 (25 °C)

2.2 Experimental Equipment and Procedure

2.2.1 Ozonation

Paper I-Experimental Equipment and Procedure

Conventional ozonation was performed in a 600 mL batch glass reactor filled with NDEA solution with initial concentration (C_0) of 10 μM ; ozone-containing air with ozone concentration of 1 or 2 $\text{mg}\cdot\text{L}^{-1}$ was fed to the solution at the flow rate of 2.5 $\text{L}\cdot\text{min}^{-1}$. Flow distribution of O_3 -containing gas is depicted in Figure 6.

Ozonation in acidic (pH 3.0) and neutral (pH 7.0) media were conducted in 50-mM phosphate buffers prepared according to Henderson-Hasselbach equation (Po and Senozan, 2001) ensuring the stability of pH throughout the experiments since preliminary treatment tests showed the decrease in pH, shifting the process towards molecular oxidation. Adjustment of pH 12.0 was provided with the addition of 10 M NaOH solution. In $\text{O}_3/\text{H}_2\text{O}_2$ experiments, hydrogen peroxide with a final concentration of 50 μM in treatment solution, was added into the reactor before the start of ozonation. Residual oxidants in samples were quenched with the addition of sodium sulphite. All experiments were conducted at an ambient temperature of 22 ± 2 °C.

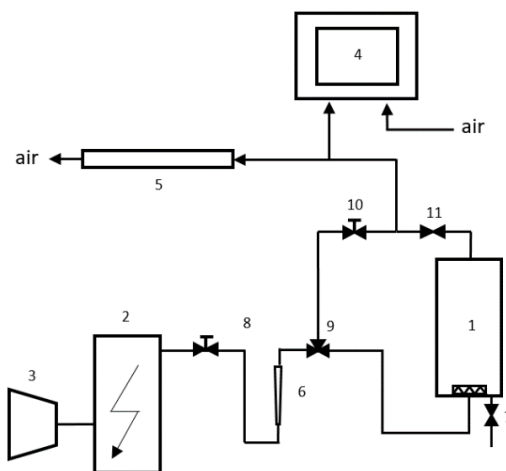


Figure 6. Schematic outline of ozonation gas distribution system: 1 – reactor; 2 – O₃ generator; 3 – compressor; 4 – O₃ monitor; 5 – residual O₃ decomposition column; 6 – rotameter; 7 – sampling port; 11 – gate valve; 8, 10 – gate valves with manual actuator; 9 – 3-way valve

Aqueous ozone was measured by means of colorimetric indigo method (Clesceri et al., 2005) calculating dissolved ozone concentration using Eq. 42:

$$C_{O_3} = \frac{100 \cdot \Delta A}{f \cdot b \cdot V} \quad (42)$$

where C_{O_3} is ozone concentration, mg·L⁻¹, ΔA is the difference between sample and blank absorbance, b is the cell path length, cm, V is the volume of sample, mL, and f is an extinction coefficient with a value of 0.42.

The energy efficiency E , g·kW⁻¹·h⁻¹, was calculated at 50% of NDEA oxidation in ozonation or O₃/H₂O₂ using Eq. 43:

$$E = \frac{\Delta C \cdot V}{t \cdot P + E_{H_2O_2} C_{H_2O_2} V} \quad (43)$$

where ΔC is the decrease of pollutant concentration, g·m⁻³, V is the volume of treated sample, m³, t is the treatment time, h, and P is the power consumed by ozone synthesis, kW, $E_{H_2O_2} C_{H_2O_2} V$ is the energy consumption for H₂O₂, kWh·g H₂O₂⁻¹. The value of power was calculated from the initial concentration of gaseous O₃, mg O₃·L⁻¹, the energy consumed by O₃ synthesis comprising 30 kWh·kg O₃⁻¹, and the flow rate of ozone-containing air, L·min⁻¹ (Katsoyiannis et al., 2011).

2.2.2 Gas-Phase Pulsed Corona Discharge

Paper I and III-Experimental Equipment

The PCD equipment (Flowrox Oy, Finland) (Figure 7) consists of 154 L reactor with 40 L storage tank, pulse generator, and circulation pump (Iwaki Co. Ltd., Japan). The treatment solution was dispersed into the plasma zone through a perforated plate with 51 holes of 1 mm diameter. High voltage pulses (ca 20 kV) were applied between horizontal high voltage electrodes made of stainless-steel wire of 0.55 mm in diameter and total length of 20 m, and two vertical grounded stainless-steel parallel plates.

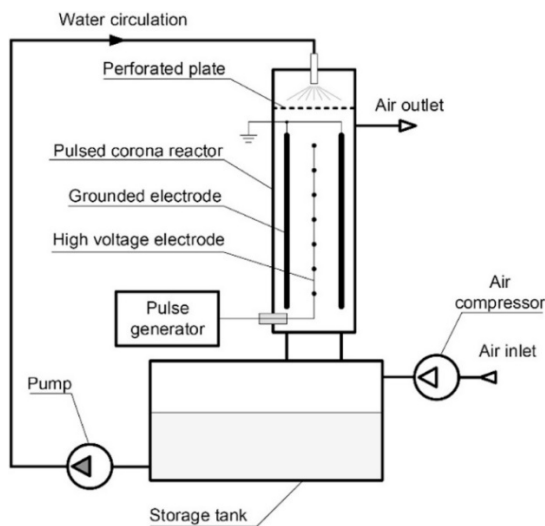


Figure 7. Schematic illustration of PCD device

Paper I-Experimental Procedure

The 10 L aqueous solution sample with initial NDEA concentration of 10 μM was pumped to the distribution box at the top of the plasma reactor and sprayed into the electric discharge zone. The experiment started once the pulse generator was turned on. It applied high voltage pulses with the repetition frequencies of 200 and 880 pulses per second (pps) providing output powers of 32 and 123 W, respectively. For sampling, the generator was turned off and the treated solution was allowed to circulate with a flow rate of 1.0 $\text{m}^3 \cdot \text{h}^{-1}$ for four minutes for equalizing the content. The procedure was repeated for each sample collected at incremental time intervals. Alkaline and acidic media were attained by adding either 5 M NaOH or 5 M H_2SO_4 to the NDEA solution, respectively. In PCD/ H_2O_2 experiments, hydrogen peroxide was added into the storage tank filled with the solution before the start of treatment, resulting in an initial concentration of 50 μM . The experiments were carried out at ambient temperature of $22 \pm 2^\circ\text{C}$.

The energy efficiency E , $\text{g} \cdot \text{kW}^{-1} \cdot \text{h}^{-1}$, was calculated at 50% NDEA oxidation using Eq. 44:

$$E = \frac{\Delta C \cdot V}{W} \quad (44)$$

where ΔC is the decrease in pollutants concentration, $\text{g} \cdot \text{m}^{-3}$, V is the volume of treated sample, m^3 , and W is the consumption of energy, kWh.

Delivered energy, $\text{kWh} \cdot \text{m}^{-3}$ was calculated using Eq. 45:

$$\text{Delivered energy} = \frac{P \cdot t}{V} \quad (45)$$

where P is the power, kW, t is the sampling time, h, and V is the volume of treatment solution, m^3 .

2.2.3 Gas-Phase Photocatalytic Oxidation

Paper II and III-Experimental Equipment

Photocatalytic oxidation was carried out in a multi-section continuous reactor consisting of five sequential sections, each equipped with UVA lamp and TiO₂-coated (P25, Evonik) borosilicate glass plates with the surface area of 120 cm². The schematic illustration of the system with photocatalytic reactor is depicted in Figure 8.

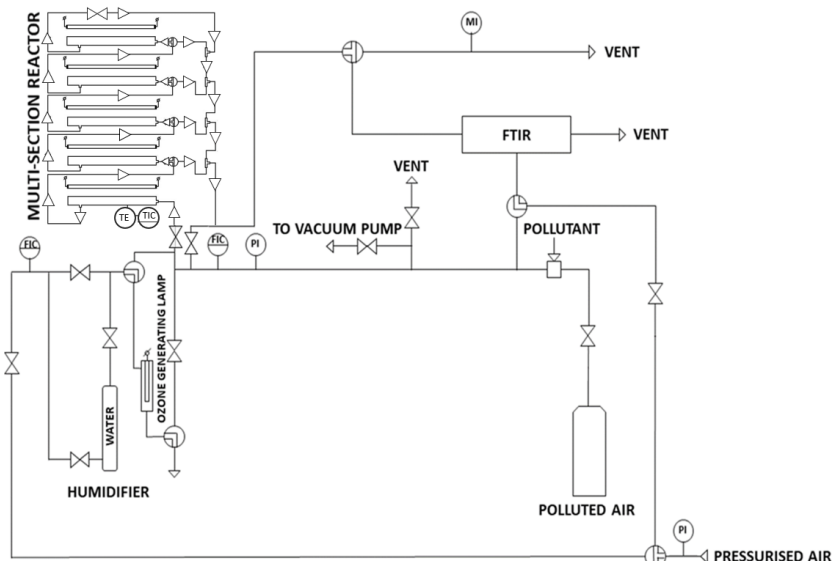


Figure 8. Schematic illustration of the system with photocatalytic reactor: FIC – flow indicator controller; MI – moisture indicator; PI – pressure indicator; TE – temperature element; TIC – temperature indicator controller

UVA-emitting fluorescent lamps (Philips, Actinic T8) with the power of 15 W were placed 6 cm above each section of the reactor. The irradiance of 3.5 mW·cm⁻² was measured at a distance corresponding to the level of the surface of the catalyst by a fibre optic spectrometer (USB-2000 + UV-VIS-ES) using cosine corrector (CC-3-UV-S, field of view 180°); the measured irradiance corresponded to 1.3 × 10⁻⁶ Einstein·s⁻¹ in one section of the reactor. The internal cross-sectional dimensions of the reactor section are 0.9 × 4.9 cm and length 29.5 cm resulting in a volume of 130 mL. The glass wall thickness is 0.2 cm. Temperature in the reactor was measured with a temperature controller supplied with K-type thermocouple (Omega, CN9000A). The gas flow rate was controlled by means of a flow metering valve (Swagelok, SS-6MG-MM) and measured by a mass flow meter (Kobold, MAS-1009-A).

Applied ozone in Paper II was generated by the UVC lamp (LSE Lighting, GPH287T5VH/4) emitting at wavelengths of 254 and 185 nm. The relative air humidity (RH) was 6 ± 1% (1.2 g·m⁻³) or 40 ± 5% (8.2 g·m⁻³) determined at 22 ± 1 °C by hygrometer/psychrometer (TPI, 597) (Paper II).

Conversion, %, was calculated using Eq. 46:

$$\text{Conversion (\%)} = \frac{C_0 - C_t}{C_0} \cdot 100 \quad (46)$$

where C_0 and C_t , ppm, are inlet and outlet concentration of pollutant, respectively.

Paper II-Experimental procedure

The air polluted with either acetone or toluene (inlet concentration, $C_0(\text{acetone})$ and $C_0(\text{toluene})$, of 20, 40, or 60 ppm) or their mixture (inlet concentration of 20 ppm of each compound) was treated in the photocatalytic reactor. The respective amounts of pollutants were injected through the injection port into the feed tank, which had been previously vacuumed. The gas mixture was allowed to evaporate for 20 min followed by the filling of the tank with compressed air to pressure of 3 bars and left for 90 min in order to balance the fluctuations in the concentration. Thereupon, it was directed into the modular reactor using up to five sections, from where the outlet gas of VOCs and ozone was led into Fourier transform infrared spectroscopy (FTIR). For the measurement of initial concentrations, the reactor was omitted by directing the gaseous mixture directly into the gas cell of FTIR.

The flow rates of 0.5 and 1.0 L·min⁻¹ were applied, providing accordingly residence times of 16.0 and 8.0 s per reactor section and specific residence times (SRT) of 0.13 and 0.065 s·cm⁻². The temperature in the reactor maintained by the heat of the lamp was 41 ± 2 °C.

2.2.4 Combination of Pulsed Corona Discharge with Photocatalytic Oxidation

Paper III-Experimental Equipment

The PCD reactor was combined with the photocatalytic one, both described in detail above, to treat residual toluene and ozone containing air exhaust. The 3D illustration of the combination is shown in Figure 9. The exhaust gas was subjected to photocatalytic treatment in the multi-section photocatalytic reactor.

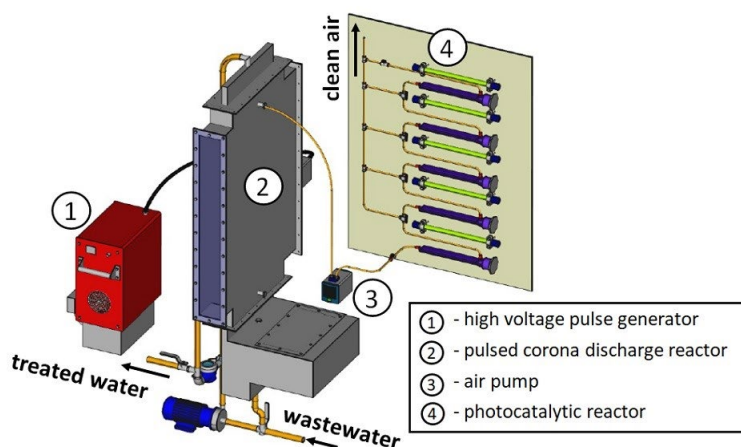


Figure 9. 3D illustration of combined PCD and photocatalytic reactor

Paper III-Experimental procedure

Solutions initially containing approximately 10, 30, and 50 mg·L⁻¹ of toluene provided equilibrium aqueous concentrations of 1.0, 3.7, and 6.3 mg·L⁻¹ in 10 L aqueous solutions at 20 ± 2 °C. These concentrations consistently provided equilibrium airborne toluene concentrations in the air phase of 0.4, 1.0, and 1.6 mg·L⁻¹, respectively, in the overall free gaseous volume of the hermetically closed PCD reactor of 144 L. In experiments at temperature elevated to 30 ± 2 °C, the equilibrium in solutions containing 30 mg L⁻¹ was established at aqueous concentration of 2.5 mg·L⁻¹ and airborne toluene content of

1.2 mg·L⁻¹. Treatment solution was recirculated for 10 min prior to the start of the experiment, and for 5 min prior to sampling after treatment to reach equilibrium concentrations of toluene in liquid and gas phases. The applied pulse repetition frequencies were 50, 200, and 880 pps, providing output powers of 9, 32, and 123W, respectively. Acidic and alkaline media were attained by adding either 5 M H₂SO₄ or 5 M NaOH to the treatment solution, respectively. Otherwise, the experimental procedure in PCD reactor is identical as previously described. An inbuilt spiral coil heater was used to obtain a higher temperature of the solution. The equilibrium state of toluene in gas–liquid system verified implementing Henry’s law (Eq. 47) (Sander, 2015) showed that the measured concentrations were close to the theoretically calculated ones:

$$H = H_0 \cdot \exp \left[\frac{\ln H}{\left(\frac{1}{T} \right)} \right] \left(\frac{1}{T} - \frac{1}{T_0} \right) \quad (47)$$

where H is Henry’s law solubility constant, H_0 is Henry’s law solubility constant at reference temperature, mol·kg⁻¹·bar⁻¹ (Leighton and Calo, 1981), T is the treated solution temperature, K, T_0 is a reference temperature of 298.15 K.

The energy efficiency E , g·kW⁻¹·h⁻¹, was calculated at 40% of toluene oxidation (Eq. 44).

The gas samples from PCD reactor were directed into the photocatalytic modular reactor for exhaust air post-treatment using an air pump (KNF Neuberger S.A.S, France) at flow rates of 0.5, 1.0, and 2.0 L·min⁻¹ that provided residence times of 16.0, 8.0, and 4.0 s per section and specific residence times (SRT) of 0.13, 0.065 and 0.033 s·cm⁻², respectively. The outlet gas of the photocatalytic reactor was directed into FTIR for the measurement of concentrations. The temperature in the reactor comprised 38 ± 1 °C maintained by the heat of the lamp.

2.3 Analytical Methods

2.3.1 Analysis of Aqueous Matrix

Paper I and III

Concentrations of aqueous solutions were measured using 9300 HPLC System high-performance liquid chromatography (YL Instrument Co., Republic of Korea) equipped with a UV/Vis detector and Waters XBridge C18 column (130 Å pore size, 3.5 µm particle size, 150 mm in length and 3.0 mm inner diameter). Eluent flow rate was 0.2 mL·min⁻¹ at the sample run time of 13 min. Isocratic elution was applied using 0.1% CH₃COOH in ultrapure water and acetonitrile: 80% and 20%, respectively, in Paper I and 70% and 30%, respectively, in Paper II. Measurements were duplicated showing a deviation of the results up to 5%.

pH was measured with S220 digital pH-meter (Mettler Toledo, Switzerland) (Paper I and II) and conductivity with multiparameter meter HQ430d (Hach Company, USA) (Paper I). Measurements (Paper I) of (i) aqueous O₃ concentration by means of indigo method at wavelength 600 nm, (ii) the concentration of H₂O₂ formed in PCD treatment using titanyl sulphate method at 410 nm (Kasprzyk-Hordern et al., 2003), and (iii) the concentration of Fe²⁺ determined by o-phenanthroline method at 410 nm (Merck, 1974) were performed by means of HeLios UV-Vis spectrophotometer (Thermo Electron Corporation, USA).

2.3.2 Analysis of Gaseous Matrix

Paper II and III

Concentrations of pollutants in the gas flow were measured using FTIR (Interspec 200-X, Estonia) with the Specac Tornado 8 m 1.33 L gas cell in the range of 500–4000 cm^{-1} . The spectra were collected every 5 min (Paper III) and 10 min (Paper II) for each reactor's section. For quantitative analysis, the peaks of acetone and toluene were measured at the IR bands 1250–1177 and 2964–2838 cm^{-1} (Paper II), respectively, and at 733–727 only for toluene (Paper III). Peak of ozone was monitored at the IR band 1100–970 cm^{-1} . The gaseous intermediate products observed in the study, such as carbon monoxide (Paper II, III) and formic acid (Paper III), were analysed at the IR bands 2225–2050 and 1150–1070 cm^{-1} , respectively. All existing peaks, except ozone, were integrated using Essential FTIR software (Operant LLC, USA) and quantitative database (FDM, HiRes VPFTIR for Quant, USA) (Papers II and III). In Paper I, ozone was produced from dry air using A2ZS-10GLAB O₃ generator (A2Z Ozone Inc., USA) and O₃ gaseous concentration in ozonation as well as the residual O₃ concentration in the exhaust air of PCD were determined with an ozone monitor (PCI-WEDECO Environmental Technologies, Inc., USA). In Papers II and III, the concentration of ozone was determined using FTIR calibrated by either colorimetric indigo method (Clesceri et al., 2005) (Paper II), or MP-6060 ozone analyser (Anseros Klaus Nonnenmacher GmbH, Germany) (Paper III) for calibration. All experiments were duplicated indicating the standard deviation less than 5%.

Catalytic coating was prepared by hand-spraying sonicated slurry of TiO₂ (5 wt%) in ethanol onto glass plates by means of

an aero spray (Stanley, 150119XSTN, USA) followed by drying at room temperature. The TiO₂ surface density was $1.4 \pm 0.2 \text{ mg}\cdot\text{cm}^{-2}$ and thickness of the coating measured using the surface profiler TENCOR P-10, USA, was in the range of 1 μm . The surface of the catalyst (Paper II, Figure S1 in Supplementary material) was visualised with field emission scanning electron microscopy (FE SEM, Dual-Beam Helios Nanolab 600, FEI, USA). The water contact angle was measured at $22 \pm 1^\circ\text{C}$ with DSA 25 (KRÜSS Instrument, Germany) applying the sessile drop fitting method.

The reference experiments, i.e., adsorption and photochemical degradation were carried out in Paper II. No decomposition of acetone, toluene, or ozone was observed under the UVA irradiation in the absence of the catalyst. No degradation of acetone and toluene was observed in the presence of ozone and the absence of TiO₂ catalyst coatings under the studied operating conditions. Slight adsorption (less than 5%) of acetone was detected in dark conditions on TiO₂ coating, whereas no decrease in toluene and ozone concentrations was detected in the FTIR spectrum referring to the lack of adsorption.

Regeneration of the catalyst was needed after the photocatalytic treatment of toluene in the absence of ozone. The air containing ozone passed through the UVA irradiated reactor for 30 min followed by the solitary UVA irradiation for 60 min. Otherwise, the photocatalytic surface was treated under UVA irradiation for 60 min.

3 Results and Discussion

3.1 Oxidation Energy Efficiency of Aqueous Pollutants by Ozonation and PCD Treatment. Content of Exhaust Air Originating from PCD Equipment

The oxidation efficiencies of (i) aqueous NDEA by ozonation, PCD, and their H₂O₂-assisted treatment, and (ii) aqueous toluene by PCD at various experimental conditions are depicted in Table 3a–s. Since toluene is a volatile compound, the energy efficiency values of simultaneous gas-phase oxidation by PCD are also shown in Table 3l–s.

Table 3. Energy efficiencies of NDEA oxidation in ozonation and PCD, and toluene oxidation in PCD treatment

	Ozonation conditions for NDEA	Efficiency of NDEA oxidation for 50%, g·kW ⁻¹ ·h ⁻¹	
		Aqueous	
(a)	C ₀ =10 μM, O ₃ [2 mg·L ⁻¹], pH=7.0, 22°C	0.034	
(b)	C ₀ =10 μM, O ₃ [2 mg·L ⁻¹], pH=12.0, 22°C	1.10	
(c)	C ₀ =10 μM, O ₃ [1 mg·L ⁻¹], pH=7.0, 22°C	0.029	
(d)	C ₀ =10 μM, O ₃ [2 mg·L ⁻¹]/H ₂ O ₂ [50 μM], pH=7.0, 22°C	0.84	
(e)	C ₀ =10 μM, O ₃ [1 mg·L ⁻¹]/H ₂ O ₂ [50 μM], pH=7.0, 22°C	0.70	
	PCD treatment conditions for NDEA	Efficiency of NDEA oxidation for 50%, g·kW ⁻¹ ·h ⁻¹	
		Aqueous	
(f)	C ₀ =10 μM, 200 pps, pH=3.0, 22°C	1.42	
(g)	C ₀ =10 μM, 200 pps, initial pH=7.0, 22°C	1.01	
(h)	C ₀ =10 μM, 200 pps, pH=12.0, 22°C	0.93	
(i)	C ₀ =10 μM, 880 pps, initial pH=7.0, 22°C	0.59	
(j)	C ₀ =10 μM, (200 pps)/H ₂ O ₂ [50 μM], initial pH=7.0, 22°C	1.05	
(k)	C ₀ =10 μM, (880 pps)/H ₂ O ₂ [50 μM], initial pH=7.0, 22°C	0.51	
	PCD treatment conditions for toluene	Efficiency of toluene oxidation for 40%, g·kW ⁻¹ ·h ⁻¹	
		Aqueous	Airborne
(l)	C ₀ =6.3 mg·L ⁻¹ , 880 pps, initial pH 7.0, 20°C	7.5	22.3
(m)	C ₀ =6.3 mg·L ⁻¹ , 200 pps, initial pH 7.0, 20°C	8.6	27.0
(n)	C ₀ =6.3 mg·L ⁻¹ , 50 pps, initial pH 7.0, 20°C	10.5	29.3
(o)	C ₀ =3.7 mg·L ⁻¹ , 200 pps, initial pH 7.0, 20°C	7.5	23.0
(p)	C ₀ =1.0 mg·L ⁻¹ , 200 pps, initial pH 7.0, 20°C	6.4	13.7
(q)	C ₀ =3.7 mg·L ⁻¹ , 200 pps, pH 3.0, 20°C	7.6	22.4
(r)	C ₀ =3.7 mg·L ⁻¹ , 200 pps, pH 12.0, 20°C	7.6	24.9
(s)	C ₀ =2.5 mg·L ⁻¹ , 200 pps, initial pH 7.0, 30°C	5.3	29.5

As is known, ozonation is a pH-sensitive process, thus the NDEA treatment solutions were buffered to maintain the desired pH throughout the experiments. The decomposition of NDEA by mere ozonation at pH 7.0 indicated energy efficiency values of 0.029 and

0.034 g·kW⁻¹·h⁻¹ at gaseous ozone concentration of 1 and 2 mg·L⁻¹, respectively (Table 3a, c; Paper I, Figure 3). Only minor, if any, oxidation was observed under acidic conditions, whereas the increase of pH to 12.0 demonstrated a significantly higher energy efficiency of 1.10 g kW⁻¹·h⁻¹ at gaseous ozone concentration of 2 mg·L⁻¹ due to the abundance of generated HO[•] (Table 3a, b; Paper I, Figure 6). Relatively low degradation efficiency of NDEA in ozonation at pH 7.0 was substantially improved with the addition of H₂O₂, explained by the accelerated decomposition of O₃ into HO[•] (Eq. 19) providing the increased oxidation efficiency of 0.70 and 0.84 g·kW⁻¹·h⁻¹ at gaseous ozone concentration of 1 and 2 mg·L⁻¹, respectively (Table 3d, e; Paper I, Figure 3). The influence of ozone gas–liquid transfer on the oxidation kinetics was tested by measuring aqueous ozone content in the NDEA solution in time of ozone delivery at pH 3.0 indicating rapid saturation of the treated water with ozone reaching an equilibrium concentration at about 250 µg·L⁻¹ in less than 1 min (Paper I, Figure S1 in Supplementary material). This indicates the mass transfer in the reactor is proceeding faster than the oxidation reaction, making the latter control the process rate.

In PCD treatment, the choice of suitable pulse repetition frequency in energy-efficient prospective is of great importance. The changes in pulse repetition demonstrated a different NDEA degradation pattern (Figure 10a) resulting in energy efficiencies of 1.01 and 0.59 g·kW⁻¹·h⁻¹ at 200 and 880 pps, respectively (Table 3g, i), thereby referring to the role of long-living O₃ in NDEA oxidation, since longer periods of time between pulses provide an extra time for O₃ transfer and reactions (Panorel et al., 2011; Preis et al., 2013 (a)). Unlike NDEA, ozone plays a minor role in aqueous toluene oxidation as only moderate variations in energy efficiency (Figure 10b) were observed, comprising 10.5, 8.6, and 7.5 g·kW⁻¹·h⁻¹ at 50, 200, and 880 pps, respectively (Table 3l–n). This is explained by the low concentration of gaseous ozone due to its reaction with toluene in air. For instance, within the first 5 min of PCD treatment, gaseous ozone concentration of 0.22 mg·L⁻¹ in the reactor (Paper III, Figure 3) may provide 0.07 mg·L⁻¹ of equilibrium aqueous ozone according to Henry's law (Gottschalk et al., 2010) affirming the smaller role of ozone in aqueous toluene oxidation. Additionally, toluene is a hydrophobic compound that possesses notably lower water solubility compared to NDEA (Table 2) referring to the occurrence of degradation process at the gas–liquid interface mostly with interface-borne short-living HO[•] (Ajo et al., 2017). It also explains the need for shorter treatment time and thus lower delivered energy in toluene decomposition seen in Figure 10b since HO[•]-based reactions generally proceed at least two orders of magnitude faster in comparison to O₃-based ones (Gottschalk et al., 2010).

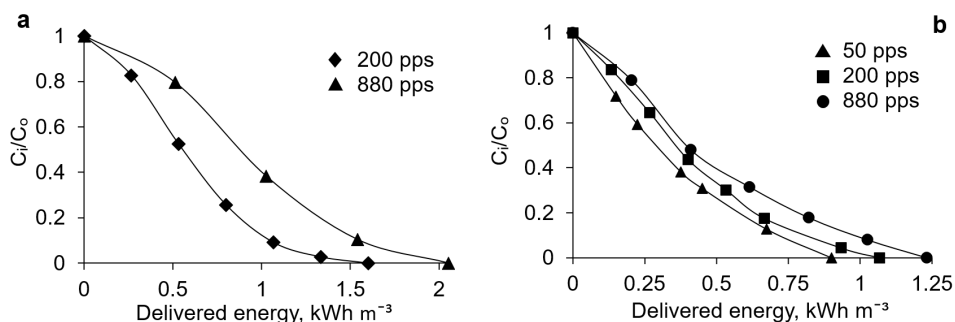


Figure 10. NDEA (a) and toluene (b) delivered energy-dependent PCD-oxidation at pulse repetition frequencies of 200 and 880 pps for NDEA and 50, 200, and 880 pps for toluene. NDEA: $C_0=10$ µM, initial pH=7.0, 22°C; toluene: $C_0=6.3$ mg L⁻¹, initial pH 7.0, 20°C

From Figure 10a one can also see a rather unusual stepwise oxidation pattern with the initial slower phase followed by degradation acceleration. This phenomenon could be explained by the occurrence of Fenton reactions in PCD setup as both H_2O_2 and Fe^{2+} were detected and quantified in concentrations growing with time and H_2O_2 also with pulse repetition frequency (Paper I, Figure 5). H_2O_2 is generated in PCD via recombination of HO^\bullet (Eq. 23) and Fe^{2+} enters the aqueous phase through the leaching from the surface of electrodes and reactor walls made of stainless-steel.

In the experiments on NDEA and toluene oxidation, the pulse frequency of 200 pps appeared to be the most optimal one for further study, affording a longer time of treatment for accurate sampling. Since different initial equilibrium concentrations of 1.0, 3.7, and 6.3 $\text{mg}\cdot\text{L}^{-1}$ were studied for toluene PCD oxidation, indicating accordingly energy efficiency values of 6.4, 7.5, and 8.6 $\text{g}\cdot\text{kW}^{-1}\cdot\text{h}^{-1}$ (Table 3m, o, p), the initial equilibrium concentration of 3.7 $\text{mg}\cdot\text{L}^{-1}$ was chosen for the same purpose as pulse frequency of 200 pps (Paper III, Figure 1a and Figure 2).

For comparative reasons, the importance of using buffered solutions was also clarified by testing PCD oxidation efficiency in conductive medium to provide stable pH as in acidic and alkaline solutions the pH remained practically unchanged throughout the treatment, whereas in neutral solutions the formation of carboxylic acids (Panorel et al., 2013) and nitrate (Kornev et al., 2013) resulted in pH decrease from 7.0 ± 0.1 to 4.2 ± 0.4 in case of NDEA and to 4.5 ± 0.2 in case of toluene. 50 mM phosphate buffer solution for pH 7.0 possessed a conductivity of $7.0 \pm 0.1 \text{ mS}\cdot\text{cm}^{-1}$ at 22 °C, which, however, demonstrated no effect on energy efficiency of complete oxidation of target compound compared to non-buffered media (Paper I, Table S1 in Supplementary material). Further discussion therefore handles PCD oxidation in non-buffered solutions. PCD oxidation of NDEA in alkaline and neutral conditions indicated similar efficiencies of 0.93 and 1.01 $\text{g}\cdot\text{kW}^{-1}\cdot\text{h}^{-1}$, respectively, whereas the acidic medium, contrary to ozonation, demonstrated the highest energy efficiency of 1.42 $\text{g}\cdot\text{kW}^{-1}\cdot\text{h}^{-1}$, exceeding the efficiency at neutral conditions of about 30% (Paper I, Figure 7). This tendency may be explained by the surface oriented HO^\bullet attack, although HO^\bullet also possesses higher redox potential in acidic medium (Wardman, 1989) as well as the radical-scavenging bicarbonates are absent in the acidic medium. Contrary to ozonation, PCD did not benefit from the addition of H_2O_2 making it evident, that the concentration of leached Fe^{2+} -ions limit the rate of Fenton oxidation discussed earlier as the content of H_2O_2 differs twofold (Table 3g, i, j, k). At neutral pH of natural water, the comparison of ozonation at gaseous ozone concentration of 2 $\text{mg}\cdot\text{L}^{-1}$ with PCD treatment at 200 pps in NDEA oxidation exhibited a considerable difference: PCD efficiency of 1.01 $\text{g}\cdot\text{kW}^{-1}\cdot\text{h}^{-1}$ surpassed 0.034 $\text{g}\cdot\text{kW}^{-1}\cdot\text{h}^{-1}$ of ozonation by at least an order of magnitude, which also exceeded the $\text{O}_3/\text{H}_2\text{O}_2$ combination for 20% (Table 3a, d, g).

In toluene PCD-oxidation, the variations in pH possessed no effect on the aqueous toluene degradation (Table 3o, q, r) although alkaline medium promotes additional HO^\bullet production via aqueous ozone decomposition (Kasprzyk-Hordern et al., 2003). As was explained earlier, this is due to the low concentration of gaseous ozone that is in accordance with an even lower equilibrium aqueous ozone content, therefore contributing to the generation of additional HO^\bullet in water only to some extent. The increase in temperature from 20 ± 2 °C to 30 ± 2 °C in the treatment solution, containing 3.7 $\text{mg}\cdot\text{L}^{-1}$ of aqueous toluene in equilibrium with air, provided a toluene aqueous concentration of 2.5 $\text{mg}\cdot\text{L}^{-1}$ and resulted in a remarkably lower energy efficiency of 5.3 $\text{g}\cdot\text{kW}^{-1}\cdot\text{h}^{-1}$ in toluene PCD oxidation (Table 3s).

The oxidation energy efficiency of airborne toluene exceeds the ones of aqueous toluene by about three times in most of the cases (Table 3l–s) pointing to toluene degradation with interface-borne HO^{*} at the gas-phase side (Ajo et al., 2017). The difference increased by about five times with temperature growth, which is consistent with the higher equilibrium concentration of 1.2 mg·L⁻¹ in gas-phase in comparison with 1.0 mg·L⁻¹, and the lower oxidation rate of aqueous admixtures at elevated temperatures (Onga et al., 2020).

The exhaust air originating from PCD setup contains residual ozone as well as a low concentration of fugitive compounds if VOCs are treated. Residual ozone, formed in NDEA PCD oxidation, was quantified at pH 3.0, 7.0, and 12.0 reaching of 0.73 mg O₃·L⁻¹ in acidic and neutral mediums and 0.66 mg O₃·L⁻¹ in alkaline (Table 4a–c). Slightly lower content of gaseous ozone residues at the highest pH is addressed to the enhanced decomposition of O₃ in alkaline solutions.

Since toluene is a volatile compound, its presence in the exhaust air is principally inevitable. In addition to ozone and toluene, a minor presence of carbon monoxide, the product of incomplete oxidation, was observed at the end of the PCD treatment (Table 4d–k).

Table 4. Toluene, O₃, and CO concentrations in PCD outlet gas

	PCD treatment conditions for NDEA	Sampling time, min	Concentration, mg·L ⁻¹		
			O ₃		
(a)	C ₀ =10 μM, 200 pps, pH=3, 22°C	25	0.73		
(b)	C ₀ =10 μM, 200 pps, pH=7, 22°C	30	0.73		
(c)	C ₀ =10 μM, 200 pps, pH=12, 22°C	45	0.66		
	PCD treatment conditions for toluene	Sampling time, min	Concentration, mg·L ⁻¹		
			Toluene	O ₃	CO
(d)	C ₀ =6.3 mg·L ⁻¹ (aq), C ₀ =1.6 mg·L ⁻¹ (gas), 880 pps, initial pH 7.0, 20°C	6	0.057	0.61	0.051
(e)	C ₀ =6.3 mg·L ⁻¹ (aq), C ₀ =1.6 mg·L ⁻¹ (gas), 200 pps, initial pH 7.0, 20°C	20	0.080	0.40	0.042
(f)	C ₀ =6.3 mg·L ⁻¹ (aq), C ₀ =1.6 mg·L ⁻¹ (gas), 50 pps, initial pH 7.0, 20°C	60	0.10	0.22	0.033
(g)	C ₀ =3.7 mg·L ⁻¹ (aq), C ₀ =1.0 mg·L ⁻¹ (gas), 200 pps, initial pH 7.0, 20°C	12.5	0.061	0.39	0.028
(h)	C ₀ =1.0 mg·L ⁻¹ (aq), C ₀ =0.4 mg·L ⁻¹ (gas), 200 pps, initial pH 7.0, 20°C	5	0.065	0.34	0.016
(i)	C ₀ =3.7 mg·L ⁻¹ (aq), C ₀ =1.0 mg·L ⁻¹ (gas), 200 pps, pH 3.0, 20°C	12.5	0.057	0.42	0.030
(j)	C ₀ =3.7 mg·L ⁻¹ (aq), C ₀ =1.0 mg·L ⁻¹ (gas), 200 pps, pH 12.0, 20°C	12.5	0.065	0.044	0.030
(k)	C ₀ =2.5 mg·L ⁻¹ (aq), C ₀ =1.2 mg·L ⁻¹ (gas), 200 pps, initial pH 7.0, 30°C	12.5	0.096	0.22	0.029

In PCD-oxidation of toluene, concentrations of both outlet gas constituents, ozone, and CO, were decreasing with declining pulse repetition frequencies at rather similar toluene content at the end of the treatment (Table 4d–f). This might refer to the potential similarity in PCD and PCO, where lower ozone in a gas phase causes the formation of lower yield of CO, observed in photocatalytic oxidation of toluene which is described in upcoming chapter. Besides, lower toluene initial concentration resulted in a lower carbon monoxide yield at almost equal O₃ content (Table 4e, g, h). The reduced

carbon monoxide yield at lower ozone concentrations monitored at higher temperature also fits into the correlation between gaseous ozone concentration and CO production (Table 4f, k). However, the PCD oxidation experiments at various pH values indicate principally identical CO yield at ozone concentrations expectedly being an order of magnitude lower in alkaline media as a result of rapid decomposition and, thus, the ozone chemisorption (Table 4g, l, j). From this, it could be concluded that CO is a toluene oxidation product without a particular role of ozone, formed through the predominant mechanism of degradation via HO^\bullet . It is also seen in Table 4 that in NDEA oxidation, the difference in O_3 concentration between acidic as well as neutral and alkaline is around 10%, while in the case of toluene, the disparity is about tenfold. In PCD outlet gas, two times higher residual O_3 content was observed at the end of NDEA treatment compared to that of toluene oxidation (Table 4b, h, where $10\text{ }\mu\text{M}$ corresponds to ca. $1\text{ mg}\cdot\text{L}^{-1}$ of NDEA), which could be addressed to the reaction between ozone and toluene in gas-phase confirmed by the measurements of gas-phase ozone concentrations exhibiting slower gaseous ozone concentration growth at higher toluene concentration (Paper III, Figure 3).

As shown in Table 4d–k the trace concentrations of toluene are present in the exhaust air after PCD treatment remaining at about $0.06\text{--}0.10\text{ mg}\cdot\text{L}^{-1}$. The complete oxidation of toluene by PCD may be a time- and energy-consuming task, and besides, residual O_3 is also considered an air pollutant. Thus, gaseous exhaust air containing residual O_3 or additionally trace amounts of VOCs requires further treatment. In such case, photocatalysis presents a reasonable approach.

3.2 Photocatalytic Treatment of Gaseous Pollutants

For successful abatement of VOCs by photocatalytic oxidation, the suitable process parameters should be opted. The changeable operating conditions comprised the presence and absence of ozone, changes in pollutant initial concentration, in residence time and specific residence time (SRT), and in relative humidity (RH) for the degradation of artificially contaminated air containing acetone and toluene, and their mixture. The humid O_3 -containing exhaust air originating from PCD equipment allowed studying only the influence of residence time and SRT as manually changeable parameters.

An explanation for the connection between residence time and SRT lies in the doubling of SRT by decreasing the gas flow rate two times that enables following VOCs' conversion at the same residence time, but at twice the smaller catalyst area. For instance, the TiO_2 -coated surface of 240 cm^2 is used at residence time of 16 s and SRT of $0.065\text{ s}\cdot\text{cm}^{-2}$, whereas at the same residence time and SRT of $0.13\text{ s}\cdot\text{cm}^{-2}$ photocatalytic process is operated over 120 cm^2 allowing to follow the changes in process performance either by increasing the overall residence time by adding the operating reactor sections or by increasing the residence time in one section and exploring the degradation over smaller catalyst surface area.

In the photocatalytic oxidation of acetone and toluene as single pollutants, the use of ozone did not indicate any major effect on the oxidation of acetone within the whole range of the studied inlet concentrations of 20, 40, and 60 ppm corresponding to 0.076, 0.15, and $0.23\text{ mg}\cdot\text{L}^{-1}$, respectively, whereas in the case of toluene, ozone apparently influenced toluene conversion at highest inlet concentration of 60 ppm through accelerated degradation of adsorbed intermediates (Figure 11a, b).

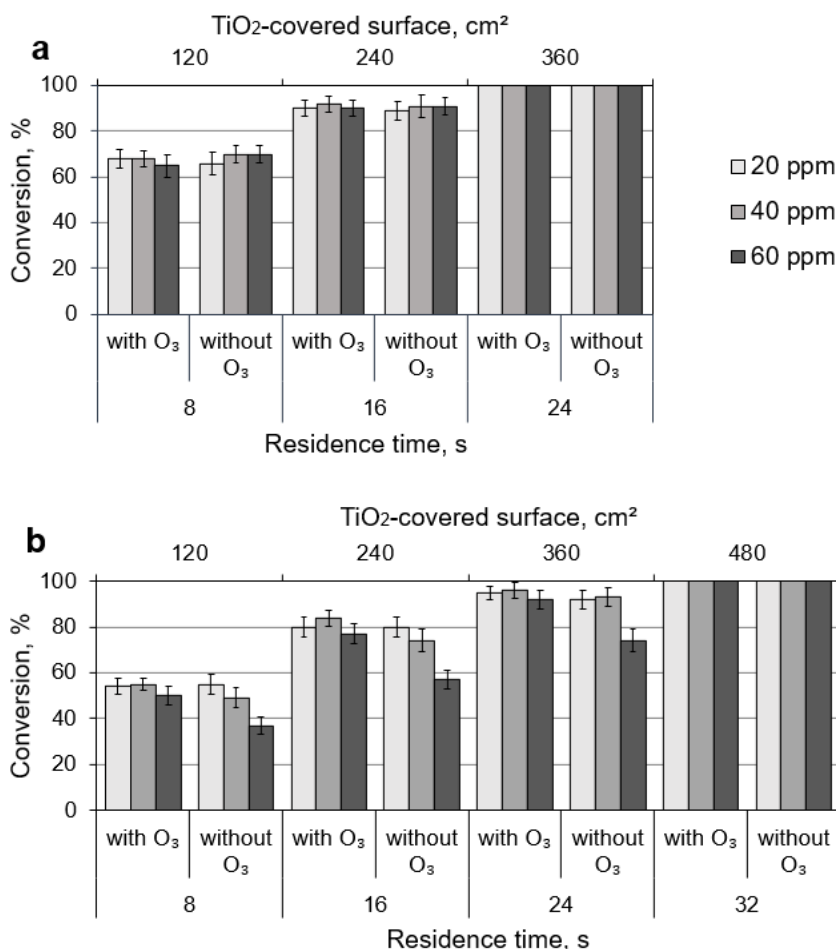


Figure 11. Influence of acetone (a) and toluene (b) concentrations on their conversion in the presence and absence of ozone. RH 6%, SRT=0.065 s·cm⁻²

Rapid deactivation of the catalyst surface by oxidation intermediates is previously reported in the literature (Augugliaro et al., 1999; d'Hennezel, 1998; Cao et al., 2000). The probable reason for the valid effect of ozone on toluene oxidation in fact is the prevention of rapid clogging of active sites by the degradation intermediates via their heterogeneous reactions with ozone. In comparison to acetone, the blocking of catalyst's active sites at higher toluene inlet concentrations is, supposedly, due to the benzene ring, which is more resistant towards oxidative degradation.

Since VOCs' inlet concentration of 20 ppm was the lowest one to allow following the degradation of the initial compounds using more than one section of the reactor, the subsequent discussion covers the results obtained at this concentration. As could be expected, the increase in residence time and TiO₂-coated area increased the efficacy of photocatalytic oxidation, resulting in complete degradation of toluene at the residence time of 32 s (SRT of 0.065 and 0.13 s·cm⁻²; coated area of 480 and 240 cm², respectively), while complete abatement of acetone was examined at residence time of 24 s and 16 s (SRT of 0.065 and 0.13 s·cm⁻²; coated area of 360 and 120 cm², respectively) (Figure 12).

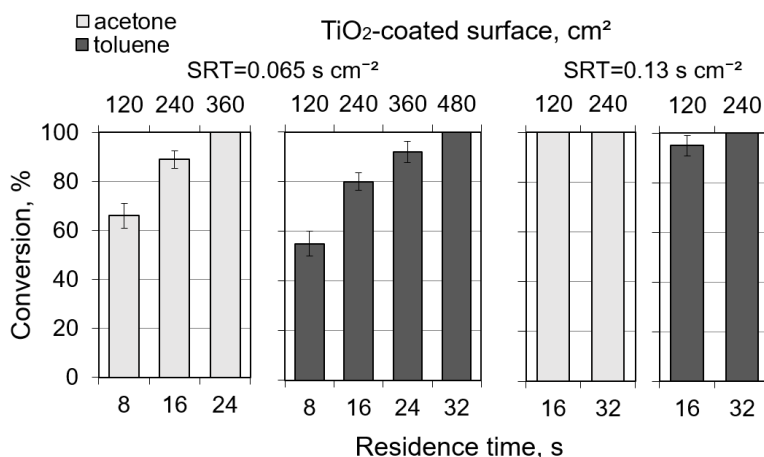


Figure 12. Influence of residence time on acetone and toluene conversion as a single VOC in the absence of ozone. $C_0(\text{acetone})=20$ ppm, $C_0(\text{toluene})=20$ ppm, RH 6%

Figure 12 also demonstrates a higher conversion of acetone and toluene at residence time of 16 s at SRT of $0.13 \text{ s} \cdot \text{cm}^{-2}$ and thus a smaller catalytic surface (coated area of 120 cm^2) compared to the SRT of $0.065 \text{ s} \cdot \text{cm}^{-2}$ (240 cm^2).

The photocatalytic degradation was also compared at different RH values of 6%, which is considered as dry air, and at RH of 40% considered as relative indoor air humidity. The higher air humidity in the presence as well as in the absence of ozone, however, showed no major influence on the oxidation of single VOCs, neither did the presence of ozone at RH of 6% in air polluted with acetone or toluene.

It is known that there are plenty of hydroxyl groups on the TiO_2 surface potentially enabling the adsorption of aromatic compounds through $\text{OH} \cdots \pi$ -electron type complex or water via hydrogen bonding (Nagao and Suda, 1989) possibly resulting in a competitive sorption process under varying experimental conditions. Water adsorption through hydrogen bonding was also confirmed in the present research by the surface wettability test. The water contact angle of TiO_2 -covered surface was measured indicating the value of 0° for an as-prepared sample, thereby showing its hydrophilicity even without the UV treatment (Banerjee et al., 2015). Thus, in the oxidation of single VOCs, the increase in the number of precursors of radicals, such as ozone and hydroxyl anions, did not assist the degradation, whereas the increase in SRT and concentration of pollutants augmented the number of pollutants degraded under the studied conditions.

The increase in RH to 40% slightly inhibited the oxidation of VOCs mixture only at longer SRT in the absence of ozone ($0.13 \text{ s} \cdot \text{cm}^{-2}$, 16 s, 120 cm^2) and in the presence of ozone at shorter SRT ($0.065 \text{ s} \cdot \text{cm}^{-2}$, 8–24 s, 120 – 360 cm^2) (Figure 13).

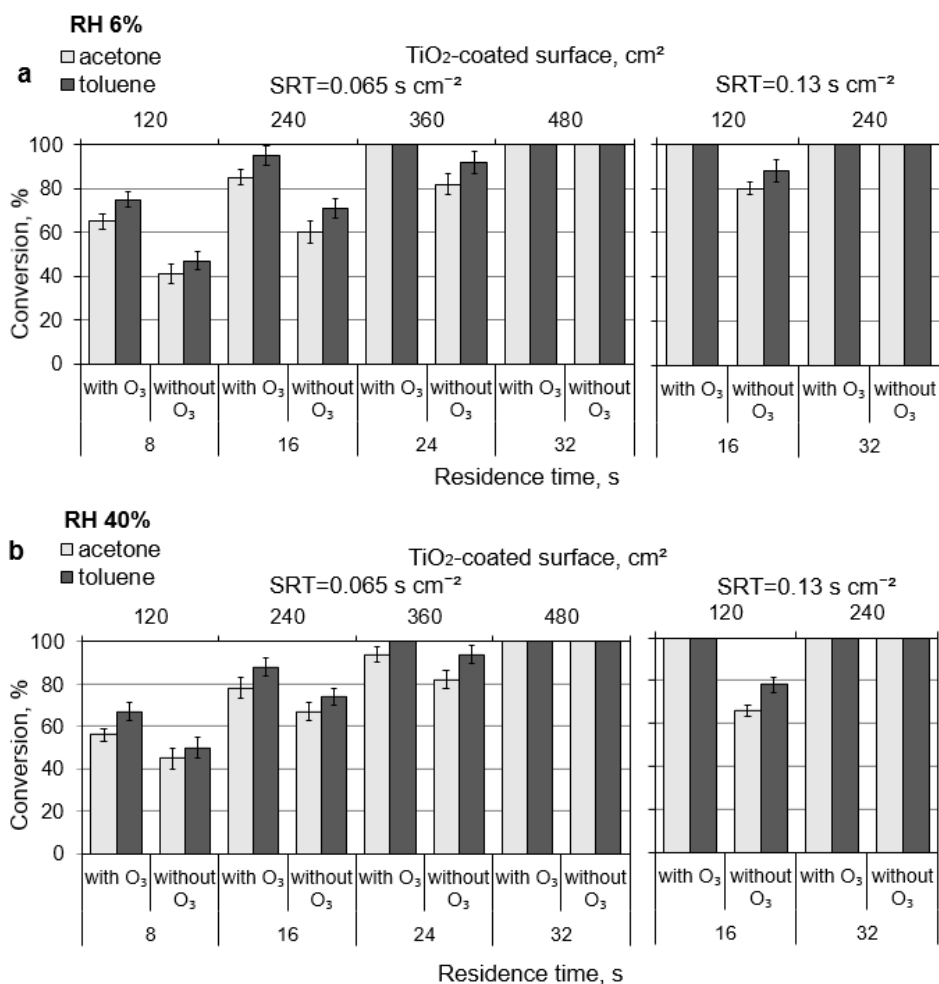


Figure 13. Influence of residence time on acetone and toluene conversion in the mixture in the absence and presence of ozone at RH of 6 (a) and 40% (b). $C_0(\text{acetone})=20$ ppm, $C_0(\text{toluene})=20$ ppm

The minor negative impact of higher relative humidity of 40% in the presence of ozone at shorter SRT could be explained by the competitive adsorption between water vapour and ozone for the active sites on the surface of the photocatalyst. At the same time, the use of ozone tends to advance the oxidation of both VOCs, which is in accordance with the foregoing assumption on the promotion of the degradation of toluene by accelerated oxidation of its intermediates. In addition, toluene presence seemingly inhibited the degradation of acetone in all experimental runs (RH of 6 and 40%, with and without ozone, SRT of 0.065 and 0.13 s·cm⁻²) explained by the adsorption–desorption equilibria, i.e., intermediate products of toluene oxidation impede the adsorption and degradation of acetone.

The complete degradation of the mixture was reached in the absence of ozone at the residence time of 32 s (SRT of 0.065 and 0.13 s·cm⁻²; coated area of 480 and 240 cm², respectively) at both humidity levels, whereas in the presence of ozone, the complete degradation was achieved at the residence time of 24 s (360 cm²) at SRT of 0.065 s·cm⁻² (except for acetone at RH of 40%) and 16 s (120 cm²) at SRT of 0.13 s·cm⁻².

In comparison to single VOCs, higher toluene conversions in the presence of ozone at SRT of $0.065 \text{ s}\cdot\text{cm}^{-2}$ and RH of 6% in the mixtures were presumably attained as a result of additionally formed radicals from acetone degradation, while the conversion of acetone in the mixture was only slightly lower than that of solitary acetone. In the absence of ozone, the catalyst deactivation with adsorbed by-products of toluene resulted in reduced conversions of acetone in the mixtures compared to that of a single VOC (Figure 13), while the toluene conversions remained practically unchanged. The degradation at SRT of $0.065 \text{ s}\cdot\text{cm}^{-2}$ and RH of 40% followed the same pattern, however, somewhat lower conversions of both compounds were noticed in the presence of ozone in comparison to that of RH of 6%, which is, as mentioned before, apparently due to the water vapour competitive adsorption.

As ozone is a toxic air pollutant, its degradation in the air mixture is required. In all studied conditions, ozone was completely degraded possibly via the reactions shown in literature overview (Eqs. 10–14). Ozone was fully degraded at RH of 6% and SRT of $0.065 \text{ s}\cdot\text{cm}^{-2}$ at residence time of 32 s (TiO_2 -coated surface of 480 cm^2), except for (i) in the presence of higher concentration of acetone (Paper II, Figure 5) or toluene (40 and 60 ppm), or (ii) in the presence of VOCs mixture (20 ppm of each pollutant) requiring residence time of 24 s (360 cm^2). This is also consistent with the previous assumption on the oxidative ability of ozone towards higher concentrations of by-products indicating faster depletion of ozone. For the total ozone degradation at higher air humidity of 40% in comparison with 6%, the VOCs' inlet concentrations of 20 ppm and their mixture needed shorter residence time of 24 and 16 s corresponding to 360 and 240 cm^2 , respectively. The presence of a higher content of water vapour favoured the ozone depletion (Masschelein, 1992) and thus somewhat lower concentrations of ozone entered the reactor. The increase in SRT up to $0.13 \text{ s}\cdot\text{cm}^{-2}$ at VOCs' inlet concentration of 20 ppm resulted in the decrease in residence time necessary for complete ozone degradation: at RH of 6% from 32 to 16 s (TiO_2 -coated surface from 480 to 240 cm^2) and at RH of 40% 24 to 16 s (from 360 to 240 cm^2). Although at longer SRT, the imperceptible amount of ozone exited the first reactor section, application of the second reactor section was needed resulting in an overall treatment time of 32 s. For the mixture, the requisite residence time for ozone depletion was 8 s less than in the case of single compounds. The need for lower residence time in order to degrade ozone at SRT of $0.065 \text{ s}\cdot\text{cm}^{-2}$ is because of the overall higher concentration of organics, which is also in accordance with the obtained results using higher VOCs concentrations.

In addition to ozone, the elimination of gaseous by-products formed in VOCs oxidation is of great importance. Plenty of studies report the detection of several adsorbed by-products on the surface of the catalyst (Bianchi et al., 2014; Huang and Li, 2011; Mo et al., 2009 (a); Sleiman et al., 2009), therefore, the present research was focused on the detection and monitoring of gas phase intermediates and by-products, which are essential from the practical point of view. The identified gaseous oxidation products in most experiments (VOCs in the inlet from 20 to 60 ppm) were water vapour, carbon dioxide (CO_2), and carbon monoxide (CO). Besides, the formation of ca. 5 ppm of formic acid (HCOOH) was detected at toluene inlet concentration of 60 ppm in the presence of ozone, nevertheless, at a residence time of 32 s (SRT of $0.065 \text{ s}\cdot\text{cm}^{-2}$, 480 cm^2) there were no traces of formic acid in the outlet gas flow (Paper II, Figure S2 in Supplementary material). Interestingly, at the same conditions, except the presence of ozone, the formation of gaseous formic acid was not noticed, possibly referring to the adsorption of HCOOH , if any, on the catalyst's surface in the absence of O_3 (Schiorlin et al., 2009;

d'Hennezel et al., 1998) whereas the presence of ozone facilitates the generation of higher amount of HCOOH followed by its partial desorption into the gaseous phase. CO was not present in the outlet flow of the reactor at acetone inlet concentration of 20 ppm in the presence and absence of ozone, confirming the total degradation of acetone in the gas phase, whereas low levels of CO (≤ 7 ppm) were observed at higher concentrations of 40 and 60 ppm. In the case of toluene PCO, the variations in toluene inlet concentration from 20 to 60 ppm resulted in the formation of CO from 2 to 8 ppm in the absence of ozone and from 13 to 20 ppm in the presence of ozone. Regarding carbon monoxide, its formation in the VOCs' oxidation within the whole range of studied concentrations was promoted by ozone. The higher CO yield in the presence of ozone confirmed the above-mentioned discussion on the larger number of formed reactive oxygen species as well as the more profound degradation of the intermediate products. In the photocatalytic treatment of mixtures of VOCs, the concentrations of formed CO were comparable or slightly higher, not exceeding 2 ppm difference, than those detected in the case of isolated toluene which is in accordance with the earlier discussion. No significant influence of higher RH of 40% on the formation of CO in PCO of toluene (20 ppm) was observed in the presence of ozone, while the formation of CO was influenced by humid conditions in the absence of ozone, resulting in higher concentrations. Higher amount of water vapour hindered the further oxidation of CO to CO₂, which is consistent with what has been reported earlier (Soliman, 2019). Carbon monoxide yields correspond to residence times, where the complete conversion of initial pollutants was accomplished.

In the combined treatment of PCD and PCO, rather low inlet concentrations of toluene in the saturated exhaust air originating from PCD setup (Table 5) became undetectable over a TiO₂-coated area of 120 cm² within various tested residence times of 4, 8, and 16 s, i.e., correspondingly at SRT values of 0.033, 0.065, and 0.13 s·cm⁻² (Figure 14).

Table 5. Toluene, O₃, and CO concentrations in PCD outlet gas entering photocatalytic reactor

	PCD treatment conditions for toluene	Sampling time, min	Concentration, mg·L ⁻¹		
			Toluene	O ₃	CO
(a)	C ₀ =6.3 mg·L ⁻¹ (aq), C ₀ =1.6 mg·L ⁻¹ (gas), 880 pps, initial pH 7.0, 20°C	20	0.034	0.29	0.038
(b)	C ₀ =3.7 mg·L ⁻¹ (aq), C ₀ =1.0 mg·L ⁻¹ (gas), 200 pps, initial pH 7.0, 20°C	12.5	0.046	0.29	0.024
(c)	C ₀ =1.0 mg·L ⁻¹ (aq), C ₀ =0.4 mg·L ⁻¹ (gas), 200 pps, initial pH 7.0, 20°C	5	0.042	0.24	0.014

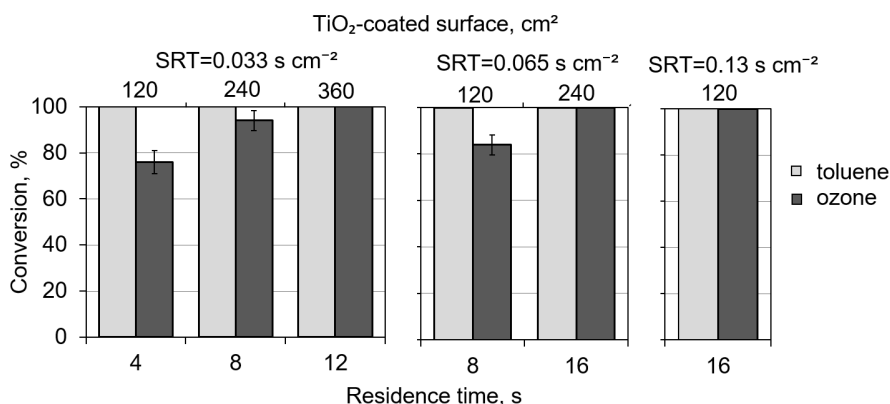


Figure 14. Conversion of airborne toluene and ozone in photocatalytic reactor dependent on residence time at the TiO_2 -coated surface, PCD treatment conditions: $C_0=3.7 \text{ mg L}^{-1}$ (aq), $C_0=1.0 \text{ mg L}^{-1}$ (gas), 200 pps, starting pH 7.0, 20 °C

The fast oxidation of residual toluene is explained by the role of residual plentiful ozone (Pichat et al., 2000). Since no major difference in O_3 conversion was noticed at several residual toluene concentrations, Figure 14 only illustrates the results obtained at an aqueous toluene starting equilibrium concentration of 3.7 mg L^{-1} (Table 5b). Ozone was fully degraded at the longest SRT of 0.13 s cm^{-2} provided by a residence time of 16 s over a TiO_2 -covered photocatalytic surface of 120 cm^2 , although at SRT of 0.065 and 0.033 s cm^{-2} , the O_3 degradation accordingly required 240 and 360 cm^2 corresponding to residence times of 16 and 12 s, respectively. At lower SRTs of 0.033 and 0.065 s cm^{-2} provided by the respective residence times of 4 and 8 s over TiO_2 -coated surface of 120 cm^2 , complete ozone depletion was not observed indicating the need for a larger area of the photocatalyst to ensure the time limit for O_3 degradation. The gradual O_3 depletion within a time span longer than the one essential for the total oxidation of residual toluene confirms a deep oxidation of toluene degradation by-products under the experimental conditions; the accelerated ozone depletion in the presence of toluene oxidation by-products adsorbed on TiO_2 -coated surface was mentioned above.

The photocatalytic treatment of the PCD exhaust air resulted in a slight addition of the CO produced from residual toluene in amounts of $0.002\text{--}0.007 \text{ mg L}^{-1}$. Variations in the CO outlet concentrations are determined by differences in the residual toluene concentrations in the air that enters the photocatalytic reactor. The probable reason for the presence of CO residues is the influence of water vapor described above. The yield of CO, however, does not exceed the maximum permissible concentration for an eight-hour exposure in a working zone comprising 0.058 mg L^{-1} (CREIA, 2011), thus proving the feasibility of the combined PCD and PCO treatment.

Conclusions

Pulsed corona discharge (PCD), photocatalytic oxidation, and their combination were studied for the energy efficient abatement of hazardous environmental pollutants. Water disinfection by-product N-nitrosodiethylamine (NDEA) was degraded as a single pollutant by PCD for the first time. A multi-section photocatalytic reactor, which allows increasing the surface of the catalyst along with the extension of residence time stepwise by adding the reactor sections, was used for the degradation of acetone, toluene, their mixture, and ozone under variable process parameters. Modular reactors with adjustable photocatalytic surface area, that allow the characterisation of the recalcitrance of volatile organic compounds (VOCs), have not been applied earlier in oxidation in continuous mode. An innovative combination of PCD with photocatalytic oxidation was studied for the elimination of residual ozone originating from PCD treatment, in which toluene was oxidised in both phases, aqueous and gaseous. Previous research in this field has not considered the combined technologies to control the removal of VOCs in both phases.

Pulsed corona discharge treatment demonstrated its unequalled energy efficiency in NDEA and toluene oxidation. The difference in energy efficiencies at different pulse repetition frequencies pointed to the role of O_3 -induced oxidation of NDEA, whereas in the case of toluene, reactions with surface-borne HO^* were dominating. At neutral pH of natural water, PCD surpassed traditional ozonation in oxidation of aqueous NDEA in energy efficiency by about twenty-nine times, surpassing also the O_3/H_2O_2 combination by about 20%. In toluene oxidation at pH 7.0, the PCD treatment showed energy efficiencies in aqueous and gaseous toluene oxidation reaching up to 10.5 and 29.6 $g \cdot kW^{-1} \cdot h^{-1}$, respectively. Residual O_3 was detected in the outlet gas of PCD in both NDEA and toluene treatment, also demonstrating the presence of low concentrations of toluene and its by-product CO in the latter case.

In photocatalytic treatment, the positive effect of ozone in toluene oxidation was conditioned by its assistance in regeneration of the catalyst deactivated by toluene oxidation by-products. The increase in specific residence time (SRT) demonstrated enhanced conversion of ozone and VOCs, i.e., acetone and toluene. Properly selected conditions of photocatalytic oxidation over TiO_2 -coated surface allowed complete degradation of VOCs, their mixture, and ozone, resulting in the formation of gaseous oxidation products such as water, CO_2 , and minor amount of carbon monoxide. CO yield, however, did not exceed the permissible concentration for an eight-hour exposure.

The findings in the study contribute to the possible application of energy efficient chemical-free PCD in water treatment in larger scale as a possible addition and/or alternative to conventional water treatment technologies, whereas multi-section photocatalytic reactor with adjustable catalytic surface allowed to obtain necessary data for the development of effective technologies for the decomposition of air pollutants. The novel combination of PCD and photocatalytic reactor contributes to a possible application of the studied approach in closed-loop energy-saving ventilation systems.

References

- Ajo, P., Kornev, I., Preis, S. (2017). Pulsed corona discharge induced hydroxyl radical transfer through the gas-liquid interface. *Sci. Rep.*, 7, 16152.
- Ajo, P., Kornev, I., Preis, S. (2015). Pulsed Corona Discharge in Water Treatment: The Effect of Hydrodynamic Conditions on Oxidation Energy Efficiency. *Ind. Eng. Chem. Res.* 54, 7452–7458.
- Anjum, H., Johari, K., Gnanasundaram, N., Appusamy, A., Thanabalana, M. (2019). Investigation of green functionalization of multiwall carbon nanotubes and its application in adsorption of benzene, toluene & p-xylene from aqueous solution. *J. Clean. Prod.* 221, 323–338.
- Augugliaro, V., Coluccia, S., Loddo, V., Marchese, L., Martra, G., Palmisano, L., Schiavello, M. (1999). Photocatalytic oxidation of gaseous toluene on anatase TiO₂ catalyst: mechanistic aspects and FT-IR investigation. *Appl. Catal. B Environ.*, 20, 15–27.
- Banerjee, S., Dionysiou, D. D., Pillai, S. C. (2015). Self-cleaning applications of TiO₂ by photo-induced hydrophilicity and photocatalysis. *Appl. Catal. B Environ.*, 176–177, 396–428.
- Batterman, S., Jia, C., Hatzivasilis, G. (2007). Migration of volatile organic compounds from attached garages to residences: A major exposure source. *Environ. Res.* 104, 224–240.
- Bechekir, S. Brahami, M., Ould Abdeslam, D., Nemmich, S., Nassour, K., Tilmatine A. (2019). Development of a Low-Cost Ozone Generator Supply --Optimization Using Response Surface Modeling--. *Plasma Environ. Sci. and Tech.*, 13, 7–13.
- Bianchi, C.L., Gatto, S., Pirola, C., Naldoni, A., Di Michele, A., Cerrato, G., Crocellà, V., Capucci, V. (2014). Photocatalytic degradation of acetone, acetaldehyde and toluene in gas-phase: Comparison between nano and micro-sized TiO₂. *Appl. Catal. B Environ.*, 146, 123–130.
- Bingbing, B. X., Zhonglin, Z. C., Qi, F., Ma, J., Wu, F. (2010). Comparison of N-nitrosodiethylamine degradation in water by UV irradiation and UV/O₃: Efficiency, product and mechanism. *J. Hazard. Mater.*, 179, 976–982.
- Bourgin, M., Borowska, E., Helbing, J., Hollender, J., Kaiser, H.-P, Kienle, C., McArde, C.S., Simon, E., von Gunten, U. (2017). Effect of operational and water quality parameters on conventional ozonation and the advanced oxidation process O₃/H₂O₂: kinetics of micropollutant abatement, transformation product and bromate formation in a surface water. *Water Res.*, 122, 234–245.
- Boyjoo, Y., Sun, H., Liu, J., Pareek, V. K., Wang, S. (2017). A review on photocatalysis for air treatment: From catalyst development to reactor design. *Chem. Eng. J.*, 310, 537–559.
- Cao, L., Gao, Z., Suib, S. L., Obee, T. N., Hay, S. O., Freihaut, J. D. (2000). Photocatalytic oxidation of toluene on nanoscale TiO₂ catalysts: Studies of deactivation and regeneration. *J. Catal.*, 196, 253–261.
- Chu, P.K., Lu, X.P. (2013). Low temperature plasma technology: Methods and applications, CRC Press. 1 - 488.
- Clesceri, L. S., Greenberg, A. E., Trussel R. R. (2005). Standard Methods for the Examination of Water and Wastewater, 21st ed., APHA, AWWA, WPCF, Washington, D.C.

- Costarramone, N., Kartheuser, B., Pecheyran, C., Pigot, T., Lacombe, S. (2015). Efficiency and harmfulness of air-purifying photocatalytic commercial devices: From standardized chamber tests to nanoparticles release. *Catal. Today*, 252, 35–40.
- CREIA, California Real Estate Inspection Association. Carbon Monoxide—Leading Cause of Poisoning Deaths. (2011). Available online: <https://www.creia.org/carbon-monoxide---leading-cause-of-poisoning-deaths>. Last access: June 29, 2021.
- Cseri, L., Razali, M., Pogany, P., Szekely, G. (2018). Chapter 3.15—Organic Solvents in Sustainable Synthesis and Engineering. *Green Chemistry: An Inclusive Approach*, 1st ed.; Elsevier Inc.: Amsterdam, The Netherlands, 513–553.
- CSWRCB, California State Water Resources Control Board. Available online: https://www.waterboards.ca.gov/drinking_water/certlic/drinkingwater/NDMA.html. Last access: June 29, 2021.
- Debono, O., Thevenet, F., Gravejat, P., Hequet, V., Raillard, C., Lecoq, L., Locoge, N. (2011). Toluene photocatalytic oxidation at ppbv levels: Kinetic investigation and carbon balance determination. *Appl. Catal. B Environ.* 106, 600–608.
- de Luis, A., Lombraña, J.I. (2018). pH-Based Strategies for an Efficient Addition of H₂O₂ During Ozonation to Improve the Mineralisation of Two Contaminants with Different Degradation Resistances. *Water Air Soil Pollut.*, 229, 372.
- d'Hennezel, O., Pichat, P., Ollis, D. F. (1998). Benzene and toluene gas-phase photocatalytic degradation over H₂O and HCl pretreated TiO₂: by-products and mechanisms. *J. Photochem. Photobiol. A Chem.*, 118, 197–204.
- EPA, United States Environmental Protection Agency. Ozone National Ambient Air Quality Standards (NAAQS). Available online: <https://www.epa.gov/ground-level-ozone-pollution/ozone-national-ambient-air-quality-standards-naaqs>. Last access: June 29, 2021.
- Fujishima, A., Zhang, X., Tryk, D. A. (2008). TiO₂ photocatalysis and related surface phenomena. *Surf. Sci. Rep.*, 63, 515–582.
- Gao, N., Deng, Y., Zhao, D. (2009). Ametryn degradation in the ultraviolet (UV) irradiation/hydrogen peroxide (H₂O₂) treatment. *J. Hazard. Mater.*, 164, 640–645.
- Ghanbari, F., Moradi, M. (2017). Application of peroxymonosulfate and its activation methods for degradation of environmental organic pollutants: Review. *Chem. Eng. J.*, 310, 41–62.
- Giri, R. R., Ozaki, H., Ishida, T., Takanami, R., Taniguchi, S. (2007). Synergy of ozonation and photocatalysis to mineralize low concentration 2,4-dichlorophenoxyacetic acid in aqueous solution. *Chemosphere*, 66, 1610–1617.
- Glaze, W. H., Kang, J-W, Chapin, D. H. (1987). The Chemistry of Water Treatment Processes Involving Ozone, Hydrogen Peroxide and Ultraviolet Radiation. *Ozone Sci. Eng.*, 9, 335–352.
- Gogate, P. R., Pandit, A. P. (2004). A review of imperative technologies for wastewater treatment I: oxidation technologies at ambient conditions. *Adv. Environ. Res.*, 8, 501–551.
- Gottschalk, C., Libra, J.A., Saupe, A. (2010). Ozonation of Water and Waste Water: A Practical Guide to Understanding Ozone and Its Applications, 2nd ed.; Wiley-VCH Verlag GmbH & Co. KGaA, Weinheim.
- Hernandez, R., Zappi, M., Colucci, J., Jones, R. (2002). Comparing the performance of various advanced oxidation processes for treatment of acetone contaminated water. *J. Hazard. Mater.*, 92, 33–50.

- Hoigné, J. (1998). Chemistry of aqueous ozone, and transformation of pollutants by ozonation and advanced oxidation processes. In: J. Hubrec, editor. The handbook of environmental chemistry quality and treatment of drinking water. Berlin: Springer.
- Huang, H., Li, W. (2011). Destruction of toluene by ozone-enhanced photocatalysis: Performance and mechanism. *Appl. Catal. B Environ.*, 102, 449–453.
- Irokawa, Y., Morikawa, T., Aoki, K., Kosaka, S., Ohwaki, T., Taga, Y. (2006). Photodegradation of toluene over TiO_2 -xNx under visible light irradiation. *PCCP*, 8, 1116–1121.
- Kang, M. S., Shin, J., Yu, T. U., Hwang, J. (2020). Simultaneous removal of gaseous NO_x and SO_2 by gas-phase oxidation with ozone and wet scrubbing with sodium hydroxide. *Chem. Eng. J.*, 381, 122601.
- Kasprzyk-Hordern, B., Ziótek, M., Nawrocki, J. (2003). Catalytic ozonation and methods of enhancing molecular ozone reactions in water treatment. *Appl. Catal. B Environ.*, 46, 639–669.
- Katsoyiannis, I.A., Canonica, S., von Gunten, U. (2011). Efficiency and energy requirements for the transformation of organic micropollutants by ozone, $\text{O}_3/\text{H}_2\text{O}_2$ and $\text{UV}/\text{H}_2\text{O}_2$. *Water Res.*, 45, 3811–3822.
- Kogelschatz, U. (2003). Dielectric-Barrier Discharges: Their History, Discharge Physics, and Industrial Applications. *Plasma Chem. Plasma Process.* 23, 1–46.
- Kornev, I., Saprykin, F., Preis, S. (2017). Stability and energy efficiency of pulsed corona discharge in treatment of dispersed high-conductivity aqueous solutions. *J. Electrostat.* 89, 42–50.
- Kornev, I., Osokin, G., Galanov, A., Yavorovskiy, N., Preis, S. (2013). Formation of nitrite- and nitrate-ions in aqueous solutions treated with pulsed electric discharges. *Ozone Sci. Eng.* 35, 22–30.
- Krichevskaya, M., Klauson, D., Portjanskaja, E., Preis, S. (2011). The cost evaluation of advanced oxidation processes in laboratory and pilot-scale experiments. *Ozone Sci. Eng.*, 33, 211–223.
- Leighton, D.T., Calo, J.M. (1981). Distribution Coefficients of Chlorinated Hydrocarbons in Dilute Air-Water Systems for Groundwater Contamination Applications. *J. Chem. Eng. Data*, 26, 382–385.
- Lukes, P., Clupek, M., Babicky, V., Janda, V., Sunka, P. (2005). Generation of ozone by pulsed corona discharge over water surface in hybrid gas-liquid electrical discharge reactor. *J. Phys. D. Appl. Phys.*, 38, 409–416.
- Luo, Y., Guo, W., Ngo, H. H., Nghiem, L. D., Hai, F. I. (2014). A review on the occurrence of micropollutants in the aquatic environment and their fate and removal during wastewater treatment. University of Wollongong Australia, Faculty of Engineering and Information Sciences.
- Magureanu, M., Bradu, C., Parvulescu, V.I. (2018). Plasma processes for the treatment of water contaminated with harmful organic compounds, *J. Phys. D. Appl. Phys.*, 51, 313002.
- Magureanu, M., Lukes, T., Parvulescu, V.I. (2013). Plasma Chemistry and Catalysis in Gases and Liquids, Wiley-VCH Verlag & Co. KGaA, 1 - 422.
- Malik, M. A. (2010). Water purification by plasmas: Which reactors are most energy efficient?. *Plasma Chem. Plasma Process.* 30, 21–31.

- Mazari, S. A., Alaba, P., Saeed, I.M. (2019). Formation and elimination of nitrosamines and nitramines in freshwaters involved in post-combustion carbon capture process. *J. Environ. Chem. Eng.*, 7, 103111.
- Masschelein, W.J. (1992). Unit Processes in Drinking Water Treatment. CRC Press, New York.
- Merck, E. (1974). The Testing of Water Quality. E. Merck, Darmstadt, Germany, p. 231.
- Mo, J., Zhang, Y., Xu, Q., Zhu, Y., Lamson, J. J., Zhao, R. (2009) (a). Determination and risk assessment of by-products resulting from photocatalytic oxidation of toluene. *Appl. Catal. B Environ.*, 89, 570–576.
- Mo, J., Zhang, Y., Xu, Q., Joaquin, J., Zhao, R. (2009) (b). Photocatalytic purification of volatile organic compounds in indoor air : A literature review. *Atmos. Environ.*, 43, 2229–2246.
- Mrowiec, B. (2014). Toluene in sewage and sludge in wastewater treatment plants. *Water Sci. Technol.* 69, 128–134.
- Nagao, M., Suda, Y. (1989). Adsorption of Benzene, Toluene, and Chlorobenzene on Titanium Dioxide. *Langmuir*, 5, 42–47.
- Onga, L.; Kornev, I.; Preis, S. (2020). Oxidation of reactive azo-dyes with pulsed corona discharge: Surface reaction enhancement. *J. Electrostat*, 103, 103420.
- Ono, R., Oda, T. (2003). Dynamics of ozone and OH radicals generated by pulsed corona discharge in humid-air flow reactor measured by laser spectroscopy. *J. Appl. Phys.* 93 5876–5882.
- Orellana-García, F., Álvarez, M. A., López-Ramón, M. V., Rivera-Utrilla, J., Sánchez-Polo, M., Fontecha-Cámara, M. A. (2016). Photoactivity of organic xerogels and aerogels in the photodegradation of herbicides from waters. *Appl. Catal. B: Environ.*, 181, 94–102.
- Padhye, L., Wang, P., Karanfil, T., Huang, C. H. (2010). Unexpected role of activated carbon in promoting transformation of secondary amines to N -nitrosamines. *Environ. Sci. Technol.*, 44, 4161–4168.
- Panorel, I.C., Preis, S., Kornev, I., Hatakka, H., Louhi-Kultanen, M. (2013). Oxidation of aqueous paracetamol by pulsed corona discharge. *Ozone Sci. Eng.*, 35, 116–124.
- Panorel, I., Kornev, I., Hatakka, H., Preis, S. (2011). Pulsed corona discharge for degradation of aqueous humic substances. *Water Supply*, 11, 238–245.
- Passalía, C., Alfano, O.M., Brandi. R.J. (2012). A methodology for modeling photocatalytic reactors for indoor pollution control using previously estimated kinetic parameters. *J. Hazard. Mater.*, 211–212, 357–365.
- Pichat, P., Disdier, J., Hoang-Van, C., Mas, D., Goutailler, G., Gaysse, C. (2000). Purification/deodorization of indoor air and gaseous effluents by TiO₂ photocatalysis. *Catal. Today*, 63, 363–369.
- Preis, S., Klauson, D., Gregor, A. (2013) (a). Potential of electric discharge plasma methods in abatement of volatile organic compounds originating from the food industry. *J. Environ. Manage.* 114, 125–138.
- Preis, S., Panorel, I. C., Kornev, I., Hatakka, H., Kallas, J. (2013) (b). Pulsed corona discharge: the role of ozone and hydroxyl radical in aqueous pollutants oxidation. *Water Sci. Technol.*, 68, 1536–1542.
- Po, H. N., Senozan, N.M. (2001). The Henderson-Hasselbalch equation: its history and limitations. *J. Chem. Educ.*, 78, 1499–1503.

- Quiroz, M. A., Bandala, E. R., Martínez-Huitle, C. A. (2011). Advanced Oxidation Processes (AOPs) for Removal of Pesticides from Aqueous Media, Pesticides – Formulations, Effects, Fate. Intech.
- Restivo, J., Orge, C. A., Guedes Gorito dos Santos, A.S., Gonçalves Pinto Soares O.S., Ribeiro Pereira, M.F. (2021). Influence of preparation methods on the activity of macro-structured ball-milled MWCNT catalysts in the ozonation of organic pollutants. *J. Environ. Chem. Eng.*, 9, 104578.
- Ren, H., Koshy, P., Chen, W, Qi, S., Sorrell, C.C. (2017). Photocatalytic materials and technologies for air purification. *J. Hazard. Mater.*, 325, 340–366.
- Ridgway, H. F., Mohan, B, Cui, X., Chua, K. J., Islam, M. R. (2017). Molecular dynamics simulation of gas-phase ozone reactions with sabinene and benzene. *J. Mol. Graph.*, 74, 241–250.
- Sander, R. (2015). Compilation of Henry’s law constants (version 4.0) for water as solvent. *Atmos. Chem. Phys.*, 15, 4399–4981.
- Schiorlin, M., Marotta, E., Rea, M., Paradisi, C. (2009). Comparison of Toluene Removal in Air at Atmospheric Conditions by Different Corona Discharges. *Environ. Sci. Technol.*, 43, 9386–9392.
- Schneider, P., Gebefügi, I., Richter, K., Wölke, G., Schnelle, J., Wichmann, H.-E., Heinrich, J., INGA Study Group. (2001). Indoor and outdoor BTX levels in German cities. *Sci. Total Environ.* 267, 41–51.
- Schneider, M., Rataj, R., Kolb, J.F., Bláha, L. (2020). Cylindrospermopsin is effectively degraded in water by pulsed corona-like and dielectric barrier discharges. *Environ. Pollut.*, 266, 115423.
- Sleiman, M., Conchon, P., Ferronato, C., Chovelon, J. M. (2009). Photocatalytic oxidation of toluene at indoor air levels (ppbv): Towards a better assessment of conversion, reaction intermediates and mineralization. *Appl. Catal. B Environ.*, 86, 159–165.
- Soliman, N. K. (2019). Factors affecting CO oxidation reaction over nanosized materials: A review. *J. Mater. Res. Technol.*, 8, 2395–2407.
- Sørensen, L., Zahlsen, K., Hyldbakk, A., da Silva, E. F., Booth, A. M. (2015). Photodegradation in natural waters of nitrosamines and nitramines derived from CO₂ capture plant operation. *Int. J. Greenh. Gas Control*, 32, 106–114.
- Stocco, C., MacNeill, M., Wang, D., Xu, X., Guay, M., Brook, J., Wheeler, A. J. (2008). Predicting personal exposure of Windsor, Ontario residents to volatile organic compounds using indoor measurements and survey data. *Atmos. Environ.* 42, 5905–5912.
- von Gunten, U. (2003). Ozonation of drinking water: Part I. Oxidation kinetics and product formation. *Water Res.*, 37, 1443–1467.
- Wang, H., Zhay, J., Yao, W., Wang, B., Deng, S., Huang, J., Yu, G., Wang, Y. (2018). Comparison of pharmaceutical abatement in various water matrices by conventional ozonation, peroxone (O₃/H₂O₂), and an electro-peroxone process. *Water Res.*, 130, 127–138.
- Zazueta, A.L.L., Destailats, H., Li Puma G. (2013). Radiation field modeling and optimization of a compact and modular multi-plate photocatalytic reactor (MPPR) for air/water purification by Monte Carlo method. *Chem. Eng. J.*, 217, 475–485.

- Zhongbia, W., Dong, F., Zhao, W., Guo, S. (2008). Visible light induced electron transfer process over nitrogen doped TiO₂ nanocrystals prepared by oxidation of titanium nitride. *J. Hazard. Mater.*, 157, 57–63.
- Zhou, C., Gao, N., Deng, Y., Chu, W., Rong, W., Zhou, S. (2012). Factors affecting ultraviolet irradiation/hydrogen peroxide (UV/H₂O₂) degradation of mixed N-nitrosamines in water. *J. Hazard. Mater.*, 231–232, 43–48.
- Wardman, P. (1989). Reduction potentials of one-electron couples involving free radicals in aqueous solution. *J. Phys. Chem. Ref. Data*, 18, 1637–1755.

Acknowledgements

I acknowledge the financial support from Estonian Ministry of Education and Research (IUT1-7), Estonian Research Council (PRG776), Executive Agency for Small and Medium Enterprises (VEU17119), Institutional Development Program of Tallinn University of Technology for 2016-2022, European Regional Development Fund (project 2014-2020.4.01.16-0032 and Dora Pluss program), TalTech Development Fund, ASTRA “TUT Institutional Development Programme for 2016-2022” Graduate School of Functional Materials and Technologies (2014-2020.4.01.16-0032), European Cooperation in Science and Technology (COST) program, Baltic Sea region university consortium for Science and Technology (BALTECH), and Tallinn city.

I would like to express my gratitude to my supervisors Dr. Juri Bolobajev and Dr. Marina Krichevskaya for their guidance and assistance as well as the share of academic knowledge and valuable ideas. I am sincerely thankful to Professor Malle Krunk and to Lead Research Scientist Mihkel Koel for providing me opportunities for my self-development. I appreciate the help of colleagues from Laboratory of Environmental Technology. My deepest gratitude is addressed to my family and friends for their continuous support and encouragement throughout the years.

Abstract

Combination of Advanced Oxidation Methods for the Energy-Efficient Abatement of Aqueous and Gaseous Hazardous Pollutants

The presence of hazardous pollutants in the environment has become a worldwide concern due to their detrimental effect on living organisms. A variety of pollutants possess refractory character towards bio-oxidation, and separation techniques, which transfer the pollutant from one phase to another, requiring further handling. A viable solution to deal with such issue is the application of advanced oxidation processes (AOPs) with the aim to degrade organics, mainly by means of highly reactive hydroxyl radicals (HO^\bullet), into harmless products like H_2O and CO_2 in as energy efficient way as possible.

One of the well-known commercially available AOP for water treatment is ozonation, yet expensive synthesis and application of ozone dictates the search for cost-effective alternatives. Pulsed corona discharge (PCD) has demonstrated its unequalled energy efficiency in the oxidation of aqueous organics as a result of more efficient utilisation of reactive species, predominantly HO^\bullet and O_3 , compared to traditional ozonation. However, PCD treatment faces the problem of residual ozone in the air exhaust discharged from the setup. Besides, low concentrations of fugitive compounds are present in the air exhaust if volatile organic compounds (VOCs) are treated, therefore requiring a post-treatment. Photocatalytic oxidation successfully degrades low concentrations of airborne VOCs at ambient temperature. Combination of electric discharge treatment with downstream catalytic utilisation and destruction of ozone along with degradation of VOCs thus presents a method of choice. The pollutants under consideration in the present thesis were N-nitrosodiethylamine (NDEA), acetone and toluene. NDEA, a water disinfection product, is known to possess carcinogenic properties, while toluene and acetone, VOCs widely used in numerous industries, may affect the central nervous and respiratory systems.

The objective of the study was (i) to carry out the comparative study of PCD energy efficiency and traditional ozonation and its combination with H_2O_2 in aqueous NDEA abatement, the oxidation kinetics of which as a single pollutant have not been investigated earlier by either of treatment technologies; (ii) to study the influence of changing process parameters, i.e., initial pollutant concentration, residence and specific residence time (SRT), and humidity, on the degradation of acetone and toluene, and their mixture in the presence and absence of ozone using the unique continuous multi-section photocatalytic reactor with adjusting catalytic surface area for the development of air purifiers; monitoring of ozone depletion was also under the scope of the study; (iii) to evaluate the feasibility of the innovative advanced combination of PCD and photocatalytic reactor for the abatement of toluene in both, aqueous and gaseous phases, and O_3 from gaseous phase, since previous studies in the field has not considered the combined technologies to control the elimination of VOCs in both phases.

Ozonation was performed by continuously feeding O_3 -containing gas flow through a 600-mL batch glass reactor containing aqueous NDEA. The air-filled plasma reactor is 154 L in volume and includes a pulse generator that applies high voltage pulses to the electrodes: horizontal high voltage electrodes are concluded between two grounded vertical parallel plates, all made of stainless steel. A solution of 10 L in volume containing either NDEA or toluene was treated in PCD equipment in recirculation mode: the treated

water was pumped to the distribution box at the top of the plasma reactor and dispersed to the electric discharge zone through a perforated plate with 51 holes of 1 mm in diameter. In toluene oxidation, the gas samples from PCD reactor were directed into the photocatalytic modular reactor for post-treatment. The exhaust air, air polluted with acetone or toluene, or their mixture were treated under UV-A irradiation in the presence and absence of ozone over the photocatalytic surface of P25 TiO₂ in a continuous photocatalytic reactor consisting of five sequential sections, each with a volume of 130 mL. A slurry containing 5% wt. of TiO₂ in ethanol was sprayed onto borosilicate glass plates comprising 120 cm² per reactor section followed by drying at room temperature.

Pulsed corona discharge treatment demonstrated its unequalled energy efficiency in NDEA and toluene oxidation. At neutral pH of natural water, PCD surpassed traditional ozonation in the oxidation of aqueous NDEA in energy efficiency by about twenty-nine times, surpassing also the H₂O₂-assisted ozonation by about 20%. In toluene oxidation at pH 7.0, the PCD treatment showed energy efficiencies in aqueous and gaseous toluene degradation reaching up to 10.5 and 29.6 g·kW⁻¹·h⁻¹, respectively. Application of different pulse repetition frequencies resulted in a notable difference in energy efficiencies pointing to the role of O₃-induced oxidation of NDEA, whereas in the case of toluene, reactions with surface-borne HO[•] were favoured. Residual O₃ was detected in the exhaust air of PCD in both NDEA and toluene treatment, also showing the presence of low concentrations of toluene and its oxidation by-product CO in the latter case.

In photocatalytic oxidation, ozone exhibited a positive effect on toluene degradation via its assistance in regeneration of the catalyst surface deactivated by toluene by-products. The increase in SRT enhanced the conversion of ozone and VOCs, i.e., acetone and toluene. All airborne pollutants were photocatalytically degraded over TiO₂ coated surface under properly selected conditions resulting in the formation of gaseous oxidation products such as water, CO₂, and minor amount of CO in case of toluene. The latter, however, did not exceed the permissible concentration for an eight-hour exposure.

The findings in the study contribute to the possible application of energy efficient chemical-free PCD equipment in water treatment in large scale, whereas the continuous multi-section photocatalytic reactor helped to obtain valuable data for the development of energy efficient air purifiers. The studied approach of combination of PCD equipment and photocatalytic reactor provide a possible solution for application in closed-loop energy-saving ventilation systems.

Lühikokkuvõte

Süvaoksüdatsiooniprotsesside kombineerimine ohtlike saasteainete energiatõhusaks lagundamiseks vees ja õhus

Ohtlike saasteainete esinemine keskkonnas on oma kahjuliku mõju tõttu elusorganismidele kerkinud ülemaailmseks probleemiks. Mitmed saasteained on biooksüdatsioonile vastupidavad ning separatsiooniprotsesside puhul toimub saasteaine lagundamise asemel selle transport ühest maatriksist teise, nõudes seega lisa puhastusetappi. Paljulubavateks töötlemisprotsessideks on süvaoksüdatsiooniprotsessid (SOP), mis põhinevad saasteainete lagundamisel tugevate oksüdantide, peamiselt hüdroksüülradikaalide (HO^\bullet), abil.

Üheks laialdaselt veetöötlustes kasutusel olevaks SOP-ks on osoonimine. Osooni sünteesimine *ex situ* ja selle rakendamine muudab antud tehnoloogia aga üsna kulukaks, mistõttu on oluline pöörata tähelepanu kulutõhusama alternatiivi leidmisele. Koroonaimpulss elektrilahendus (KIEL) on osutunud mitmete saasteainete oksüdeerimisel vägagi energiatõhusaks meetodiks ning seda just KIEL reaktoris *in situ* tekkivate oksüdantide, enamasti HO^\bullet ja osoon, tõttu. KIEL tehnoloogia üheks puuduseks on jääksooni esinemine seadmest väljuvas õhus, mis võib lisaks sisaldada veel ka lenduvaid orgaanilisi ühendeid (LOÜ). Sellest johtuvalt on vajalik heitgaasi edasine töötlemine. Järeltöötlusena sobib fotokatalüütiline oksüdatsioon, mis võimaldab lagundada madalaid LOÜ-de kontsentratsioone. Käesolevas töös olid vaatluse all kolm saasteainet: N-nitrosodietüülamiin (NDEA), toluen ja atsetoon. NDEA on kantserogeenne vee desinfitseerimisel kloorühenditega tekkiv kõrvalprodukt. Toluen ja atsetoon on tööstuses laialt kasutusel olevad LOÜ-d, mis võivad avaldada kahjulikku mõju närvisüsteemile ja hingamisteedele.

Töö üheks eesmärgiks oli võrrelda omavahel KIEL-i ja osoonimise ning viimase kombinatsiooni vesinikperoksiidiga, energiaefektiivsusi NDEA lagundamisel vesifaasis. NDEA lagundamise kineetikat SOP-dega üksiku saasteainena ei oldud vaarasevalt uuritud. Töö eesmärgiks oli ka uurida erinevate töötingimuste, nagu saasteaine algne kontsentratsioon, viibe- ja eriviibeaeg ja suhteline õhuniiskus, mõju tolueni ja atsetooni ning nende segu lagundamisele osooni juuresolekul ja ilma, kasutades unikaalset fotokatalüütilist pidevas režiimis töötavat reaktorit, mis võimaldab muuta fotokatalüütilise pinna suurust vastavalt vajadusele. Oluline oli jälgida ka osooni kui toksilise õhusaasteaine lagundamist. Saadud tulemused on väärtuslikud tõhusate õhupuhastustehnoloogiate välja töötamiseks. Lisaks seati töös eesmärk hinnata KIEL-i ja fotokatalüütilise reaktori kombineerimise otstarbekust tolueni lagundamiseks nii vedelkui gaasifaasist ja osooni lagundamiseks gaasifaasist, kuna varasemalt puudusid uuringud LOÜ-de lagundamiseks kombineeritud tehnoloogiaid kasutades.

Osoonimise katsed viidi läbi 600 ml NDEA lahust sisaldavas segureaktoris, millest puhuti pidevalt läbi osooni sisaldavat gaasi. Gaasifaasiline KIEL-i reaktor on mahult 154 l ning hõlmab endas lisaks veel pulsigeneraatorit, mis rakendab elektroodidele kõrgepinge impulsse. Kõrgpinge elektroodid asetsevad horisontaalselt kahe maandatud vertikaalse paralleelse elektroodi vahel. Lahust töödeldi retsirkuleerivas režiimis. 10 l töötlemislahust, mis sisaldas vastavalt kas NDEA-d või tolueni, pumbati plasmareaktori ülemises osas asuvasse jaotuskambris ja piserdati plasmatsiooni läbi perforatsioonplaadi. Tolueni töötlemise puhul koguti hetkel, mil tolueni kontsentratsiooni vees enam ei tuvastatud, gaasiproovid, mis suunati edasiseks töötamiseks fotokatalüütilisse reaktoris. KIEL reaktorist pärineva tolueni ja osooni sisaldava heitgaasi ning kunstlikult valmistatud

gaasisegude, mis sisaldasid vastavalt kas atsetooni, tolueeni, või mõlemat saasteainet ja mida töödeldi osooni juuresolekul ja ilma, puhastamiseks kasutati fotokatalüütilist reaktorit. Reaktor koosneb viiest sektsioonist, millest igaüks on mahult 130 ml ning varustatud UVA lambiga. Iga sektsiooni sisse on paigutatud 120 cm² suurune borosilikaatklaas, mis kateti käsitsi spreitamise teel suspensiooniga, mis sisaldas 5 massi% TiO₂ etanoolis. Katted kuivatati toatemperatuuril.

KIEL tehnoloogia osutus nii NDEA kui ka tolueeni lagundamisel energiatõhusaks meetodiks. Loodusliku vee tavapärase neutraalse pH juures ületas KIEL NDEA lagundamisel traditsioonilist osoonimist ligikaudu 29 korda ning osooni kombineerimist vesinikperoksiidiga ligikaudu 20%. Tolueeni oksüdeerimise puhul neutraalses keskkonnas ulatusid KIEL-i energiaefektiivsuse väärtused vee- ja gaasifaasis vastavalt 10.5 ja 29.6 g·kW⁻¹·h⁻¹. Erinevate pulsisageduste rakendamine tõi NDEA lagundamise puhul kaasa märgatava erinevuse energiaefektiivsuses, viidates seega osooni mõjule lagundamisprotsessis. Tolueeni puhul oli erinevus pigem väike, mis viitab hoopis HO[•] rollile. Nii NDEA kui ka tolueeni töötlemisel tuvastati KIEL seadmest väljuvas heitgaasis jääkosooni ning tolueeni puhul ka madalaid tolueeni ning selle laguprodukti – CO, kontsentratsioone.

Fotokatalüütilisel töötlemisel takistas osooni juuresolek katalüsaatori pinna saastumist tolueeni laguproduktidega. Eriviibeaja suurendamisega kaasnes osooni ja LOÜ-de – atsetoon ja tolueen, kõrgem konversioon. Sobilikud katsetingimused tagasid õhusaasteainete lagundamise veeks ja süsihappegaasiks. Tolueeni puhul tuvastati ka CO teket, mis siiski ei ületanud lubatavat kontsentratsiooni kaheksatunnise kokkupuute korral.

Töös uuritud saasteainete energiatõhusat lagundamist tõestanud kemikaalivaba KIEL tehnoloogia võib tulevikus leida laialdasemat kasutust. Pidevas režiimis töötava mitmesektsioonilise katalüütilise õhupuhastusreaktoriga saadud tulemused omavad kõrget väärtust olemasolevate õhupuhastusreaktorite arendamisel ja uute välja töötamisel. KIEL reaktori ja fotokatalüütilise reaktori innovaatilist kombinatsiooni saab potentsiaalselt rakendada suletud energiasäästlikes ventilatsioonisüsteemides.

Appendix 1

Paper I

Kask, M.; Krichevskaya, M.; Preis, S.; Bolobajev, J. (2021). Oxidation of Aqueous N-Nitrosodiethylamine: Experimental Comparison of Pulsed Corona Discharge with H₂O₂-Assisted Ozonation. *Journal of Environmental Chemical Engineering*, 9, #105102.



Contents lists available at ScienceDirect

Journal of Environmental Chemical Engineering

journal homepage: www.elsevier.com/locate/jeceOxidation of aqueous N-nitrosodiethylamine: Experimental comparison of pulsed corona discharge with H₂O₂-assisted ozonationMaarja Kask, Marina Krichevskaya, Sergei Preis, Juri Bolobajev^{*}

Department of Materials and Environmental Technology, Tallinn University of Technology, Ehitajate tee 5, 19086 Tallinn, Estonia

ARTICLE INFO

Editor: V. Victor

Keywords:

Advanced oxidation processes
Electric discharge
Ozonation
N-nitrosamine
Plasma
Water purification

ABSTRACT

Hazardous nitrosamines formed in drinking water disinfection present serious public health and environmental concerns. Pulsed corona discharge (PCD) known for its unequalled energy efficiency in aqueous pollutants oxidation was experimentally compared with ozonation in degradation of N-nitrosodiethylamine (NDEA). Both methods were combined with H₂O₂ for advancement testing. In neutral media, PCD surpassed conventional ozonation for about twenty-nine times in energy efficiency; ozonation efficiency was substantially improved with H₂O₂ addition, whereas PCD did not benefit from it still surpassing O₃/H₂O₂ combination for about 20% at pH 7.0. The Fenton-mediated oxidation was noticed in PCD accelerating oxidation of NDEA. The increase of pH to 12.0 predictably accelerated ozonation whereas PCD demonstrated the opposite outcome resulting in higher oxidation efficiency at pH 3.0.

1. Introduction

Hazardous nitrosamines (NAs) formed as water disinfection by-products present serious public health and environmental concerns. Roughly, 80–90% of more than 300 identified NAs are known for their carcinogenic, mutagenic, and teratogenic properties [1–3]. One of the most carcinogenic NAs is N-nitrosodiethylamine (NDEA), that is linked to human gastrointestinal tumors having 1 ng L⁻¹ as a calculated value of concentration in potable water associated with a lifetime cancer risk level of 10⁻⁶ [4]. Hence, the allowable limit for NDEA concentration in water was legislated by a few governments: State of California Department of Public Health and Australian Government set the NDEA notification level at 10 ng L⁻¹, and Norwegian Public Health Institute at 4 ng L⁻¹ in drinking water [4,5].

Since NAs are known to be recalcitrant towards conventional water treatment, advanced oxidation processes (AOPs) are considered as a viable solution [6,7]. Successful degradation of NDEA in ozonation, UV photolysis, O₃/UV treatment, and Fenton process has been reported [2, 8]. Ozonation, as a commercially available technology, is extensively studied for abatement of organic pollutants oxidized with ozone and/or HO-radicals (HO•) formed with O₃ decomposition in water [9–11]. For slowly degrading refractory pollutants, addition of H₂O₂ to O₃-treated solutions is recommended for accelerated HO-radicals production at improved radicals yield (Eq. 1) [12]:



Zhang with co-workers studied degradation of NAs mixture including NDEA using O₃ and O₃/H₂O₂ combination [13]. The authors of the present study failed to find, however, data on oxidation kinetics of NDEA as a single pollutant.

Expensive synthesis and application of ozone hinder its implementation in water treatment dictating the search for cost-effective alternatives [14]. One of the promising AOPs is application of non-thermal plasma, where most common reactive species generated at atmospheric pressure are HO•, O₃, NO•, H₂O₂, atomic oxygen, superoxide anion as well as excited molecules and atoms, positive and negative ions, free electrons and free radicals, which formation and abundance is dependent on the type of plasma source [15,16]. Gas-phase pulsed corona discharge (PCD) plasma treatment demonstrated unequalled energy efficiency in oxidation of various aqueous organic pollutants [17,18]. Main short-living reactive species, HO-radicals and atomic oxygen generated in plasma from water and gas-phase oxygen (Eqs. 2 and 3) utilize the discharge energy in more efficient way than in traditional ozonation [19]:

^{*} Corresponding author.E-mail address: juri.bolobajev@taltech.ee (J. Bolobajev).<https://doi.org/10.1016/j.jece.2021.105102>

Received 22 November 2020; Received in revised form 8 January 2021; Accepted 16 January 2021

Available online 18 January 2021

2213-3437/© 2021 Elsevier Ltd. All rights reserved.

Ozone synthesized in PCD provides additional oxidant amount contributing to pollutant oxidation dependently on the reaction kinetics to be taken into account for optimizing the treatment control parameters [18].

The present study focuses on PCD oxidation of aqueous NDEA for clarifying its efficiency compared to traditional ozonation and its combination with H_2O_2 .

2. Experimental

2.1. Chemicals

N-nitrosodiethylamine ($\text{C}_4\text{H}_{10}\text{N}_2\text{O}$, $\geq 99\%$), phosphoric acid (H_3PO_4 , 85%), ammonium acetate ($\text{CH}_3\text{COONH}_4$, $\geq 98\%$), acetic acid (CH_3COOH , 99%), sodium hydroxide (NaOH , $\geq 98\%$), sodium sulphite (Na_2SO_3 , $\geq 99\%$), sodium dihydrogen phosphate (NaH_2PO_4 , $\geq 99\%$), titanium sulphate ($\text{TiO}_2\cdot\text{SO}_3\cdot 2\text{H}_2\text{O}$, $\geq 99\%$), potassium indigotrisulfonate ($\text{C}_{16}\text{H}_7\text{N}_2\text{O}_{11}\text{S}_3\text{K}_3$, $\geq 99\%$), and hydroxylamine hydrochloride ($\text{NH}_2\text{OH}\cdot\text{HCl}$, $\geq 99\%$) were purchased from Sigma-Aldrich. Dipotassium phosphate (K_2HPO_4 , 99%), potassium dihydrogen phosphate (KH_2PO_4 , 99%), sulfuric acid (H_2SO_4 , 96%), and 1,10-phenanthroline monohydrate ($\text{C}_{12}\text{H}_8\text{N}_2\cdot\text{H}_2\text{O}$) were provided by LACH-NER (Czech Republic). Hydrogen peroxide (H_2O_2 , $\geq 30\%$, w/w) was purchased from Honeywell.

All aqueous solutions were prepared using distilled water.

2.2. Experimental conditions

Aqueous solutions with initial concentrations $[\text{NDEA}]_0 = 10 \mu\text{M}$ were treated by means of ozonation and PCD at various pH values. Ozonation experiments in acidic and neutral media were carried out in 50-mM phosphate buffers prepared according to Henderson–Hasselbach equation [20] ensuring stable pH throughout the experiments since preliminary treatment tests demonstrated decreasing pH. Adjustment of pH 12.0 was provided with addition of 10 M NaOH solution. In PCD experiments, acidic and alkaline media were attained by adding either 5 M H_2SO_4 or 5 M NaOH to the NDEA solution, respectively. The initial concentration of H_2O_2 in $\text{O}_3/\text{H}_2\text{O}_2$ and PCD/ H_2O_2 experiments comprised 50 μM . All experiments were conducted at ambient temperature, $22 \pm 2^\circ\text{C}$.

2.3. Experimental equipment and procedure

Pure NDEA is a volatile organic liquid with vapor pressure of 5.7 mmHg at 25°C [21]. Preliminary reference tests with N_2 as a stripping gas were conducted under ozonation experimental conditions (see below) for possible evaporation of NDEA; nitrogen was provided using LCMS30–1 generator (Parker, Dominick Hunter). Concentration of NDEA did not change for 60 min of stripping, thus attributing NDEA concentration decline in ozonation experiments solely to its oxidation.

Conventional ozonation was performed in a 600 mL batch glass reactor filled with NDEA solution; ozone-containing air with ozone concentration of 1 or 2 mg L^{-1} was fed at the flow rate of 2.5 L min^{-1} . Flow distribution of O_3 -containing gas is depicted in Fig. 1; ozone was produced from dry air using A2ZS-10GLAB O_3 generator (A2Z Ozone Inc., USA) with its gaseous concentration determined with an O_3 monitor (PCI-WEDECO Environmental Technologies, Inc., USA). Ozonation experiments lasted for 10–60 min with sampling at incremental time intervals. In $\text{O}_3/\text{H}_2\text{O}_2$ experiments, hydrogen peroxide was added once into the reactor before the start of ozonation. Residual oxidants in samples were quenched with addition of sodium sulphite.

Aqueous dissolved ozone was measured using colorimetric indigo method [22] calculating dissolved ozone concentration using Eq. 4:

$$C_{\text{O}_3} = \frac{100 \cdot \Delta A}{f \cdot b \cdot V} \quad (4)$$

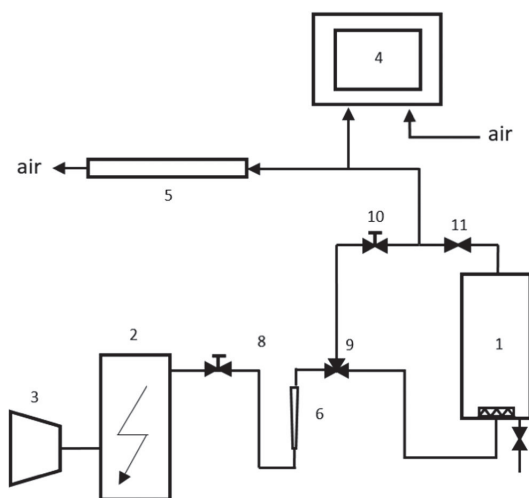


Fig. 1. Schematic outline of ozonation gas distribution system: 1 – reactor; 2 – O_3 generator; 3 – compressor; 4 – O_3 monitor; 5 – residual O_3 decomposition column; 6 – rotameter; 7 – sampling port, 11 – gate valve; 8, 10 – gate valves with manual actuator, 9 – 3-way valve.

where C_{O_3} is ozone concentration, mg L^{-1} , ΔA is the difference between sample and blank absorbances, b is the cell path length, cm, V is the volume of sample, mL, and f is an extinction coefficient being 0.42.

The energy efficiency (E) of NDEA oxidation with O_3 or $\text{O}_3/\text{H}_2\text{O}_2$, $\text{g kW}^{-1} \text{ h}^{-1}$, was calculated using Eq. 5:

$$E = \frac{\Delta C \cdot V}{t \cdot P + E_{\text{H}_2\text{O}_2} C_{\text{H}_2\text{O}_2} V} \quad (5)$$

where ΔC is the decrease of NDEA concentration, g m^{-3} , V is the volume of treated sample, m^3 , t is the treatment time, h, and P is the power consumed by ozone synthesis, kW, $E_{\text{H}_2\text{O}_2} C_{\text{H}_2\text{O}_2} V$ is the energy consumption for H_2O_2 , $\text{kWh g H}_2\text{O}_2^{-1}$. The power was calculated from gaseous O_3 initial concentration, $\text{mg O}_3 \text{ L}^{-1}$, the flow rate of ozone-containing air, L min^{-1} , and the energy consumed by O_3 synthesis comprising 30 kWh kg O_3^{-1} [23]. Energy efficiency calculations were made for 50% decrease in NDEA concentration.

The PCD equipment (Flowrox Oy, Finland) (Fig. 2) consists of reactor with 40 L storage tank, pulse generator, and circulation pump (Iwaki Co. Ltd., Japan). The air-filled plasma reactor consists of horizontal high voltage electrodes of 0.55 mm in diameter and total length of 20 m concluded between two grounded vertical parallel plates with the distance from the wire electrode to the grounded plate of 19 mm. The generator applies high voltage pulses to electrodes with the repetition frequencies of 200 and 880 pulses per second (pps) providing output powers of 32 and 123 W, respectively. The 10-L solution samples were treated while circulating in the PCD reactor with a flow rate of $1.0 \text{ m}^3 \text{ h}^{-1}$. Solutions were pumped to the distribution box at the top of reactor and dispersed to the discharge zone through a perforated plate with 51 holes with a diameter of 1 mm. The experiment started once the pulse generator was turned on. For sampling, the latter was turned off and the treated solution was allowed to circulate for four minutes for equalizing the content. The procedure was repeated for each sample collected at incremental time intervals, i.e., at received pulsed energy doses. In PCD/ H_2O_2 experiments, hydrogen peroxide was added into the storage tank filled with the solution before the start of treatment. The setup was ventilated for oxygen replenishment in PCD reactor at 2.0 L min^{-1} using an air compressor.

The energy efficiency of NDEA oxidation E , $\text{g kW}^{-1} \text{ h}^{-1}$, was

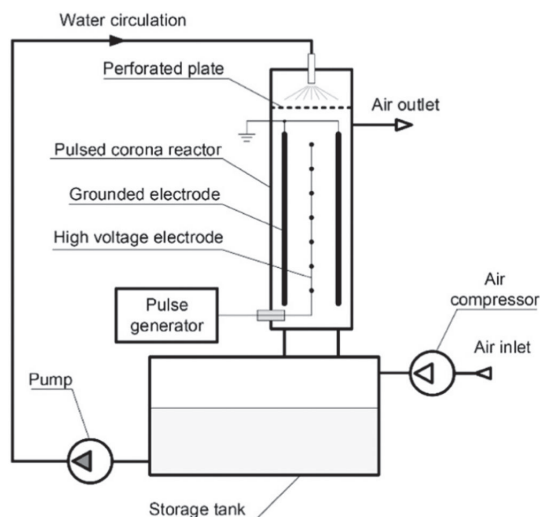


Fig. 2. Schematic outline of PCD equipment.

calculated using Eq. 6:

$$E = \frac{\Delta C \cdot V}{W} \quad (6)$$

where ΔC is the decrease of NDEA concentration, g m^{-3} , V is the volume of treated sample, m^3 , and W is the energy consumption derived as a product of applied pulsed power and treatment time, kWh. Energy efficiency calculations were made for 50% decrease in NDEA concentration.

2.4. Analyses

Concentration of aqueous NDEA was determined using 9300 HPLC System high-performance liquid chromatograph (YL Instrument) equipped with a Waters XBridge C18 column (130 Å, 150 mm×3.0 mm inner diameter, 3.5 µm particle size) and UV/Vis detector. The flow rate 0.2 mL min^{-1} and sample run time 13 min were applied. Isocratic elution was applied using 80% of eluent A - 0.1% CH_3COOH in ultrapure water, and 20% of eluent B - acetonitrile. Measurements were duplicated showing deviation of results smaller than 5%.

Measurements of (i) aqueous O_3 concentration using indigo method at wavelength 600 nm, (ii) concentration of H_2O_2 formed in PCD treatment using titanyl sulphate method at 410 nm [24], and (iii) concentration of Fe^{2+} determined by o-phenanthroline method at 410 nm [25] were performed by means of Helios UV-Vis spectrophotometer (Thermo Electron Corporation, USA). pH and conductivity were measured using accordingly S220 digital pH-meter (Mettler Toledo, Switzerland) and multiparameter meter HQ430d (Hach Company, USA). The residual O_3 concentration in the exhaust air of PCD and ozonation was measured using ozone monitors (Anseros Klaus Nonnenmacher GmbH, Germany and PCI-WEDECO Environmental Technologies, Inc., USA).

3. Results and discussion

3.1. Ozonation and PCD-oxidation of NDEA assisted with H_2O_2

Ozone possessing the redox potential of 2.07 V slowly reacts directly with NDEA (Fig. 3). Even the reactivity of HO-radical (2.80 V) with the N-nitroso group was reported to be low [26] making the oxidation rate

determined by unselective HO-radicals reacting with other functional groups in the NDEA molecule [27,28].

Relatively low NDEA degradation efficiency in ozonation at neutral pH was substantially improved with addition of H_2O_2 explained by accelerated decomposition of O_3 into non-selective HO-radicals (Eq. 2). Fig. 3 demonstrates spectacular impact of H_2O_2 addition on NDEA oxidation rate.

The increased gaseous O_3 concentration resulted in expectedly higher NDEA degradation rates in both ozonation and $\text{O}_3/\text{H}_2\text{O}_2$ processes. Doubled ozone concentration resulted in approximately twofold faster decomposition of NDEA in ozonation, showing even stronger effect in $\text{O}_3/\text{H}_2\text{O}_2$ oxidation (Fig. 3).

Oxidation of NDEA improved with H_2O_2 addition was reported earlier [13]. A mixture of nine aqueous NAs dissolved at 2 mg L^{-1} of aggregate NAs' concentration including NDEA was oxidized in tap water with ozone at its gaseous inlet concentration of 2 mg L^{-1} . As a result, NDEA was removed for about 20% in 30 min of ozonation, and for 45%, i.e., roughly doubled with H_2O_2 addition. The effect of hydrogen peroxide addition observed in the present research is noticeably stronger, which may be explained by the difference in NDEA absolute concentrations.

In PCD experiments, the importance of using buffered solutions was clarified by testing PCD oxidation efficiency in conductive media: ohmic losses are known to reduce energy efficiency of oxidation in reactors of certain construction [29]. 50 mM phosphate buffer solutions for pH 7.0 possess conductivity of $7.0 \pm 0.1 \text{ mS cm}^{-1}$ at 22 °C. Oxidation of NDEA in buffered and a non-buffered solutions, however, indicated no difference in energy efficiency at complete oxidation of target compound at both pulse repetition frequencies of 880 and 200 pps used in the study (Table S1 in Supplementary material). Further discussion thus handles PCD-oxidation in non-buffered solutions at lower pulse repetition frequency of 200 pps for more accurate sampling within longer time of treatment.

Fig. 4 illustrates the results of NDEA PCD-oxidation. One can see a difference in NDEA degradation dependent on the delivered energy at various pulse rates. Such disparity refers to the role of O_3 in NDEA oxidation since longer pauses between pulses provide an extra time for O_3 transfer and reactions [17,18].

Contrary to ozonation, addition of hydrogen peroxide to the PCD-treated NDEA solutions in concentration of 50 µM resulted in no particular acceleration of the target compound oxidation regardless pH of treated solutions.

Interestingly, the degradation of NDEA consistently follows an unusual pattern undergoing stepwise oxidation along the initial slower phase with subsequent acceleration (Fig. 4). A similar phenomenon was observed by Bolobajev et al. [30], where chlorophenol was oxidized in water by H_2O_2 in the presence of insoluble ferric oxyhydroxide. Iron

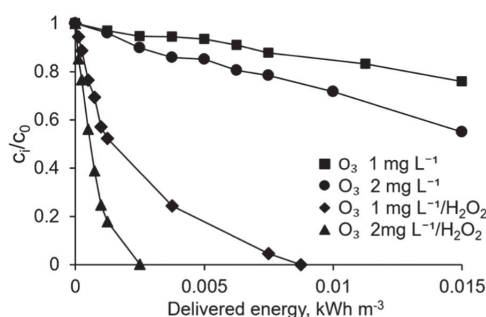


Fig. 3. Oxidation of NDEA dependent on delivered energy with ozone and $\text{O}_3/\text{H}_2\text{O}_2$ at inlet gaseous O_3 concentrations of 1 and 2 mg L^{-1} ; $[\text{NDEA}]_0 = 10 \text{ µM}$, $[\text{H}_2\text{O}_2]_0 = 50 \text{ µM}$, pH = 7.

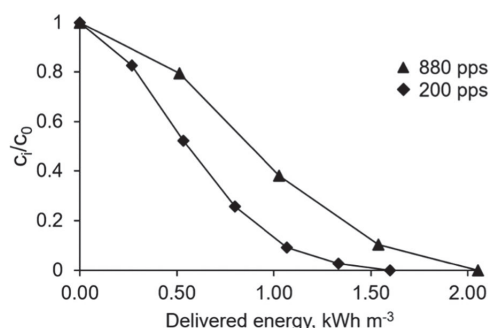


Fig. 4. NDEA PCD-oxidation dependent on delivered energy at pulse repetition frequencies of 200 and 880 pps. $[NDEA]_0 = 10 \mu M$, $pH = 7$.

leaching took place initiating the stagewise oxidation of chlorophenol induced by Fenton-like process.

In the present study, the credible Fenton reactions may occur due to the presence of Fe^{2+} at concentrations growing on course of oxidation originated, presumably but exclusively, from the contact of treated solution with stainless steel walls of the reactor, and growing concentrations of H_2O_2 (Fig. 5). Both admixtures were quantified in the NDEA solutions in the course of PCD treatment.

H_2O_2 most probably was generated in PCD through recombination of HO-radicals (Eq. 7) observed in a different type of electric discharge [31]. This hypothesis is indirectly confirmed by the higher pulse repetition frequency ensuring higher concentrations of H_2O_2 (Fig. 5). Formation of hydrogen peroxide was observed in both PCD- and PCD/ H_2O_2 -treated NDEA solution at approximately equal rates of growth. As iron leaching process is dependent on pH of the solution, the concentration of iron was measured at pH 3.0, 7.0, and 12.0 only at 200 pps.



Co-existent ferrous ions and H_2O_2 in NDEA solutions may lead to the accelerated oxidation of substrate induced by Fenton reaction (Fig. 4). Since no difference in oxidation rates was observed in PCD and PCD/ H_2O_2 treatment differing in H_2O_2 content about twofold, one can make a conclusion about the Fe^{2+} -ions concentration limiting the rate of Fenton oxidation. Possible acceleration of PCD oxidation with addition of ferrous ions deserves further studies.

Residual ozone formed in PCD and present in outlet stream of ventilation air was quantified in NDEA oxidation experiments at pH 3.0, 7.0, and 12.0 reaching the highest of $0.728 \text{ mg O}_3 \text{ L}^{-1}$ in acidic and neutral solutions and $0.663 \text{ mg O}_3 \text{ L}^{-1}$ in alkaline. Lower concentrations of residual gaseous ozone at high pH is addressed to the enhanced

decomposition of O_3 in alkaline solutions. That low concentrations of residual O_3 , however, are easily eliminated in photocatalytic reactors [32].

3.2. pH impact on NDEA ozonation and PCD treatment

Ozonation is sensitive towards pH for ozone decomposition forming HO-radicals via slow reaction with hydroxyl ion [33]. Acidic medium thus favors direct reactions between molecular ozone and pollutants, whereas the share of indirect radical oxidation should grow with increasing pH [24]. This is consistent with the results observed for NDEA (Fig. 6), where ozone in acidic medium barely oxidized NDEA within an hour, whereas oxidation rate increased with pH demonstrating nearly complete oxidation in just 10 min at pH 12.0. The negative predicted number of NDEA pKa [34] indicates that within the experimental range of pH no influence of pH on NDEA ozonation is exhibited from the substrate properties side.

The impact of ozone gas-liquid transfer on the oxidation kinetics was tested by measuring aqueous ozone concentration in the NDEA solution-filled reactor in time of ozone delivery at pH 3.0. Fig. S in Supplementary material shows rapid saturation of the treated water with O_3 reaching an equilibrium concentration at about $250 \mu g \text{ L}^{-1}$ in less than 1 min. This indicates the mass transfer in the reactor proceeding faster than oxidation reaction making the latter control the process rate.

Contrary to ozonation, NDEA PCD-degradation is less dependent on pH of treated solution showing the reverse tendency in the dependence itself. Oxidation of NDEA proceeded twofold faster in acidic media than in alkaline – complete oxidation at pH 3.0 was observed in 20 min and at pH 12.0 in 45 min corresponding to the delivered energy doses of 1.07 and 2.40 kWh m^{-3} , respectively (Fig. 7). Although higher redox potential of HO-radical in acidic medium [35] and the absence of

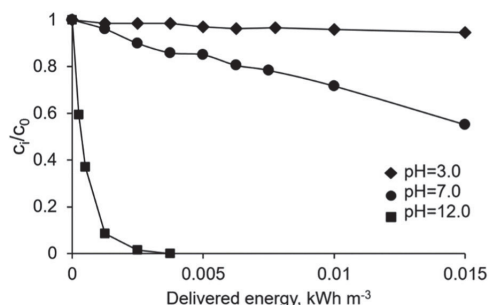


Fig. 6. pH effect on NDEA oxidation with ozone dependent on delivered energy: inlet O_3 concentration 2 mg L^{-1} , $[NDEA]_0 = 10 \mu M$.

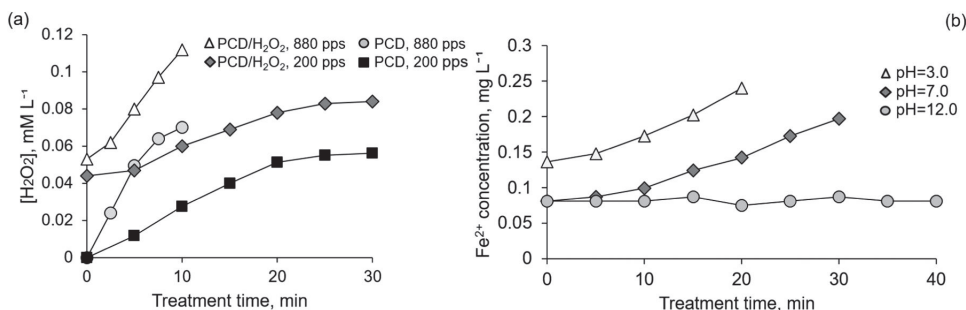


Fig. 5. Formation of H_2O_2 dependent on pulse repetition frequency (a) and Fe^{2+} at 200 pps (b) in PCD-treated NDEA solutions with and without addition of H_2O_2 : $[NDEA]_0 = 10 \mu M$, $pH = 7.0$, $[H_2O_2]_0 = 50 \mu M$.

radical-scavenging bicarbonates may explain the tendency, the surface character of HO-radical attack explains efficient oxidation in acidic medium. Besides, with an exception of pH 12.0, oxidation of NDEA, slower at the beginning of treatment, proceeds with acceleration referring to the abovementioned Fenton oxidation (Fig. 4). pH plays an important role in the Fenton process providing the highest oxidation efficacy in acidic media [36]. Acidic media also provides a faster iron leaching from the surface of equipment (Fig. 5). Thus, contrary to ozonation, alkaline conditions obstruct the Fenton reaction and less inflection if any in the NDEA degradation curves is seen at pH 12.0 (Fig. 7). As a result, higher growing concentrations of Fe^{2+} were observed in acidic solutions followed by the ones in neutral media. In alkaline conditions, the concentration of Fe^{2+} remained constantly low at around 0.08 mg L^{-1} throughout the treatment (Fig. 5). The presence of ferrous ions in small but growing concentrations in acidic and neutral media is explained by the Fenton cyclic reaction maintaining both ferrous and ferric ions in the solution. Smaller concentration of ferrous ions in alkaline medium is due to ferric iron partly precipitating in its insoluble hydroxide form thus interrupting the Fenton cycle [37].

As mentioned above, NDEA solutions treated with PCD were not buffered. pH of acidic and alkaline solutions remained practically unchanged throughout the treatment, while in neutral solutions pH decreased from 7 ± 0.1 – 4.2 ± 0.4 within half an hour. This, however, had no impact since, as noticed earlier, the difference between buffered at pH 7.0 and non-buffered solutions treatment was experimentally found insignificant. The latter may be due to minor pH change, down to 6.0 ± 0.2 within the first 15 min of treatment when NDEA oxidation was accomplished.

3.3. NDEA oxidation energy efficiency

The results of energy efficiency calculations for ozonation, $\text{O}_3/\text{H}_2\text{O}_2$, and PCD treatment are brought together in Fig. 8. Table S1 in Supplementary material depicts energy efficiencies of NDEA oxidation of all studied processes including PCD-oxidation conducted with H_2O_2 additions and in buffered solutions. The calculations were made at 50% of NDEA degradation.

The highest oxidation energy efficiency of $1.10 \text{ g kW}^{-1}\text{h}^{-1}$ was observed in ozonation at pH 12.0 and gaseous ozone concentration of 2 mg L^{-1} followed by the $\text{O}_3/\text{H}_2\text{O}_2$ oxidation at pH 7 with the efficiency of $0.87 \text{ g kW}^{-1}\text{h}^{-1}$. Ozone-based oxidation at other experimental conditions was significantly less effective. At pH 3.0, the ozonation efficiency was negligible if any (see Fig. 6).

The highest energy efficiency of 1.42 g kWh^{-1} by PCD treatment was observed at a pulse frequency of 200 pps at pH 3.0. At neutral pH of natural water, the comparison of NDEA ozonation with PCD at 200 pps showed a remarkable difference: PCD efficiency of $1.01 \text{ g kW}^{-1}\text{h}^{-1}$ exceeds $0.034 \text{ g kW}^{-1}\text{h}^{-1}$ of ozonation by at least an order of magnitude

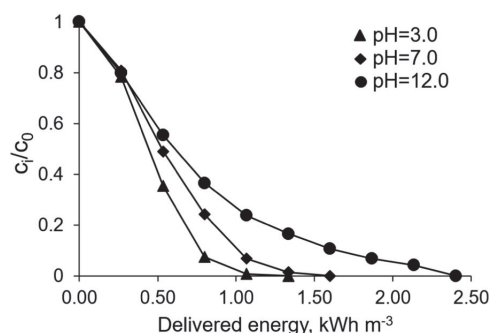


Fig. 7. NDEA PCD-oxidation in delivered energy dependent on pH: pulse repetition frequency 200 pps, $[\text{NDEA}]_0 = 10 \text{ }\mu\text{M}$.

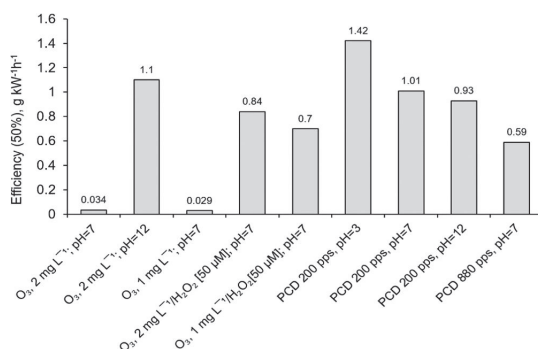


Fig. 8. Comparison of energy efficiency results for ozonation, $\text{O}_3/\text{H}_2\text{O}_2$, and PCD treatment.

(Fig. 8). Addition of hydrogen peroxide assisting ozonation in neutral medium substantially improved oxidation efficiency providing $0.84 \text{ g kW}^{-1}\text{h}^{-1}$ still yielding 20% to PCD under similar conditions at 200 pps.

4. Conclusions

Advanced oxidation involving HO-radicals appears feasible in removal of toxic water disinfection by-product – N-nitrosodiethylamine: the target pollutant is oxidized mainly with HO-radical comprising a basic oxidant in ozonation of alkaline solutions and hydrogen peroxide-assisted ozonation. Predominant character of HO-radical as an oxidant was also seen in treatment with gas-phase pulsed corona discharge plasma confirmed by moderate difference in oxidation at various pulse repetition frequencies. A comparative study clarified the energy efficiency advantage of chemical-free PCD over ozonation in all studied combinations.

At neutral pH, PCD surpasses ozonation in energy efficiency by at least an order of magnitude. The $\text{O}_3/\text{H}_2\text{O}_2$ combination, although being substantially more effective than unassisted ozonation, still yields to PCD in efficiency for 20%.

Fenton reaction was detected spontaneously developing in PCD: both Fe^{2+} and H_2O_2 were quantified in concentrations growing with treatment time and pulse repetition frequency thus increasing the overall NDEA oxidation rate on the way of treatment. Addition of H_2O_2 to the PCD-treated NDEA solutions, however, did not result in an increased oxidation rate indicating (i) Fe^{2+} concentration limiting the reaction kinetics and (ii) inability of PCD to activate H_2O_2 .

CRedit authorship contribution statement

Maarja Kask: Conceptualization, Methodology, Investigation, Formal analysis, Writing - original Draft, Visualization. **Marina Krichevskaya:** Conceptualization, Writing - review & editing, Supervision. **Sergei Preis:** Conceptualization, Writing - review & editing, Funding acquisition. **Juri Bolobajev:** Conceptualization, Methodology, Visualization, Writing - review & editing, Supervision.

Declaration of Competing Interest

The authors declare that they have no known competing financial interests or personal relationships that could have appeared to influence the work reported in this paper.

Acknowledgement

This work was supported by the Institutional Development Program

of Tallinn University of Technology for 2016–2022, project 2014-2020.4.01.16-0032 from the EU Regional Development Fund, and the Research Group Support project PRG776 of Estonian Research Council.

Appendix A. Supporting information

Supplementary data associated with this article can be found in the online version at doi:10.1016/j.jece.2021.105102.

References

- [1] C. Zhou, N. Gao, Y. Deng, W. Chu, W. Rong, S. Zhou, Factors affecting ultraviolet irradiation/hydrogen peroxide (UV/H₂O₂) degradation of mixed N-nitrosamines in water, *J. Hazard. Mater.* 231–232 (2012) 43–48, <https://doi.org/10.1016/j.jhazmat.2012.06.032>.
- [2] B. Xu, Z. Chen, F. Qi, J. Ma, F. Wu, Comparison of N-nitrosodiethylamine degradation in water by UV irradiation and UV/O₃: Efficiency, product and mechanism, *J. Hazard. Mater.* 179 (2010) 976–982, <https://doi.org/10.1016/j.jhazmat.2010.03.100>.
- [3] S.A. Mazari, P. Alaba, I.M. Saeed, Formation and elimination of nitrosamines and nitramines in freshwaters involved in post-combustion carbon capture process, *J. Environ. Chem. Eng.* 7 (2019), 103111, <https://doi.org/10.1016/j.jece.2019.103111>.
- [4] California State Water Resources Control Board, (https://www.waterboards.ca.gov/drinking_water/certific/drinkingwater/NDMA.html). Last access: Nov 08, 2020.
- [5] L. Sørensen, K. Zahlsen, A. Hyldebakk, E.F. da Silva, A.M. Booth, Photodegradation in natural waters of nitrosamines and nitramines derived from CO₂ capture plant operation, *Int. J. Greenh. Gas Control* 32 (2015) 106–114, <https://doi.org/10.1016/j.jggc.2014.11.004>.
- [6] L. Padhye, P. Wang, T. Karanfil, C.H. Huang, Unexpected role of activated carbon in promoting transformation of secondary amines to N-nitrosamines, *Environ. Sci. Technol.* 44 (2010) 4161–4168, <https://doi.org/10.1021/es903916t>.
- [7] N. Gao, Y. Deng, D. Zhao, Ametryn degradation in the ultraviolet (UV) irradiation/hydrogen peroxide (H₂O₂) treatment, *J. Hazard. Mater.* 164 (2009) 640–645, <https://doi.org/10.1016/j.jhazmat.2008.08.038>.
- [8] K. Hiramoto, Y. Ryuno, K. Kikugawa, Decomposition of N-nitrosamines, and concomitant release of nitric oxide by Fenton reagent under physiological conditions, *Mutat. Res. Genet. Toxicol. Environ. Mutagen.* 520 (2002) 103–111, [https://doi.org/10.1016/S1383-5718\(02\)00168-7](https://doi.org/10.1016/S1383-5718(02)00168-7).
- [9] H. Wang, J. Zhay, W. Yao, B. Wang, S. Deng, J. Huang, G. Yu, Y. Wang, Comparison of pharmaceutical abatement in various water matrices by conventional ozonation, peroxide (O₂/H₂O₂), and an electro-peroxide process, *Water Res.* 130 (2018) 127–138, <https://doi.org/10.1016/j.watres.2017.11.054>.
- [10] M. Bourgin, E. Borowska, J. Helbing, J. Hollender, H.-P. Kaiser, C. Kienle, C. S. McArdell, E. Simon, U. von Gunten, Effect of operational and water quality parameters on conventional ozonation and the advanced oxidation process O₃/H₂O₂: kinetics of micropollutant abatement, transformation product and bromate formation in a surface water, *Water Res.* 122 (2017) 234–245, <https://doi.org/10.1016/j.watres.2017.05.018>.
- [11] J. Restivo, C.A. Orge, A.S. Guedes Gorito dos Santos, O.S. Gonçalves Pinto Soares, M.F. Ribeiro Pereira, Influence of preparation methods on the activity of macro-structured ball-milled MWCNT catalysts in the ozonation of organic pollutants (in press), *J. Environ. Chem. Eng.* (2020), 104578, <https://doi.org/10.1016/j.jece.2020.104578>.
- [12] C. Gottschalk, J.A. Libra, A. Saupe, *Ozonation of Water and Waste Water: A Practical Guide to Understanding Ozone and its Applications*, second ed., Wiley, New Jersey, 2009, pp. 267–343.
- [13] Z. Zhang, Q. Zhao, H. Song, J. Zhang, L. Wang, J. Qi, Y. Liu, J. Ma, Comparative study about oxidation of trace N-nitrosamines by seven oxidation processes with a sensitivity improved determination method, *Sep. Purif. Technol.* 236 (2020), 116009, <https://doi.org/10.1016/j.seppur.2019.116009>.
- [14] M. Krichevskaya, D. Klauson, E. Portjanskaja, S. Preis, The cost evaluation of advanced oxidation processes in laboratory and pilot-scale experiments, *Ozone Sci. Eng.* 33 (2011) 211–223, <https://doi.org/10.1080/01919512.2011.554141>.
- [15] M. Schneider, R. Rataj, J.F. Kolb, L. Bláha, Cy lindropermopsin is effectively degraded in water by pulsed corona-like and dielectric barrier discharges, *Environ. Pollut.* 266 (2020), 115423, <https://doi.org/10.1016/j.envpol.2020.115423>.
- [16] V. Scholtz, J. Pazlarova, H. Souskova, J. Khun, J. Julak, Nonthermal plasma – a tool for decontamination and disinfection, *Biotechnol. Adv.* 33 (2015) 1108–1119, <https://doi.org/10.1016/j.biotechadv.2015.01.002>.
- [17] I. Panorel, I. Kornev, H. Hatakka, S. Preis, Pulsed corona discharge for degradation of aqueous humic substances, *Water Supply* 11 (2011) 238–245, <https://doi.org/10.2166/ws.2011.045>.
- [18] S. Preis, I.C. Panoral, I. Kornev, H. Hatakka, J. Kallas, Pulsed corona discharge: the role of ozone and hydroxyl radical in aqueous pollutants oxidation, *Water Sci. Technol.* 68 (2013) 1536–1542, <https://doi.org/10.2166/wst.2013.399>.
- [19] P. Ajo, I. Kornev, S. Preis, Pulsed corona discharge induced hydroxyl radical transfer through the gas-liquid interface, *Sci. Rep.* 7 (2017), 16152, <https://doi.org/10.1021/acs.iecr.5b01915>.
- [20] H.N. Po, N.M. Senozan, The Henderson-Hasselbalch equation: its history and limitations, *J. Chem. Educ.* 78 (2001) 1499–1503, <https://doi.org/10.1021/ed078p1499>.
- [21] NCBI, PubChem Compound Summary for CID 5921, N-Nitrosodiethylamine. <https://pubchem.ncbi.nlm.nih.gov/compound/N-Nitrosodiethylamine>. Last access: Nov 11, 2020.
- [22] E.W. Rice, R.B. Baird, A.D. Eaton, *Standard Methods for The Examination of Water and Wastewater*, twenty third ed., APHA, AWWA, WEF, Washington, D.C., 2017 <https://doi.org/10.1016/j.cj.2020.125815>.
- [23] I.A. Katsoyiannis, S. Canonica, U. von Gunten, Efficiency and energy requirements for the transformation of organic micropollutants by ozone, O₃/H₂O₂ and UV/H₂O₂, *Water Res.* 45 (2011) 3811–3822, <https://doi.org/10.1016/j.watres.2011.04.038>.
- [24] B. Kasprzyk-Hordern, M. Ziółek, J. Nawrocki, Catalytic ozonation and methods of enhancing molecular ozone reactions in water treatment, *Appl. Catal. B Environ.* 46 (2003) 639–669, [https://doi.org/10.1016/S0926-3373\(03\)00326-6](https://doi.org/10.1016/S0926-3373(03)00326-6).
- [25] E. Merck, *The Testing of Water Quality*, E. Merck, Darmstadt, Germany, 1974, p. 231.
- [26] H. Mestankova, K. Schirmer, S. Canonica, U. von Gunten, Development of mutagenicity during degradation of N-nitrosamines by advanced oxidation processes, *Water Res.* 66 (2014) 399–410, <https://doi.org/10.1016/j.watres.2014.08.012>.
- [27] N.A. Landsman, K.L. Swancutt, C.N. Bradford, C.R. Cox, J.J. Kiddle, S.P. Mezyk, Free radical chemistry of advanced oxidation process removal of nitrosamines in water, *Environ. Sci. Technol.* 41 (2007) 5818–5823, <https://doi.org/10.1021/es070275f>.
- [28] S.P. Mezyk, W.J. Cooper, K.P. Madden, D.M. Bartels, Free radical destruction of N-nitrosodimethylamine in water, *Environ. Sci. Technol.* 38 (2004) 3161–3167, <https://doi.org/10.1021/es0347742>.
- [29] I. Kornev, F. Saprykin, S. Preis, Stability and energy efficiency of pulsed corona discharge in treatment of dispersed high-conductivity aqueous solutions, *J. Electroanal. Chem.* 89 (2017) 42–50, <https://doi.org/10.1016/j.jelstat.2017.07.001>.
- [30] J. Bolobajev, M. Trapido, A. Goi, Interaction of tannic acid with ferric iron to assist 2,4,6-trichlorophenol catalytic decomposition and reuse of ferric sludge as a source of iron catalyst in Fenton-based treatment, *Appl. Catal. B Environ.* 187 (2016) 75–82, <https://doi.org/10.1016/j.apcatb.2016.01.015>.
- [31] S. Mededovic, W.C. Finney, B.R. Locke, Electrical discharges in mixtures of light and heavy water, *Plasma Process Polym.* 5 (2008) 76–83, <https://doi.org/10.1002/ppap.200700090>.
- [32] M. Kask, J. Bolobajev, M. Krichevskaya, Gas-phase photocatalytic degradation of acetone and toluene, and their mixture in the presence of ozone in continuous multi-section reactor as possible air post-treatment for exhaust from pulsed corona discharge, *Chem. Eng. J.* 399 (2020), 125815, <https://doi.org/10.1016/j.cj.2020.125815>.
- [33] J. Hoigné, H. Bader, Rate constants of reactions of ozone with organic and inorganic compounds in water II: dissociating organic compounds, *Water Res.* 17 (1983) 185–194, [https://doi.org/10.1016/0043-1354\(83\)90099-4](https://doi.org/10.1016/0043-1354(83)90099-4).
- [34] Chemical Book, N-Nitrosodiethylamine, (https://www.chemicalbook.com/ChemicalProductProperty_EN_CB8732709.htm). Last access: Jan 7, 2021.
- [35] P. Wardman, Reduction potentials of one-electron couples involving free radicals in aqueous solution, *J. Phys. Chem. Ref. Data* 18 (1989) 1637–1755, <https://doi.org/10.1063/1.555843>.
- [36] C.-M. Dai, X.-F. Zhou, Y.-L. Zhang, Y.-P. Duan, Z.-M. Qiang, T.C. Zhang, Comparative study of the degradation of carbamazepine in water by advanced oxidation processes, *Environ. Technol.* 33 (2012) 1101–1109, <https://doi.org/10.1080/09593330.2011.610359>.
- [37] W.G. Barb, J.H. Baxendale, P. George, K.R. Hargrave, Reactions of ferrous and ferric ions with hydrogen peroxide, *Trans. Faraday Soc.* 47 (1951) 591–616, <https://doi.org/10.1039/TF9514700462>.

Supplementary material for

Oxidation of aqueous N-nitrosodiethylamine: experimental comparison of pulsed corona discharge with H₂O₂-assisted ozonation

*Maarja Kask, Marina Krichevskaya, Sergei Preis, Juri Bolobajev**

Department of Materials and Environmental Technology, Tallinn University of Technology,
Ehitajate tee 5, 19086 Tallinn, Estonia

*Corresponding author: juri.bolobajev@taltech.ee

Table S1. Energy efficiencies of NDEA oxidation in PCD and ozonation

Solution	Process	Efficiency 50%, g kW ⁻¹ h ⁻¹
Buffered	O ₃ [2 mg L ⁻¹], pH=7	0.034
	O ₃ [2 mg L ⁻¹], pH=12	1.10
	O ₃ [1 mg L ⁻¹], pH=7	0.029
	O ₃ [2 mg L ⁻¹]/H ₂ O ₂ [50 μM], pH=7	0.84
	O ₃ [1 mg L ⁻¹]/H ₂ O ₂ [50 μM], pH=7	0.70
	PCD 200 pps, pH=7	0.83
	PCD 880 pps, pH=7	0.64
	PCD (200 pps)/H ₂ O ₂ [50 μM], pH=7	0.99
	PCD (880 pps)/H ₂ O ₂ [50 μM], pH=7	0.71
Non-buffered	PCD 200 pps, pH=3	1.42
	PCD 200 pps, pH=7	1.01
	PCD 200 pps, pH=12	0.93
	PCD 880 pps, pH=7	0.59
	PCD (200 pps)/H ₂ O ₂ [50 μM], pH=7	1.05
	PCD (880 pps)/H ₂ O ₂ [50 μM], pH=7	0.51

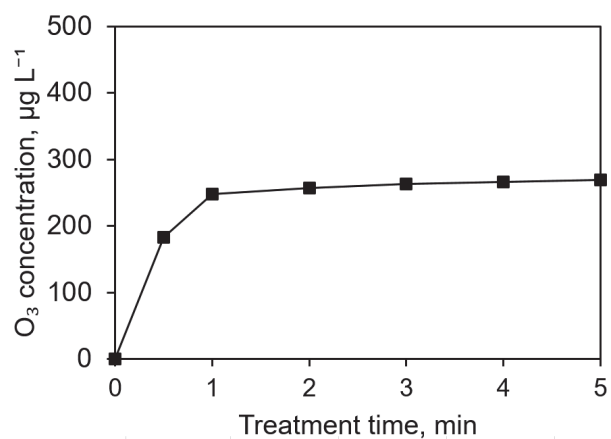


Figure S1. Accumulation of aqueous O₃ in NDEA solution bubbled with ozone-containing air: ozone inlet concentration 2 mg L⁻¹, 22 °C, pH 3.0

Appendix 2

Paper II

Kask, M.; Bolobajev, J.; Krichevskaya, M. (2020). Gas-Phase Photocatalytic Degradation of Acetone and Toluene, and their Mixture in the Presence of Ozone in Continuous Multi-Section Reactor as Possible Air Post-Treatment for Exhaust from Pulsed Corona Discharge. *Chemical Engineering Journal*, 399, #125815.



Contents lists available at ScienceDirect

Chemical Engineering Journal

journal homepage: www.elsevier.com/locate/cej

Gas-phase photocatalytic degradation of acetone and toluene, and their mixture in the presence of ozone in continuous multi-section reactor as possible air post-treatment for exhaust from pulsed corona discharge

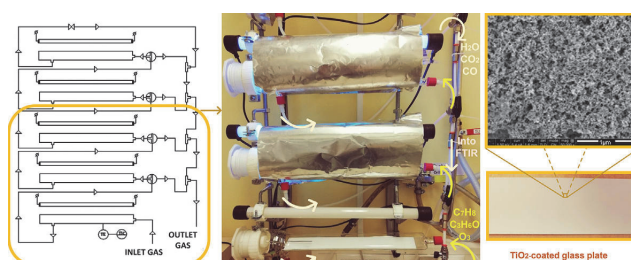
M. Kask, J. Bolobajev, M. Krichevskaya*

Department of Materials and Environmental Technology, Tallinn University of Technology, Ehitajate tee 5, 19086 Tallinn, Estonia

HIGHLIGHTS

- Modular reactor to differentiate the character of degradation of VOCs in mixtures.
- Total depletion of residual ozone from pulsed corona discharge process.
- Prevention of catalyst deactivation with toluene by-products by means of ozone.
- H_2O , CO_2 , and CO were detected as only gas-phase photocatalytic oxidation products.

GRAPHICAL ABSTRACT



ARTICLE INFO

Keywords:

Air purification
Photocatalysis
Ozone
Titanium dioxide
VOCs
Continuous reactor

ABSTRACT

Photocatalytic oxidation (PCO) of acetone and toluene, and their mixture was performed using a unique multi-section photocatalytic apparatus with adjustable catalytic surface area. Both volatile organic compounds (VOCs) were treated under the UVA irradiation and over the photocatalytic surface of P25 TiO_2 in the presence and absence of ozone at humidity levels of 6 and 40%. The presence of ozone along with the VOCs in the air simulated the exhaust from pulsed corona discharge treatment. The degradation of ozone as a toxic air pollutant in addition to the study of its effect on the PCO process performance was also monitored. The contribution of ozone to the oxidation of acetone and toluene was not observed at any inlet concentration of a single present VOC, except for higher concentration (60 ppm) of toluene as well as for mixtures, where higher conversions of acetone and toluene were obtained. The presence of ozone in the air hindered the deactivation of the catalyst by toluene oxidation by-products. Changes in relative humidity demonstrated no major effect on the oxidation of acetone and toluene either in the presence or absence of ozone, while higher humidity slightly inhibited the oxidation of VOCs in the mixture. The only PCO products observed in gas-phase were water vapour, CO_2 , and CO . The multi-section configuration of the reactor allowed obtaining prompt PCO results, characterising the degree of recalcitrance of VOCs under consideration as well as essential operating conditions including photocatalytic surface.

* Corresponding author. Tel.: +372 6202851.

E-mail address: marina.kritsevskaja@taltech.ee (M. Krichevskaya).<https://doi.org/10.1016/j.cej.2020.125815>

Received 12 February 2020; Received in revised form 28 May 2020; Accepted 5 June 2020

Available online 09 June 2020

1385-8947/ © 2020 Elsevier B.V. All rights reserved.

1. Introduction

Photocatalytic oxidation (PCO) is a promising technology to handle very low concentrations of pollutants in the air [1,2]. Moreover, it serves the possibility to conduct the process at a low flow rate as well as at room temperature and under atmospheric pressure [2,3]. The most commonly used catalyst in PCO reactors is TiO_2 due to its availability, cost-effectiveness, non-toxicity, chemical stability, and high photocatalytic activity possessing a band gap of 3.23 and 3.02 eV for anatase and rutile, respectively [4–6]. Volatile organic compounds (VOCs) are abundant hazardous air pollutants that may cause several health problems, e.g., skin, eye, nose, and throat irritation, and harm the central nervous system [1,4]. Photocatalytic decomposition of VOCs generally leads, however, to the formation of intermediates, and by-products, which amount is strongly dependent on the process operating parameters. Hence, the incomplete decomposition of VOCs in oxidation processes is one of the challenges to be faced. The formation of intermediate products of gaseous-phase acetone and toluene oxidation in the presence of P25 under the UVA-light has been widely examined [7–10]. For example, in the study of Bianchi et al. the only product detected in the decomposition of acetone was CO_2 without the formation of adsorbed by-products on the surface of the catalyst. In contrast, unreacted toluene and by-products like benzyl alcohol, benzoic acid, and benzaldehyde were identified on the surface of catalytic samples after the PCO of toluene [7].

Another advanced oxidation method applied towards VOCs abatement, such as pulsed corona discharge (PCD) plasma, also demonstrates promising potential in, for instance, oxidation of aqueous aromatic VOCs [11], although short-chain stable acetone molecules appear to be rather refractory towards airborne hydroxyl radicals [12]. The abatement of VOCs from gases by non-thermal PCD plasma is a promising technique as well as it is non-selective towards a wide range of indoor air pollutants [13,14]. One of the most commonly studied compounds are aromatic hydrocarbons (benzene, toluene) [15,16], aliphatic hydrocarbons (n-hexane) [17], alcohols (isopropyl alcohol) [18], and others. As an example, the oxidation of toluene (at the initial concentration of 500 ppm) in the air applying positive pulsed high voltages, compared to that of positive and negative direct current, has demonstrated the increase in efficiency of the treatment process as follows: $+\text{DC} < -\text{DC} < +\text{pulsed}$ [14]. Though, low concentrations of certain VOCs, including residual initial compounds, and trace amounts of ozone discharged from the setup could require post-treatment [14,15,19,20]. Jarrige and Vervisch have detected the formation of acetone as a main degradation product in the exhaust gas from $+\text{pulsed}$ corona treatment formed during the oxidation of isopropyl alcohol (500 ppm) in dry air conditions, wherein the presence of CO and CO_2 was observed as well [18]. Marotta et al., in contrast, have mainly detected CO_2 , CO, O_3 and N_2O after n-hexane (500 ppm) oxidation in dry air, however, low quantities of various VOCs were also monitored, among them acetone [17]. Thus, a combination of electric discharge treatment with downstream catalytic utilization and destruction of ozone along with degradation of VOCs presents a method of choice.

The photocatalytic reactors for the air treatment incorporate immobilised catalyst generally in the plate, annular, honeycomb or packed and fluidized bed types of constructions [21–25]; their advantages and drawbacks are discussed, for example, by Boyjoo et al. [26]. Most of the studies regarding the degradation of VOCs are carried out in batch reactors [27–29]. In the case of an examination of potentially commercialisable systems, photocatalytic reactors operating in continuous mode are under research and development. These reactors are characterised by a fixed area of the photocatalytic surface, whereas, modular reactors, where the surface covered with photocatalyst could be steadily increased by a certain increment, are useful for the testing and collection of essential data necessary for successful application of the systems operating in continuous mode. To the best of our knowledge, the reactors with changing photocatalytic surface area have not

been applied earlier for the study of photocatalytic degradation of VOCs in a continuous mode.

In the present research, the use of a multi-section photocatalytic reactor allowed to gradually increase the surface area of titanium dioxide coating along with the extension of residence time by adding the reactor sections. Such a unique photocatalytic apparatus allows specifying the required operating conditions following the degradation of initial compounds and their intermediates. The present study investigated the PCO of acetone and toluene, and their mixture under different operating conditions including the presence and absence of ozone. The total degradation of ozone in the presence of VOCs was a desired outcome along with the PCO of VOCs with the formation of zero or trace amounts of gaseous by-products. The objective of the study was to demonstrate the influence of (i) the presence of ozone in low concentrations ($100\text{--}150\text{ }\mu\text{g L}^{-1}$), (ii) concentration of acetone/toluene, (iii) residence and specific residence time (SRT, the residence time of pollutants' molecule per unit of TiO_2 -coated surface) and (iv) air humidity on the degradation of the organic pollutants using the photocatalytic apparatus with adjustable catalytic surface.

2. Experimental

The air polluted with either acetone or toluene (inlet concentration, $[\text{acetone}]_0$ or $[\text{toluene}]_0$, of 20, 40 or 60 ppm) or their mixture (inlet concentration of 20 ppm of each compound) was treated in the presence or absence of ozone on TiO_2 -coated (P25) glass plates under UVA irradiation in a continuous photocatalytic reactor.

Materials: Acetone ($\text{C}_3\text{H}_6\text{O}$, $\geq 99\%$), toluene (C_7H_8 , $\geq 99\%$), and ethanol ($\text{C}_2\text{H}_5\text{OH}$, $\geq 99\%$) were purchased from Sigma-Aldrich. P25 TiO_2 was provided by Evonik Industries.

Catalytic coating: Sonicated slurry of TiO_2 (5 wt%) in ethanol was hand-sprayed onto borosilicate glass plates using aero spray (Stanley, 150119XSTN) followed by drying at room temperature. The surface of the TiO_2 -covered glass plate, which was afterwards inserted into the reactor section, was 120 cm^2 with a TiO_2 surface density of $1.4 \pm 0.2\text{ mg cm}^{-2}$. The thickness of the photocatalytic coating measured using surface profiler TENCOR P-10 was in the range of $1\text{ }\mu\text{m}$. The surface of the catalyst was visualised by means of field emission scanning electron microscopy (FE SEM, Dual-Beam Helios Nanolab 600, FEI) (Supplementary material, Fig. S1).

Experimental procedure: UVA-emitting fluorescent lamps (Philips, Actinic T8) with the power of 15 W were placed 6 cm above each section of the reactor. The irradiance of 3.5 mW cm^{-2} was measured at a distance corresponding to the level of the surface of the catalyst by a fibre optic spectrometer (USB-2000 + UV-VIS-ES) using cosine corrector (CC-3-UV-S, field of view 180°); the measured irradiance corresponded to $1.3 \times 10^{-6}\text{ Einstein s}^{-1}$ in one section of the reactor. The internal cross-sectional dimensions and length of the reactor section are $0.9 \times 4.9\text{ cm}$ and 29.5 cm , respectively, resulting in a volume of 130 mL. The glass wall thickness is 0.2 cm. The schematic illustration of the experimental device is shown in Fig. 1. The respective amounts of the pollutants were injected through the injection port into the feed tank, which had been previously vacuumed. The gas mixture was allowed to evaporate for 20 min followed by the filling of the tank with compressed air to pressure of 3 bars and left for 90 min in order to balance the fluctuations in the concentration. Thereupon it was directed into the modular reactor using from one to five sections, where, accordingly, the outlet concentration of VOCs and ozone was followed by Fourier transform infrared spectroscopy (FTIR). For the measurements of the initial concentrations, the reactor was omitted with a gaseous mixture directed straight into the gas cell of FTIR.

The temperature in the reactor maintained by the heat of the lamp and the use of a reflector was $41 \pm 2^\circ\text{C}$, measured with a temperature controller (Omega, CN9000A). The gas flow rate was regulated employing a flow metering valve (Swagelok, SS-6MG-MM) and measured by a mass flow meter (Kobold, MAS-1009-A). Two regimes were

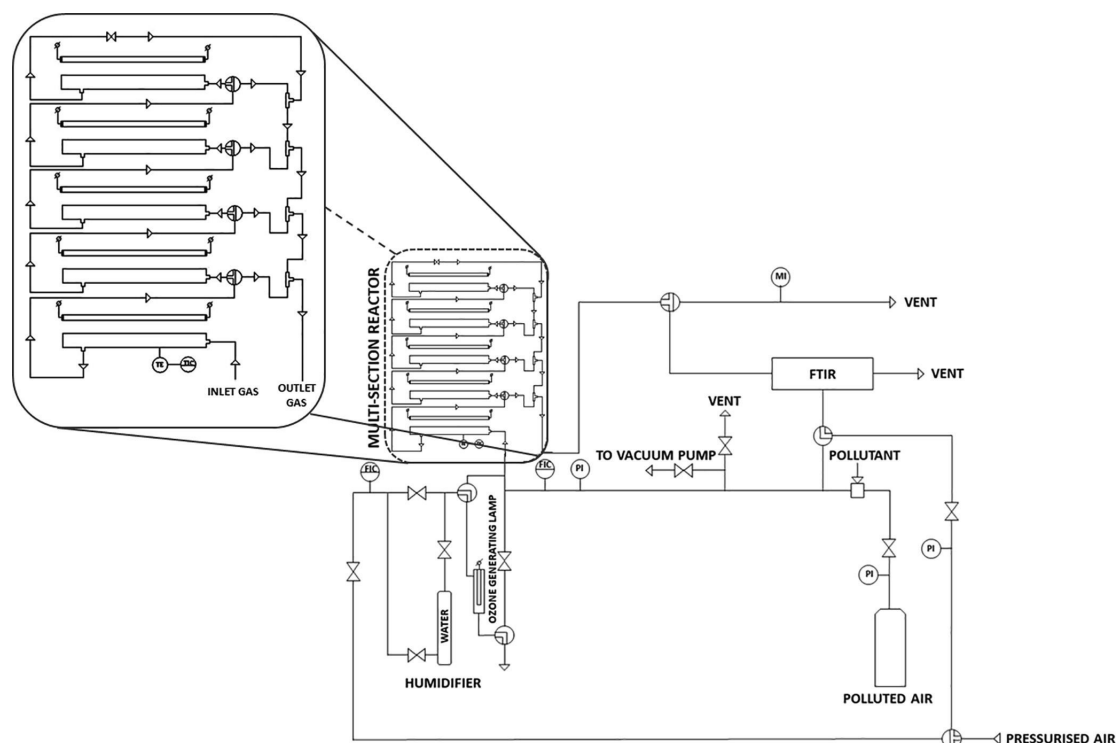


Fig. 1. Experimental device (FIC – gas flow controllers, MI – gas humidity meter, PI – manometers, TE – thermo-pair, TIC – temperature controller).

applied: flow rate of 0.5 L min^{-1} corresponding to the residence time of 16 s per section and SRT of 0.13 s cm^{-2} ; flow rate of 1 L min^{-1} corresponding to the residence time of 8 s per section and SRT of 0.065 s cm^{-2} (the following simplification was made: residence time is calculated for the ideal plug flow reactor, the residence time distribution was not taken into account). Applied ozone (inlet concentrations of 100 or $150 \pm 15 \mu\text{g L}^{-1}$ corresponding to ca. 47 or 70 ppm at an overall air flow rate of 1 and 0.5 L min^{-1} , respectively) was generated by the UVC lamp (LSE Lighting, GPH287T5VH/4) emitting at 254 and 185 nm. The relative air humidity (RH) was $6 \pm 1\%$ (1.2 g m^{-3}) or $40 \pm 5\%$ (8.2 g m^{-3}) determined at $22 \pm 1^\circ\text{C}$ by hygrometer/psychrometer (TPI, 597).

Analytical procedures: The concentration of the pollutants in outlet gas flow was followed using FTIR spectroscopy (Interspec, 200-X) with the Specac Tornado 8-m 1.33 L gas cell in the range of $500\text{--}4000 \text{ cm}^{-1}$. The spectra were collected twice after every 10 min for each required section. For quantitative analysis the peaks of acetone and toluene were measured at the IR bands $1250\text{--}1177$ and $2964\text{--}2838 \text{ cm}^{-1}$, respectively. Peak of ozone was monitored at the IR band $1100\text{--}970 \text{ cm}^{-1}$. The gaseous intermediate products observed in the study, such as carbon monoxide and formic acid, were analysed at the IR bands $2225\text{--}2050$ and $1150\text{--}1070 \text{ cm}^{-1}$, respectively. All existing peaks, except ozone, were integrated using Essential FTIR software (Operant LLC) and quantitative database (FDM, HiRes VPFTIR for Quant). The concentration of ozone was determined by means of FTIR using the colorimetric indigo method [30] for calibration. All the experiments were duplicated. The standard deviation of the results was less than 5%.

The reference experiments, i.e., adsorption and photochemical degradation were carried out. No decomposition of acetone, toluene, or ozone was observed under the UV irradiation in the absence of the catalyst. No degradation of acetone and toluene was observed in the

presence of ozone and the absence of TiO_2 catalyst coatings under studied operating conditions. Slight adsorption (less than 5%) of acetone was detected in dark conditions on TiO_2 coating, whereas no decrease in toluene and ozone concentrations was detected in the FTIR spectrum referring to the lack of adsorption.

Regeneration of the catalyst was needed after the photocatalytic treatment of the air polluted with toluene in the absence of ozone. The air containing ca. $100 \mu\text{g L}^{-1}$ of ozone passed through the UVA irradiated reactor for 30 min followed by the solitary UVA irradiation for 60 min. Otherwise, the photocatalytic surface was treated under UVA irradiation for 60 min.

The water contact angle was measured at $22 \pm 1^\circ\text{C}$ with DSA 25 (KRÜSS Instrument) applying the sessile drop fitting method.

3. Results and discussion

3.1. Photocatalytic degradation of VOCs with different inlet concentrations. Effect of ozone

The application of ozone in the photocatalytic process has been observed earlier [8,31–33]. In the present study, ozone did not possess any major effect on the degradation process, i.e., low concentrations of ozone did not promote the oxidation of acetone within the whole range of studied inlet concentrations (Fig. 2 (a); Supplementary material, Table S1).

In the case of toluene, ozone apparently influenced its oxidation at a higher inlet concentration of 60 ppm (Fig. 2(b); Supplementary material, Table S1) via accelerated degradation of adsorbed intermediates.

The probable reason for the valid effect of ozone on toluene degradation in fact is the avoidance of rapid blocking of active sites by the oxidation intermediates through their heterogeneous reactions with

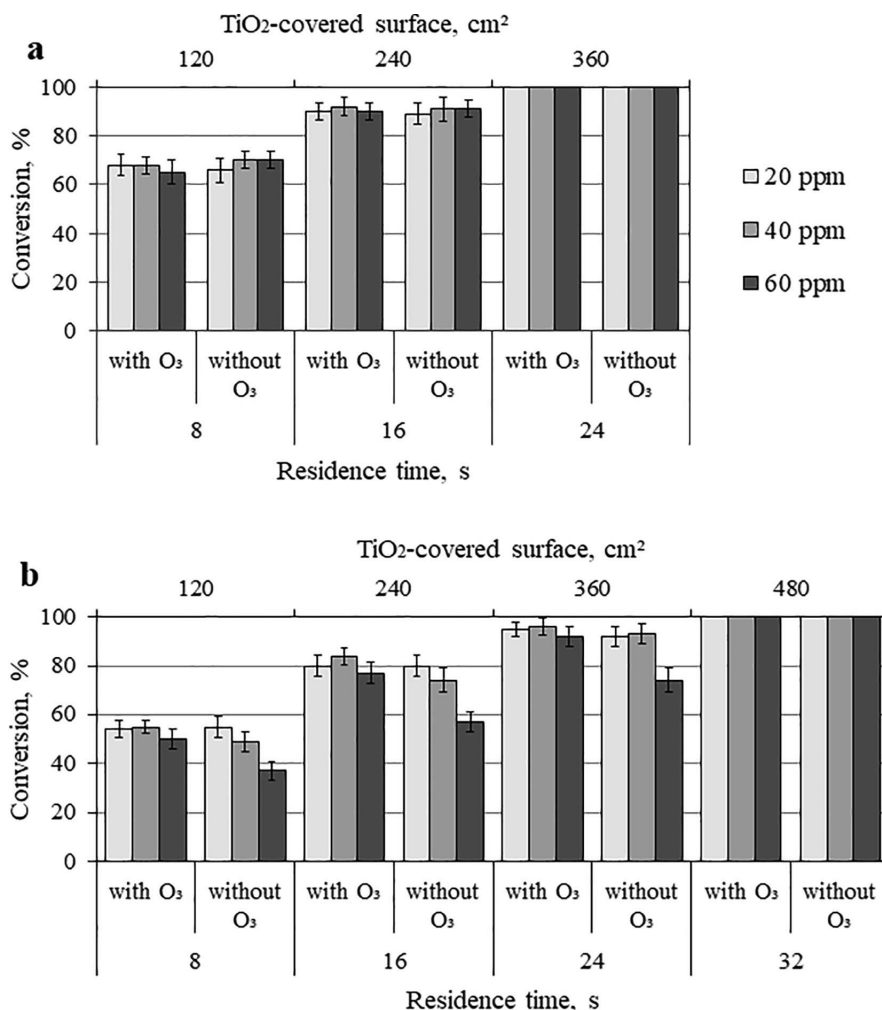


Fig. 2. Influence of acetone (a) and toluene (b) concentrations on their conversions in the presence and absence of ozone. RH 6%, SRT = 0.065 s cm⁻².

ozone. This is in accordance with catalyst's durability test, where the exposure of toluene (20 ppm, SRT of 0.065 s cm⁻², RH of 40%) over the 240 cm² of titanium dioxide coating under the UVA irradiation in the absence of ozone in 190 min of experiment time resulted in yellowish surface of the catalyst, therefore demonstrating the adsorption of by-products on the surface of the catalyst, while 90% of toluene was oxidised. Fast deactivation of the catalyst by oxidation intermediates has also been previously reported in the literature [34,35,36]. Compared to acetone, the clogging of catalyst at higher toluene inlet concentrations is, presumably, due to the aromatic ring, which oxidation, knowingly, is significantly more demanding. However, the presence of ozone (ca. 100 µg L⁻¹) led to the remarkable improvement in the durability of the catalyst under the same experimental conditions, as the colour of the surface remained unchanged along with 90% conversion of toluene.

The construction of the reactor allows emphasising explicitly "on-line" the more recalcitrant character of toluene: under the same operating conditions (SRT of 0.065 s cm⁻², RH 6%), greater catalytic surface (coated area of 480 cm²), and longer residence time (32 s) are needed to degrade toluene if compared to acetone (360 cm² and 24 s, respectively). Although in the case of acetone and toluene as model air

pollutants such a conclusion is obvious, it should be taken into account that acquisition of kinetic data in continuous flow systems is complicated in comparison to batch reactors, where a lot of data could be obtained even from one experiment. The kinetic model of decomposition of gas-phase toluene and acetone in a photocatalytic monolith and batch reactors was previously represented by Langmuir-Hinshelwood equation [37,38,39]. However, reaction mechanisms in heterogeneous photocatalysis are complex and their description using Langmuir-Hinshelwood mechanism or pseudo first-order rate constants is often inconsistent [40]. Thus, the ascertainment of empirical pollutant-specific data in the present reactor configuration, which allows to gradually increase the photocatalytic surface and follow online the pollutant degradation, is simplified.

Herein, it is noteworthy, that the following experiments were conducted at VOCs' inlet concentration of 20 ppm, the lowest concentration that allowed to follow the degradation of initial compounds applying more than one section of the reactor.

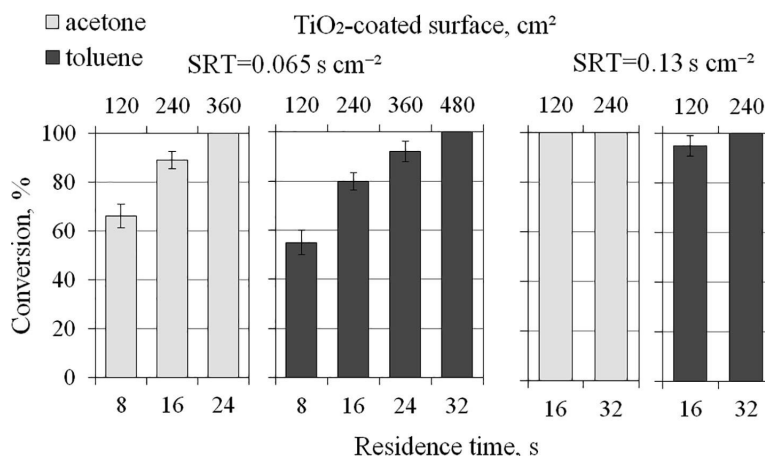


Fig. 3. Influence of residence time on acetone and toluene conversion as a single VOC in the absence of ozone. $[\text{acetone}]_0 = 20$ ppm, $[\text{toluene}]_0 = 20$ ppm, RH 6%.

3.2. Influence of residence time and air humidity on the conversion of acetone and toluene, and their mixture

Doubling the SRT enables following the conversions of VOCs at the same residence time, but at twice the lower catalyst area. For example, the TiO_2 -coated surface of 240 cm^2 is used for the operation at a residence time of 16 s and SRT of 0.065 s cm^{-2} , while at the same residence time and SRT of 0.13 s cm^{-2} photocatalytic process is operated over 120 cm^2 . Thus, the changes in process performance could be followed either by increasing the overall residence time by adding the operating reactor sections or by increasing the residence time in one section and exploring the degradation over smaller catalyst surface area.

In the present study, the increase in residence time and photocatalytic surface area amplified the process as expected: higher conversions of acetone and toluene were observed (Fig. 3; Supplementary material, Table S1). The complete oxidation of toluene was achieved at the residence time of 32 s (SRT of 0.065 and 0.13 s cm^{-2} ; coated area of 480 and 240 cm^2 , respectively), whereas no acetone in the air at the outlet of the reactor was observed at the residence time of 24 s and 16 s (SRT of 0.065 and 0.13 s cm^{-2} ; coated area of 360 and 120 cm^2 , respectively).

It could be also seen that at the same residence time of 16 s the longer specific residence time of 0.13 s cm^{-2} and thus smaller catalytic surface (coated area of 120 cm^2) resulted in higher conversions of acetone and toluene compared to the SRT of 0.065 s cm^{-2} (240 cm^2). In both cases the air flow is laminar as the calculated value of Reynolds number is 17 and 34 (at a temperature of 41°C) (Supplementary material, Eq. S1-S3 and Fig. S3) at SRT of 0.13 and 0.065 s cm^{-2} corresponding to air flow of 0.5 and 1 L min^{-1} , respectively. If two sections of the reactor are applied, the intensive mixing of air occurs as air velocity is substantially changed with the air moving through piping to the next section of the reactor. Despite the enhanced mass transfer at shorter SRT and higher photocatalytic surface area, i.e., a higher number of potentially formed active radical species, the conversion of VOCs is not facilitated, which means that surface-reaction-limited process could not be primarily assumed. Usually, first-order kinetics could be assumed, which in the case of the photocatalytic surface reaction refers to the diffusion-limited process, in which the reaching of VOCs to the surface of the catalyst is a limiting process. Nevertheless, if different adsorption patterns of the pollutants are considered (toluene is weakly adsorbed; acetone is more readily adsorbed if compared to toluene) along with the formation of intermediate products, which adsorption, degradation, and desorption interfere the process; none of the

above-mentioned kinetic models can describe in fact the overall process. This is the reason why the continuous multi-section reactor with adjustable catalytic surface area could help to receive a fast response on the “degree of recalcitrance” of the compounds to be treated.

While the initial experimental runs (Fig. 2) were conducted under dry air conditions, the relative indoor air humidity of around 40% is usually assumed comfortable, and therefore, the process performance under more humid conditions was studied as well. The increase in air humidity from 6 to 40% (in the presence or absence of ozone), however, demonstrated no major effect on the oxidation of single VOCs neither did the presence of ozone in the dry air polluted with either acetone or toluene (Supplementary material, Table S1).

As is known, hydroxyl groups are abundantly present on the surface of TiO_2 enabling the adsorption of aromatic compounds via $\text{OH}\cdots\pi$ -electron type complex or water via hydrogen bonding [41] possibly resulting in a competitive environment under different experimental conditions. The latter, water adsorption via hydrogen bonding, was likewise confirmed in the present research by the surface wettability test. The TiO_2 coating was studied by measuring the water contact angle indicating the value of 0° for an as-prepared sample, thereby demonstrating its strongly hydrophilic properties even without the UV treatment [42]. Therefore, during the oxidation of single VOC the increase in the number of precursors of radicals, such as ozone and hydroxyl anions, did not assist the degradation process, while the rise of the SRT and concentration of pollutants did augment the amount of pollutant degraded under studied conditions.

Although several previous studies have demonstrated the positive effect of higher air humidity on the degradation rate of toluene and acetone [43,44] it has been reported that an increase in humidity could also hinder the oxidation rate of toluene and acetone [36,45]. The RH of 40% compared to that of 6% inhibited the oxidation process of acetone and toluene mixture in the air (inlet concentration of both VOCs of 20 ppm) to some minor extent only at longer SRT in the absence of ozone (0.13 s cm^{-2} , 16 s, 120 cm^2) and in the presence of ozone at shorter SRT (0.065 s cm^{-2} , 8–24 s, $120\text{--}360 \text{ cm}^2$) (Fig. 4; Supplementary material, Table S1). The slightly negative effect of higher humidity in the presence of ozone at shorter SRT could be attributed to the competitive adsorption between ozone and water vapour for the active sites on the surface of the photocatalyst. At the same time, the application of ozone tends to promote the degradation of both VOCs, which is consistent with the above-mentioned assumption regarding the promotion of the oxidation of toluene as an initial compound by accelerated degradation of its intermediates. Moreover, the presence of toluene seemingly inhibited the oxidation of acetone in all

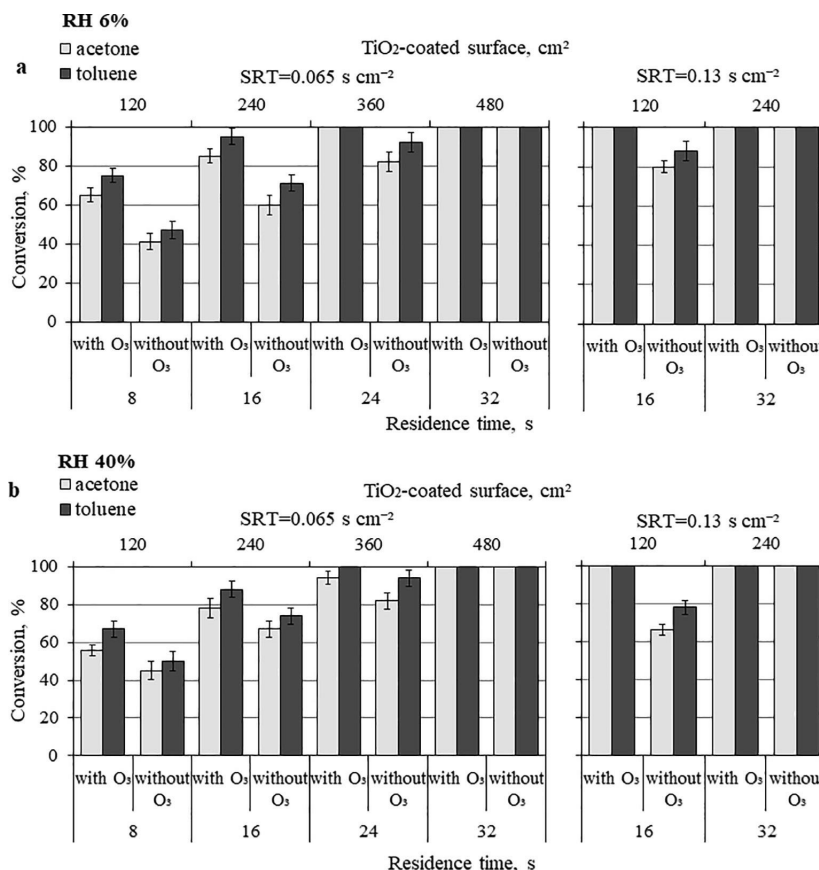


Fig. 4. Influence of residence time on acetone and toluene conversion in the mixture in the absence and presence of ozone at RH of 6 (a) and 40% (b). [acetone]₀ = 20 ppm, [toluene]₀ = 20 ppm.

conducted experiments (RH of 6 and 40%, with and without ozone, SRT of 0.065 and 0.13 s cm⁻²). The plausible explanation lies in the alteration of the adsorption-desorption equilibria, i.e., degradation intermediate products of toluene hinder the adsorption and oxidation of acetone.

The complete oxidation of the mixture of air pollutants was achieved in the absence of ozone at the residence time of 32 s (SRT of 0.065 and 0.13 s cm⁻²; coated area of 480 and 240 cm², respectively) at both humidity levels, while in the presence of ozone the complete degradation was obtained at the residence time of 24 s (360 cm²) at SRT of 0.065 s cm⁻² (except for acetone at RH of 40%) and 16 s (140 cm²) at SRT of 0.13 s cm⁻².

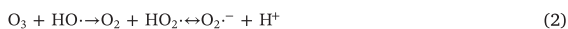
In comparison to the oxidation of single VOCs, higher conversions of toluene in the presence of ozone at SRT of 0.065 s cm⁻² and RH of 6% in the mixtures were supposedly achieved as a result of additionally formed radicals from acetone oxidation, whereas the conversion of acetone in the mixture was only to some extent lower than that of acetone alone. In the absence of ozone, the conversions of acetone in the mixtures compared to that of a single VOC were reduced due to the presence of adsorbed by-products of toluene deactivating the catalyst, while the conversions of toluene remained virtually unchanged. The degradation at SRT of 0.065 s cm⁻² and RH of 40% followed the same principle, however, somewhat lower conversions of both compounds were achieved in the presence of ozone compared to that of RH of 6%. As mentioned hereinbefore, it is apparently due to the water vapour

competitive adsorption.

3.3. Degradation of ozone

Ozone that is present in air mixture originating from environmental applications of pulsed corona discharge technology is a dual phenomenon. Firstly, it is a toxic air pollutant, which total degradation is required. Secondly, ozone is a strong oxidiser, which combination with PCO is generally expected to promote the overall process performance.

In this study, the degradation of ozone was not observed in the absence of TiO₂ coatings and under UVA irradiation at a slightly elevated temperature of about 41 °C. However, ozone was degraded in the PCO experimental runs; several possible reactions are presented below (Reactions 1–4, [46]).



The complete depletion of ozone at RH of 6% and SRT of 0.065 s cm⁻² was achieved at a residence time of 32 s (TiO₂-coated surface of 480 cm²), except for (1) presence of a higher concentration of acetone (Fig. 5; Supplementary material, Table S2) or toluene (40 and

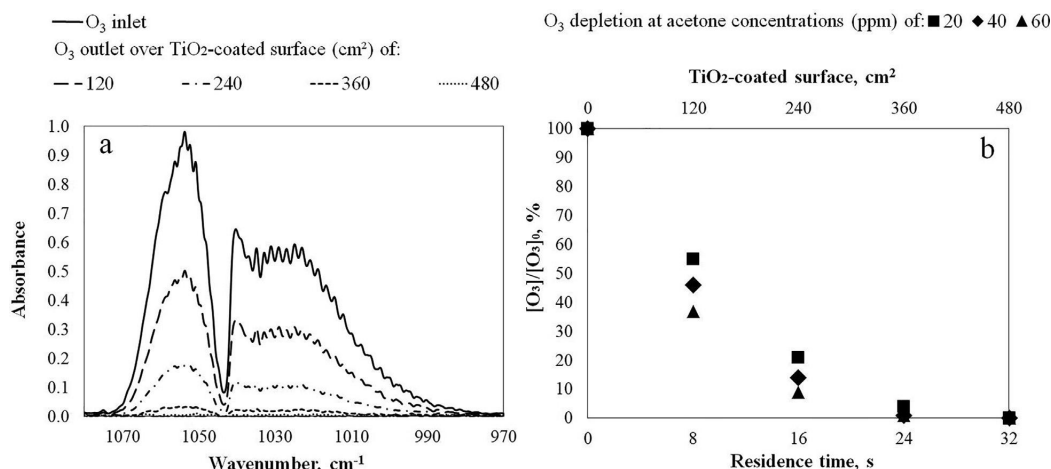


Fig. 5. Depletion of ozone over the TiO₂-covered surface up to 480 cm². A: [acetone]₀ = 20 ppm, B: [acetone]₀ = 20, 40 and 60 ppm; SRT = 0.065 s cm⁻², RH 6%.

60 ppm), or (2) presence of a mixture of VOCs (20 ppm of each contaminant) requiring residence time of 24 s (360 cm²). This is consistent with the previously established assumptions regarding the oxidative ability of ozone towards high concentrations of by-products indicating the more prompt depletion of ozone.

The increase in air humidity up to 40% in case of VOCs' inlet concentrations of 20 ppm and their mixture resulted in the need for shorter residence time (24 and 16 s corresponding to 360 and 240 cm², respectively) for the total ozone degradation compared to that of at RH of 6%. The presence of a higher concentration of water vapour favoured the depletion of ozone [46] and thus slightly lower concentrations of ozone entered the reactor.

The increase in the SRT up to 0.13 s cm⁻² at VOCs' inlet concentration of 20 ppm led to the decrease in residence time needed for total ozone degradation: from 32 to 16 s (coated area from 480 to 240 cm²) and 24 to 16 s (from 360 to 240 cm²) at RH of 6 and 40%, respectively. At longer SRT, the amount of ozone exiting the first reactor section was imperceptible, however, indicating the need for the second reactor section to be applied and resulting in an overall treatment time of ca. 32 s. Thus, under studied conditions in plug flow reactor the enhanced mass transfer, i.e., the mixing of the gas medium between the several sections of the reactor through changing gas velocity entering and exiting the tubing could favour the complete oxidation of small quantities of ozone.

For the mixture of studied compounds, the required residence time in order to degrade ozone was 8 s lower than in the case of single compounds. The necessity for a lower residence time for the depletion of ozone at SRT of 0.065 s cm⁻² is due to the overall higher concentration of organics, which is consistent with the results obtained while using higher concentrations of VOCs.

3.4. Formation of gaseous by-products during photocatalytic oxidation of VOCs

Since many studies have reported the detection of various adsorbed by-products on the surface of the catalyst [7–10], the present study focused on the detection and monitoring of gaseous intermediates and by-products, which are important from the practical point of view.

The gaseous oxidation products detected in most experiments (VOCs in the inlet from 20 to 60 ppm) were carbon dioxide (CO₂), water vapour, and carbon monoxide (CO). The latter, however, was not observed in the reactor outlet flow at acetone inlet concentration of 20 ppm in the presence and the absence of ozone, thereby confirming

the complete oxidation of acetone in the gaseous phase. Besides that, the formation of ca. 5 ppm of formic acid (HCOOH) was detected at toluene inlet concentration of 60 ppm in the presence of ozone, nevertheless, at a residence time of 32 s (SRT of 0.065 s cm⁻², 480 cm²) there were no traces of formic acid in the outlet gas flow. It is worth mentioning that in the study of Jarrige and Vervisch the presence of HCOOH was also reported in the exhaust gas from + pulsed corona treatment [18], therefore, once again, confirming the relevance of the present study since the positive effect of PCO was observed towards the degradation of HCOOH. Fig. S2 (Supplementary material) illustrates the obtained reactor inlet (VOC inlet concentration of 60 ppm) and outlet FTIR spectra of the oxidation of acetone and toluene over the TiO₂-coated surface of 240 (16 s) and 120 cm² (8 s), respectively, in the presence of ozone (RH 6%, SRT of 0.065 s cm⁻²). The formation of gaseous HCOOH in PCO of toluene and possible oxidation pathways of toluene has been reported earlier [9]. Huang and Li [8] studied ozone-enhanced PCO of toluene and proposed the potential degradation pathways for toluene by HO• (mainly formed in the UV/TiO₂, UV/O₃, O₃/TiO₂ and O₃-PCO processes) and O• (formed in the catalytic ozonation) as oxidants. The results indicated the presence of formic acid only in UV/TiO₂ and UV/O₃ processes, whereas the formation of this oxidation product was not observed in the combined O₃-PCO process. This might be attributed to the higher concentration of ozone compared to that of the present research (up to 8-fold difference) while the studied concentration of toluene was also lower (ca. 1.5-fold difference). Interestingly, in the present study, the formation of gaseous formic acid was not observed during the oxidation of toluene (60 ppm) in mere PCO, thereby giving us the basis to presume the influence of ozone on the formation of HCOOH. It could be assumed that in the absence of ozone the formed HCOOH, if any, may be adsorbed on the surface of the catalyst [14,35]. However, in the presence of ozone, a larger number of reactive oxygen species supposedly facilitate the formation of a greater amount of formic acid followed by its partial desorption into the gas-phase. Moreover, since ozone facilitates the regeneration of the photocatalytic surface, the low concentrations of ozone should presumably favour the formation of volatile low molecular intermediates while degrading the by-products adsorbed on the catalyst surface. In any case, the experimental study followed by the choice of process operating parameters should set the conditions, where gaseous by-products except water and carbon dioxide are not formed.

Regarding carbon monoxide, the formation of thereof in the VOCs' oxidation within the whole range of studied concentrations was promoted by ozone. However, in the case of acetone oxidation, rather low

levels of CO (≤ 7 ppm) were observed at higher acetone inlet concentrations (40 and 60 ppm) in the presence and absence of ozone. Besides, no CO was monitored during the PCO of acetone with an inlet concentration of 20 ppm. The PCO of toluene at higher concentration resulted in the greater amount of carbon monoxide formed: the rise in toluene inlet concentration from 20 to 60 ppm led to the formation of CO from 13 to 20 ppm in the presence of ozone and from 2 to 8 ppm in the absence of ozone. The higher CO levels produced in the presence of ozone confirm the foregoing discussion on the larger number of reactive oxygen species formed as well on the more profound oxidation of the intermediate products. In the case of the PCO of the mixture of VOCs (20 ppm of each compound), the concentrations of formed carbon monoxide were comparable or slightly higher (not exceeding 2 ppm difference) than those obtained in the PCO of toluene as a single pollutant, which is in accordance with earlier discussion. It should be also noted that no significant influence of higher water vapour content on the formation of CO during the PCO of toluene (20 ppm) was observed in the presence of ozone, whereas the formation of CO was affected by more humid conditions in the absence of ozone, resulting in higher concentrations. It is likely that greater amounts of water vapour hindered the further oxidation of carbon monoxide to carbon dioxide, which is consistent with what has been reported earlier [47]. It is worthwhile to mention that all the concentrations of CO discussed here were measured at residence times, where the total conversion of the initial pollutants was achieved.

4. Conclusions

The positive effect of ozone within the whole range of studied inlet concentrations (20–60 ppm) of a single present VOC at relative air humidity (RH) of 6% and specific residence time (SRT) of 0.065 s cm^{-2} was only observed in the case of toluene at a concentration of 60 ppm. In addition to the presence or absence of ozone, the changes in RH also did not influence the oxidation of acetone and toluene at an initial concentration of 20 ppm resulting in similar conversions, while the conversion of both compounds was enhanced at higher SRT of 0.13 s cm^{-2} . However, the application of ozone prolonged the lifetime of the photocatalyst impeding the deactivation by toluene oxidation by-products. Moreover, the total depletion of ozone was monitored throughout the study. The contribution of ozone towards VOCs oxidation was also observed with mixtures resulting in the highest conversions of acetone and toluene at SRT of 0.13 s cm^{-2} and RH of 6%. In comparison to the oxidation of single VOCs, in the mixture the presence of ozone led to higher conversions of toluene and the absence of ozone resulted in reduced conversion of acetone. An increase in RH up to 40% maintained a similar degradation pattern, however, somewhat lower conversions of both VOCs in the mixture in the presence of ozone at shorter SRT were achieved. The only PCO products observed in gas-phase were water vapour, CO_2 , and CO. The presence of ozone favoured the formation of higher concentrations of CO during the oxidation of VOCs as single pollutants and as a mixture.

The general assumption of using a unique multi-section apparatus with an adjustable TiO_2 -covered surface to study photocatalysis as a post-treatment for the exhaust from pulsed corona discharge was found to be feasible.

Declaration of Competing Interest

The authors declare that they have no known competing financial interests or personal relationships that could have appeared to influence the work reported in this paper.

Acknowledgement

This work was supported by the Institutional Development Program

of Tallinn University of Technology for 2016–2022, project 2014-2020.4.01.16-0032 from the EU Regional Development Fund, and the Research Group Support project PRG776 of Estonian Research Council. The authors would also like to thank MSc Irina Petrotsenko for her assistance with the experiments.

Appendix A. Supplementary data

Supplementary data to this article can be found online at <https://doi.org/10.1016/j.cej.2020.125815>.

References

- [1] O. Debono, F. Thevenet, P. Gravejat, V. Hequet, C. Raillard, L. Lecoq, N. Locoge, Toluene photocatalytic oxidation at ppbv levels: Kinetic investigation and carbon balance determination, *Appl. Catal. B Environ.* 106 (2011) 600–608, <https://doi.org/10.1016/j.apcatb.2011.06.021>.
- [2] N. Costarramone, B. Kartheuser, C. Pechevran, T. Pigot, S. Lacombe, Efficiency and harmfulness of air-purifying photocatalytic commercial devices: From standardized chamber tests to nanoparticles release, *Catal. Today* 252 (2015) 35–40, <https://doi.org/10.1016/j.cattod.2015.01.008>.
- [3] S. Preis, J.L. Falconer, R.D.P. Asensio, N.C. Santiago, A. Kachina, J. Kallas, Photocatalytic oxidation of gas-phase methyl tert-butyl ether and tert-butyl alcohol, *Appl. Catal. B Environ.* 64 (2006) 79–87, <https://doi.org/10.1016/j.apcatb.2005.11.002>.
- [4] J. Mo, Y. Zhang, Q. Xu, J. Joaquin, R. Zhao, Photocatalytic purification of volatile organic compounds in indoor air: A literature review, *Atmos. Environ.* 43 (2009) 2229–2246, <https://doi.org/10.1016/j.atmosenv.2009.01.034>.
- [5] W. Zhongbia, F. Dong, W. Zhao, S. Guo, Visible light induced electron transfer process over nitrogen doped TiO_2 nanocrystals prepared by oxidation of titanium nitride, *J. Hazard. Mater.* 157 (2008) 57–63, <https://doi.org/10.1016/j.jhazmat.2007.12.079>.
- [6] Y. Irokawa, T. Morikawa, K. Aoki, S. Kosaka, T. Ohwaki, Y. Taga, Photodegradation of toluene over $\text{TiO}_2 - \text{xNx}$ under visible light irradiation, *PCCP* 8 (2006) 1116–1121, <https://doi.org/10.1039/B517653K>.
- [7] C.L. Bianchi, S. Gatto, C. Pirola, A. Naldoni, A. Di Michele, G. Cerrato, V. Crocellà, V. Capucci, Photocatalytic degradation of acetone, acetaldehyde and toluene in gas-phase: Comparison between nano and micro-sized TiO_2 , *Appl. Catal. B Environ.* 146 (2014) 123–130, <https://doi.org/10.1016/j.apcatb.2013.02.047>.
- [8] H. Huang, W. Li, Destruction of toluene by ozone-enhanced photocatalysis: Performance and mechanism, *Appl. Catal. B Environ.* 102 (2011) 449–453, <https://doi.org/10.1016/j.apcatb.2010.12.025>.
- [9] J. Mo, Y. Zhang, Q. Xu, Y. Zhu, J.J. Lamson, R. Zhao, Determination and risk assessment of by-products resulting from photocatalytic oxidation of toluene, *Appl. Catal. B Environ.* 89 (2009) 570–576, <https://doi.org/10.1016/j.apcatb.2009.01.015>.
- [10] M. Sleiman, P. Conchon, C. Ferronato, J.M. Chovelon, Photocatalytic oxidation of toluene at indoor air levels (ppbv): Towards a better assessment of conversion, reaction intermediates and mineralization, *Appl. Catal. B Environ.* 86 (2009) 159–165, <https://doi.org/10.1016/j.apcatb.2008.08.003>.
- [11] I. Kornev, S. Preis, Aqueous benzene oxidation in low-temperature plasma of pulsed corona discharge, *J. Adv. Oxid. Technol.* 19 (2016) 284–289, <https://doi.org/10.1515/jaots-2016-0212>.
- [12] P. Ajo, I. Kornev, S. Preis, Pulsed corona discharge induced hydroxyl radical transfer through the gas-liquid interface, *Sci. Rep.* 7 (2017) article number 16152, <https://doi.org/10.1038/s41598-017-16333-1>.
- [13] M. Ondarts, W. Hajji, J. Outin, T. Bejat, E. Gonze, Non-Thermal Plasma for indoor air treatment: Toluene degradation in a corona discharge at ppbv levels, *Chem. Eng. Res. Des.* 118 (2017) 194–205, <https://doi.org/10.1016/j.chemd.2016.12.015>.
- [14] M. Schiorlin, E. Marotta, M. Rea, C. Paradisi, Comparison of Toluene Removal in Air at Atmospheric Conditions by Different Corona Discharges, *Environ. Sci. Technol.* 43 (2009) 9386–9392, <https://doi.org/10.1021/es9021816>.
- [15] J. Durme, J. Dewulf, W. Sysmans, C. Leys, H. Van Langenhove, Abatement and degradation pathways of toluene in indoor air by positive corona discharge, *Chemosphere* 68 (2007) 1821–1829, <https://doi.org/10.1016/j.chemosphere.2007.03.053>.
- [16] X. Fan, T. Zhu, Y. Wan, X. Yan, Effects of humidity on the plasma-catalytic removal of low-concentration BTX in air, *J. Hazard. Mater.* 80 (2010) 616–621, <https://doi.org/10.1016/j.jhazmat.2010.04.078>.
- [17] E. Marotta, A. Callea, X. Ren, M. Rea, C. Paradisi, A Mechanistic Study of Pulsed Corona Processing of Hydrocarbons in Air at Ambient Temperature and Pressure, *Int. J. Plasma Environ. Sci. Tech.* 1 (2007) 39–45, http://www.iesj.org/content/files/pdf/Volume%201,%20Number%201,%202007/7_Marotta.pdf.
- [18] J. Jarrigea, P. Vervisch, Decomposition of three volatile organic compounds by nanosecond pulsed corona discharge: Study of by-product formation and influence of high voltage pulse parameters, *J. Appl. Phys.* 99 (113303) (2006) 1–10, <https://doi.org/10.1063/1.2202700>.
- [19] S. Preis, D. Klauson, A. Gregor, Potential of electric discharge plasma methods in abatement of volatile organic compounds originating from the food industry, *J. Environ. Manage.* 114 (2013) 125–138, <https://doi.org/10.1016/j.jenvman.2012.10.042>.
- [20] W. Liang, J. Li, J. Li, Y. Jin, Abatement of toluene from gas streams via ferro-electric

- packed bed dielectric barrier discharge plasma, *J. Hazard. Mater.* 170 (2009) 633–638, <https://doi.org/10.1016/j.jhazmat.2009.05.019>.
- [21] R. Yang, Y. Zhang, Q. Xu, J. Mo, A mass transfer based method for measuring the reaction coefficients of a photocatalyst, *Atmos. Environ.* 41 (2007) 1221–1229, <https://doi.org/10.1016/j.atmosenv.2006.09.043>.
 - [22] W.A. Jacoby, D.M. Blake, R.D. Noble, C.A. Koval, Kinetics of the Oxidation of Trichloroethylene in Air via Heterogeneous Photocatalysis, *J. Catal.* 157 (1995) 87–96, <https://doi.org/10.1006/jcat.1995.1270>.
 - [23] M.M. Hossain, G.B. Raupp, S.O. Hay, T.N. Obee, Three-dimensional developing flow model for photocatalytic monolith reactors, *AIChE J.* 45 (1999) 1309–1321, <https://doi.org/10.1002/aic.690450615>.
 - [24] M. Mehrvar, W.A. Anderson, M. Moo-Young, Preliminary analysis of a tellerette packed-bed photocatalytic reactor, *Adv. Environ. Res.* 6 (2002) 411–418, [https://doi.org/10.1016/S1093-0191\(01\)00068-5](https://doi.org/10.1016/S1093-0191(01)00068-5).
 - [25] F. Chen, J.C. Zhao, H. Hidaka, Adsorption factor and photocatalytic degradation of dye-constituent aromatics on the surface of TiO₂ in the presence of phosphate anions, *Res. Chem. Intermediat.* 29 (2003) 733–748, <https://doi.org/10.1163/156856703322601744>.
 - [26] Y. Boyjoo, H. Sun, J. Liu, V.K. Pareek, S. Wang, A review on photocatalysis for air treatment: From catalyst development to reactor design, *Chem. Eng. J.* 310 (2017) 537–559, <https://doi.org/10.1016/j.cej.2016.06.090>.
 - [27] D. Wood, S. Shaw, T. Cawte, E. Shanen, B. Van Heyst, An overview of photocatalyst immobilization methods for air pollution remediation, *Chem. Eng. J.* (2019), <https://doi.org/10.1016/j.cej.2019.123490>.
 - [28] K. Vikrant, C.M. Park, K.H. Kim, S. Kumar, E.C. Jeon, Recent advancements in photocatalyst-based platforms for the destruction of gaseous benzene: Performance evaluation of different modes of photocatalytic operations and against adsorption techniques, *J. Photochem. Photobiol. C* 41 (2019), <https://doi.org/10.1016/j.jphotochemrev.2019.08.003>.
 - [29] C.H.A. Tsang, K. Li, Y. Zeng, W. Zhao, T. Zhang, Y. Zhan, R. Xie, D.Y.C. Leung, H. Huang, Titanium oxide based photocatalytic materials development and their role of in the air pollutants degradation: Overview and forecast, *Environ. Int.* 125 (2019) 200–228, <https://doi.org/10.1016/j.envint.2019.01.015>.
 - [30] L. S. Clesceri, A. E. Greenberg, R. R. Trussel, Standard Methods for the Examination of Water and Wastewater, 21st ed., APHA, AWWA, WPCF, Washington, D.C, 2005.
 - [31] B. Ohtani, S.-W. Zhang, T. Ogita, S. Nishimoto, T. Kagiya, Photoactivation of silver loaded on titanium(IV) oxide for room-temperature decomposition of ozone, *J. Photochem. Photobiol. A Chem.* 71 (1993) 195–198, <https://doi.org/10.1016/j.jphotochem.2004.05.015>.
 - [32] P. Zhang, J. Liu, Photocatalytic degradation of trace hexane in the gas phase with and without ozone addition: Kinetic study, *J. Photochem. Photobiol. A Chem.* 167 (2004) 87–94.
 - [33] M. Krichevskaya, S. Preis, A. Moiseev, N. Pronina, J. Deubener, Gas-phase photocatalytic oxidation of refractory VOCs mixtures: Through the net of process limitations, *Catal. Today* 280 (2017) 93–98, <https://doi.org/10.1016/j.cattod.2016.03.041>.
 - [34] V. Augugliaro, S. Coluccia, V. Loddo, L. Marchese, G. Martra, L. Palmisano, M. Schiavello Photocatalytic oxidation of gaseous toluene on anatase TiO₂ catalyst : mechanistic aspects and FT-IR investigation, *Appl. Catal. B Environ.* 20 (1999) 15–27, [https://doi.org/10.1016/S0926-3373\(98\)00088-5](https://doi.org/10.1016/S0926-3373(98)00088-5).
 - [35] Olga d'Hennezel, P. Pichat, D. F. Ollis, Benzene and toluene gas-phase photocatalytic degradation over H₂O and HCl pretreated TiO₂: by-products and mechanisms, *J. Photochem. Photobiol. A Chem.* 118 (1998) 197–204, [https://doi.org/10.1016/S1010-6030\(98\)00366-9](https://doi.org/10.1016/S1010-6030(98)00366-9).
 - [36] L. Cao, Z. Gao, S.L. Suib, T.N. Obee, S.O. Hay, J.D. Freihaut, Photocatalytic oxidation of toluene on nanoscale TiO₂ catalysts: Studies of deactivation and regeneration, *J. Catal.* 196 (2000) 253–261, <https://doi.org/10.1006/jcat.2000.3050>.
 - [37] M.L. Sauer, D.F. Ollis, Acetone Oxidation in a Photocatalytic Monolith Reactor, *J. Catal.* 149 (1994) 81–91, <https://doi.org/10.1006/jcat.1994.1274>.
 - [38] A. Maudhuit, C. Raillard, V. Héquet, L. Le Coq, J. Sablayrolles, L. Molins, Adsorption phenomena in photocatalytic reactions: The case of toluene, acetone and heptane, *Chem. Eng. J.* 170 (2011) 464–470, <https://doi.org/10.1016/j.cej.2011.02.040>.
 - [39] M. Le Becq, N. Kinadjian, D. Ollis, R. Backov, S. Lacombe, Comparison of kinetics of acetone, heptane and toluene photocatalytic mineralization over TiO₂ micro-fibers and Quartzel® mats, *Appl. Catal. B Environ.* 179 (2015) 78–87, <https://doi.org/10.1016/j.apcatb.2015.05.015>.
 - [40] B. Ohtani, Preparing Articles on Photocatalysis—Beyond the Illusions, Misconceptions, and Speculation, *Chem. Lett.* 37 (2008) 216–229, <https://doi.org/10.1246/cl.2008.216>.
 - [41] M. Nagao, Y. Suda, Adsorption of Benzene, Toluene, and Chlorobenzene on Titanium Dioxide, *Langmuir* 5 (1989) 42–47, <https://doi.org/10.1021/la00085a009>.
 - [42] S. Banerjee, D.D. Dionysiou, S.C. Pillai, Self-cleaning applications of TiO₂ by photo-induced hydrophilicity and photocatalysis, *Appl. Catal. B Environ.* 176–177 (2015) 396–428, <https://doi.org/10.1016/j.apcatb.2015.03.058>.
 - [43] J. Jeong, K. Sekiguchi, W. Lee, K. Sakamoto, Photodegradation of gaseous volatile organic compounds (VOCs) using TiO₂ photoirradiated by an ozone-producing UV lamp : decomposition characteristics, identification of by-products and water-soluble organic intermediates, *Photochem. Photobiol. A Chem.* 169 (2005) 279–287, <https://doi.org/10.1016/j.jphotochem.2004.07.014>.
 - [44] M. El-Maazawi, A.N. Finken, A.B. Nair, V.H. Grassian, Adsorption and photocatalytic oxidation of acetone on TiO₂: An in situ transmission FT-IR study, *J. Catal.* 191 (2000) 138–146, [https://doi.org/10.1016/0021-9517\(92\)90085-V](https://doi.org/10.1016/0021-9517(92)90085-V).
 - [45] J. Peral, D.F. Ollis, Heterogeneous photocatalytic oxidation of gas-phase organics for air purification: Acetone, 1-butanol, butyraldehyde, formaldehyde, and m-xylene oxidation, *J. Catal.* 136 (1992) 554–565.
 - [46] W.J. Masschelein, Unit Processes in Drinking Water Treatment, CRC Press, New York, 1992.
 - [47] N.K. Soliman, Factors affecting CO oxidation reaction over nanosized materials: A review, *J. Mater. Res. Technol.* 8 (2019) 2395–2407, <https://doi.org/10.1016/j.jmrt.2018.12.012>.

Supplementary material for

Gas-phase photocatalytic degradation of acetone and toluene, and their mixture in the presence of ozone in continuous multi-section reactor as possible air post-treatment for exhaust from pulsed corona discharge

M. Kask, J. Bolobajev, M. Krichevskaya

Department of Materials and Environmental Technology, Tallinn University of Technology,

Ehitajate tee 5, 19086 Tallinn, Estonia (marina.kritsevskaja@taltech.ee)

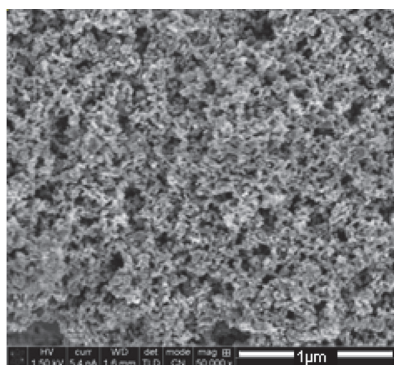


Fig. S1. SEM image of P25 TiO₂ photocatalytic coating.

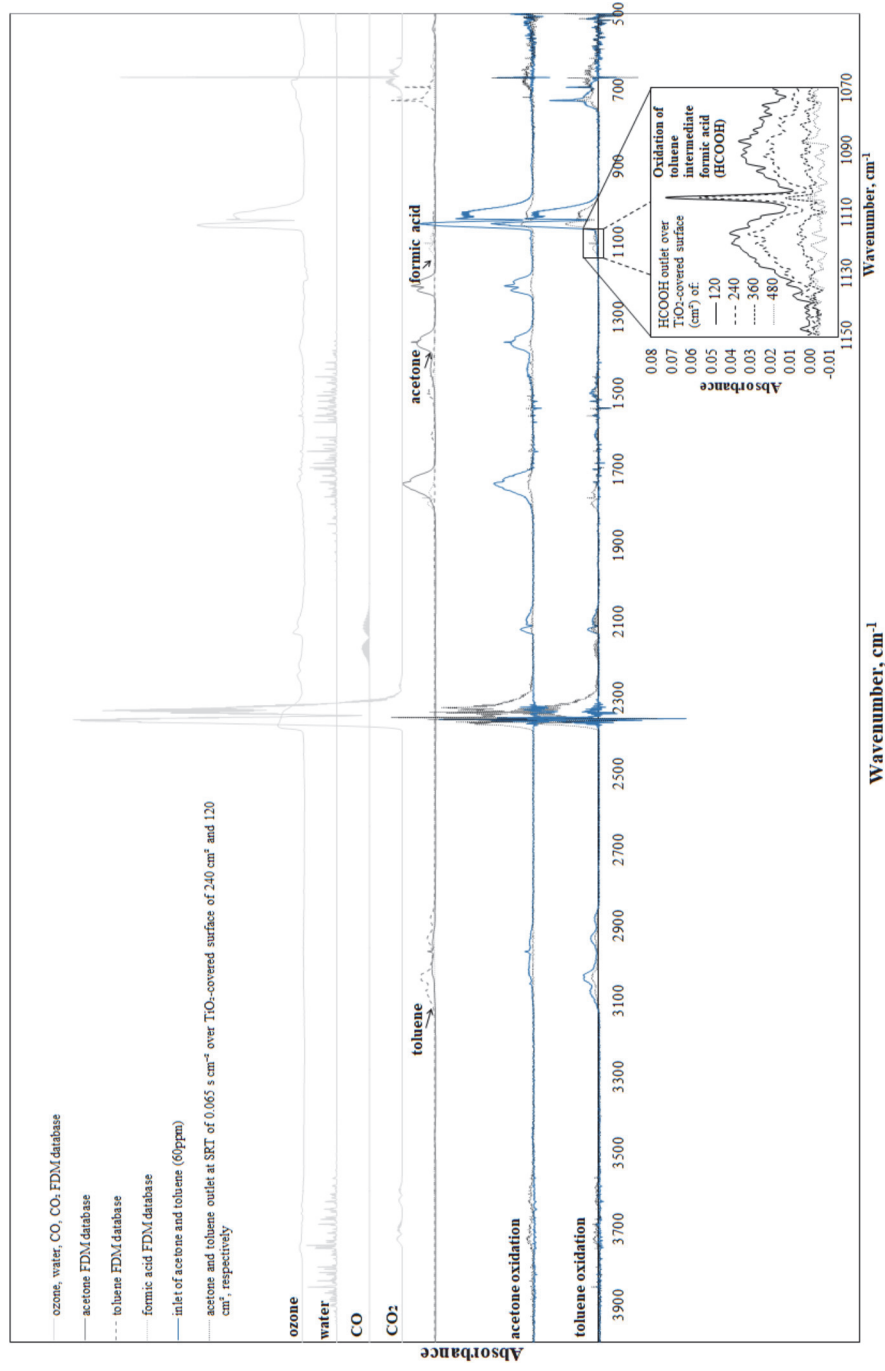


Fig. S2. Reactor inlet and outlet FTIR spectra of acetone (60ppm) and toluene (60ppm) oxidation in the presence of ozone. Decomposition of formic acid and formation of CO .

Calculations of Reynolds number

For the characterisation of the gas flow regime in the reactor section Reynolds number (Re) was calculated (Eq. S1).

$$Re = \frac{\rho \cdot V \cdot L}{\mu} \quad (S1)$$

Where: ρ – density of the fluid, kg m^{-3}

V – characteristic velocity of the flow, m s^{-1}

L – characteristic length scale of flow, m

μ – dynamic viscosity of the fluid, Pa s

Gas velocity (V) through the reactor section was calculated considering the measurements of a reactor section (4.9×0.9 cm), and gas flow rates of 0.5 and 1.0 L min^{-1} using an Eq. S2.

$$V = \frac{\text{Gas flow rate}}{\text{Internal cross-sectional area}} \quad (S2)$$

Characteristic length (L) was calculated using an Eq. S3.

$$L = \frac{4 \cdot a \cdot b}{2(a+b)} \quad (S3)$$

Where: a and b – internal cross-sectional dimensions, m

Re number for both flow rates was calculated by substituting Eq. S2 and Eq. S3 to Eq. S1, thereby using extrapolated density and dynamic viscosity values at a temperature of 41 °C [1].

$$Re_{0.5 \text{ l min}^{-1}} = \frac{1.1252 \cdot 0.019 \cdot 0.015}{1.878 \cdot 10^{-5}} = 17$$

$$Re_{1.0 \text{ l min}^{-1}} = \frac{1.1252 \cdot 0.038 \cdot 0.015}{1.878 \cdot 10^{-5}} = 34$$

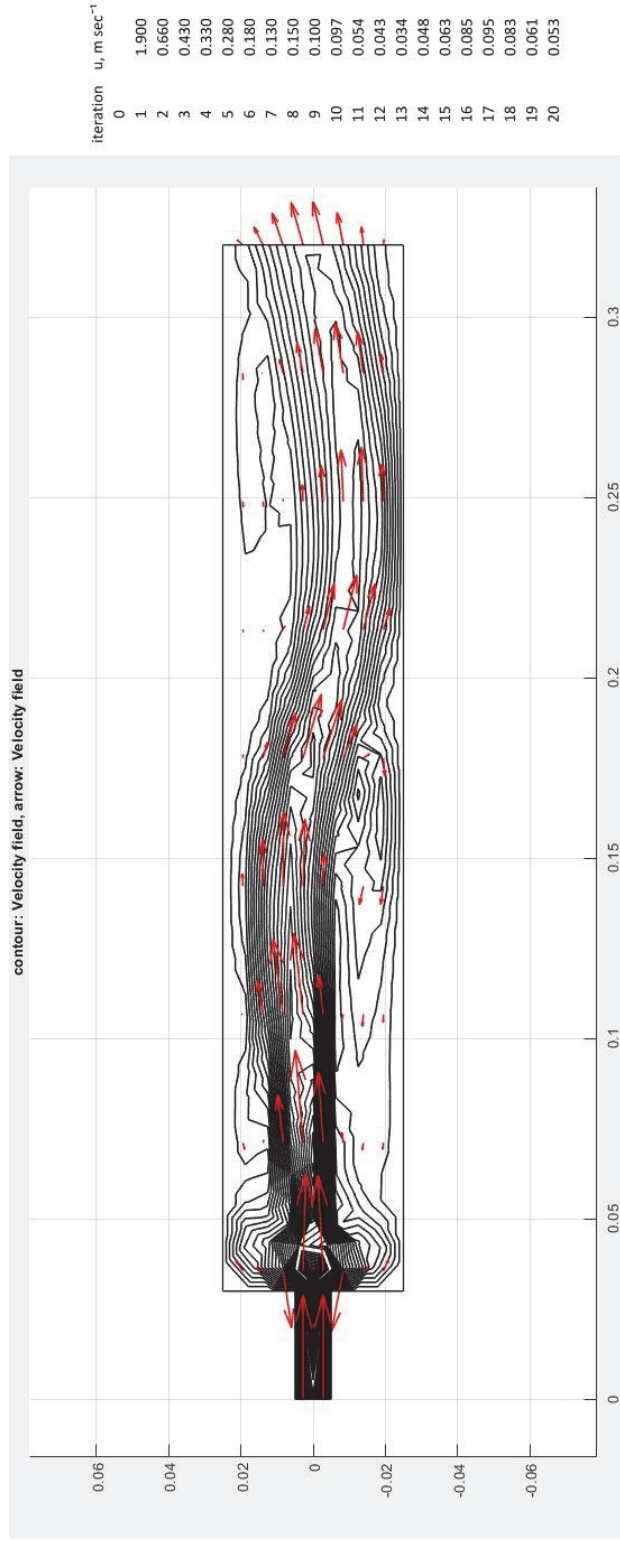


Fig. S3. Air flow streamlines simulated by two-dimensional computational fluid dynamics in a reaction section and average air velocities calculated by iterative procedure (air flow of 1 L min⁻¹; Matlab R2020a software with integrated FEATool Multiphysics).

Table S1. Conversion of acetone and toluene as a single VOC, and their mixture under different operating conditions.

Pollutant concent- ration, ppm	Relative humidity, %	Specific residence time, s cm ⁻²	Conversion after 1st reactor section (120 cm ² *), %				Conversion after 2 reactor sections (240 cm ² *), %				Conversion after 3 reactor sections (360 cm ² *), %				Conversion after 4 reactor sections (480 cm ² *), %			
			acetone with O ₃	with- out O ₃	toluene with O ₃	with- out O ₃	acetone with O ₃	with- out O ₃	toluene with O ₃	with- out O ₃	acetone with O ₃	with- out O ₃	toluene with O ₃	with- out O ₃	acetone with O ₃	with- out O ₃	toluene with O ₃	with- out O ₃
Single VOC	40	0.065 ^a	68	64	55	54	87	86	80	76	100	100	90	88	100	100	100	100
		0.13 ^b	100	100	95	94	100	100	100	100	-	-	-	-	-	-	-	-
		0.065 ^a	68	66	54	55	90	89	80	80	100	100	95	92	100	100	100	100
		0.13 ^b	100	100	100	95	100	100	100	100	-	-	-	-	-	-	-	-
Mixture	6	0.065 ^a	68	70	55	49	92	91	84	74	100	100	96	93	100	100	100	100
		0.065 ^a	65	70	50	37	90	91	77	57	100	100	92	74	100	100	100	100
		0.065 ^a	56	45	67	50	78	67	88	74	94	82	100	94	100	100	100	100
		0.13 ^b	100	66	100	78	100	100	100	100	-	-	-	-	-	-	-	-
	6	0.065 ^a	65	41	75	47	85	60	95	71	100	82	100	92	100	100	100	100
		0.13 ^b	100	80	100	88	100	100	100	100	-	-	-	-	-	-	-	-

* – TiO₂-covered surface

^a – residence time of 8 s per reactor section

^b – residence time of 16 s per reactor section

Table S2. Depletion of ozone in the presence of acetone.

Acetone concent- ration, ppm	O ₃ concent- ration, µg L ⁻¹	Relative humidity, %	Specific residence time, s cm ⁻²	[O ₃]/[O ₃] ₀ after 1st reactor section (120 cm ² *), %	[O ₃]/[O ₃] ₀ after 2 reactor sections (240 cm ² *), %	[O ₃]/[O ₃] ₀ after 3 reactor sections (360 cm ² *), %	[O ₃]/[O ₃] ₀ after 4 reactor sections (480 cm ² *), %
20	100	6	0.065 ^a	55	21	4	0
40				46	14	0	0
60				37	9	0	0

* – TiO₂-covered surface

^a – residence time of 8 s per reactor section

Supplementary references

[1] R. D. Blevins, Applied Fluid Dynamics Handbook, Van Nostrand Reinhold Co., Inc., New York, 1984.

Appendix 3

Paper III

Kask, M.; Krichevskaya, M.; Preis, S.; Bolobajev, J. (2021). Oxidation of Aqueous Toluene by Gas-Phase Pulsed Corona Discharge in Air-Water Mixtures Followed by Photocatalytic Exhaust Air Cleaning. *Catalysts*, *11*, #549.



Article

Oxidation of Aqueous Toluene by Gas-Phase Pulsed Corona Discharge in Air-Water Mixtures Followed by Photocatalytic Exhaust Air Cleaning

Maarja Kask *, Marina Krichevskaya , Sergei Preis and Juri Bolobajev *

Department of Materials and Environmental Technology, Tallinn University of Technology, Ehitajate Tee 5, 19086 Tallinn, Estonia; marina.kritsevskaja@taltech.ee (M.K.); sergei.preis@taltech.ee (S.P.)

* Correspondence: maarja.kask@taltech.ee (M.K.); juri.bolobajev@taltech.ee (J.B.)

Abstract: The treatment of wastewaters containing hazardous volatile organic compounds (VOCs) requires the simultaneous treatment of both water and air. Refractory toluene, extensively studied for its removal, provides a basis for the comparison of its abatement methods. The oxidation of aqueous toluene by gas-phase pulsed corona discharge (PCD) in combination with the subsequent photocatalytic treatment of exhaust air was studied. The PCD treatment showed unequalled energy efficiencies in aqueous and gaseous toluene oxidation, reaching, respectively, up to 10.5 and 29.6 g·kW⁻¹·h⁻¹. The PCD exhaust air contained toluene residues and ozone in concentrations not exceeding 0.1 and 0.6 mg·L⁻¹, respectively. As a result of the subsequent photocatalytic treatment, both airborne residues were eliminated within a contact time with TiO₂ as short as 12 s. The results contribute to the possible application of the studied approach in closed-loop energy-saving ventilation systems.



Citation: Kask, M.; Krichevskaya, M.; Preis, S.; Bolobajev, J. Oxidation of Aqueous Toluene by Gas-Phase Pulsed Corona Discharge in Air-Water Mixtures Followed by Photocatalytic Exhaust Air Cleaning. *Catalysts* **2021**, *11*, 549. <https://doi.org/10.3390/catal11050549>

Academic Editors: Chantal Guillard and Didier Robert

Received: 30 March 2021

Accepted: 21 April 2021

Published: 27 April 2021

Publisher's Note: MDPI stays neutral with regard to jurisdictional claims in published maps and institutional affiliations.



Copyright: © 2021 by the authors. Licensee MDPI, Basel, Switzerland. This article is an open access article distributed under the terms and conditions of the Creative Commons Attribution (CC BY) license (<https://creativecommons.org/licenses/by/4.0/>).

Keywords: electric discharge; plasma; ozone; VOCs; water purification; air purification

1. Introduction

Volatile organic compounds (VOCs) in industrial wastewaters present a challenge in their removal if stripping to the atmosphere is avoided. Toluene is a hydrophobic aromatic hydrocarbon of moderate toxicity occurring in wastewaters with concentrations recorded within the interval of 0.2–12,900 µg·L⁻¹ in several industries, such as paint and coating production, oil refinery, and gas processing [1–3]. Wastewaters subjected to the appropriate treatment may still contain residual toluene [3] that can be released to the ambient air, thereby having a detrimental impact on ecosystems. In urban air, toluene concentrations range from 5 to 150 µg·m⁻³, and in places with high traffic density they can reach 1310 µg·m⁻³ [4,5]. Human exposure to toluene has been reported to affect the central nervous and respiratory systems, also causing eye irritation [6–8]. Toluene is a refractory compound that is known due to extensive studies of its oxidation in air [7], thus providing a reasonable basis for the comparison of its abatement with various methods.

Advanced oxidation processes (AOPs) have proven their ability to degrade organic pollutants in various matrices [9–11]. The present research explores an alternative to conventional AOPs in the form of low-temperature plasma of pulsed corona discharge (PCD) as a source of active short-living oxidants. The abatement of aqueous and gaseous toluene using non-thermal plasma of electric discharges has been studied previously [12–15]. These studies only report the results obtained in either the aqueous or the gaseous phase, without considering the necessity to control pollutant removal in both phases. The pulsed corona discharge used in the study has shown an energy-efficient degradation of various aqueous pollutants [16–18], although the volatile acetone demonstrated its refractory character [19]. Therefore, the PCD not only faces the problem of ozone (O₃) present in the discharge, but also of residual VOCs in the air exhaust, requiring their elimination. Ozone is formed in

plasma reactions together with HO-radicals (HO^\bullet), hydrogen peroxide (H_2O_2), and atomic oxygen [17,20–22]. Photocatalytic oxidation successfully degrades low concentrations of airborne VOCs, converting them into harmless products, often H_2O and CO_2 [7]. The successful photocatalytic abatement of O_3 and VOCs, including toluene, was reported earlier [11]: toluene at a concentration of 60 ppm ($0.23 \text{ mg}\cdot\text{L}^{-1}$), in the presence of ozone, was degraded at the energy efficiency of $12.1 \text{ g}\cdot\text{kW}^{-1}\cdot\text{h}^{-1}$. The efficiency was calculated for 40% toluene removal at a photocatalyst irradiance of $3.5 \text{ mW}\cdot\text{cm}^{-2}$ (365 nm).

A composite approach simultaneously removing toluene from polluted aqueous media and air is applied in the present study, combining gas-phase electric discharge with the subsequent photocatalytic oxidation of exhaust air.

2. Results and Discussion

2.1. PCD Oxidation of Aqueous and Gaseous Toluene

A second-order kinetic law (Equation (1)) was used for the characterization of PCD oxidation [20]:

$$\frac{dC}{dt} = -\frac{k_2 \cdot C \cdot P}{V}, \tag{1}$$

where k_2 is the second-order reaction rate constant for PCD, $\text{m}^3\cdot\text{J}^{-1}$; C is the concentration of toluene, $\text{mol}\cdot\text{m}^{-3}$; P is the power of pulsed corona discharge, W; and V is the volume of plasma zone, m^3 .

Aqueous toluene oxidation at its initial equilibrium concentration (C_0) of $6.3 \text{ mg}\cdot\text{L}^{-1}$ at pulse repetition frequencies of 50, 200, and 800 pulses per second (pps) is depicted in Figure 1. It can be observed that the oxidation rates grow with the pulse repetition frequency (Figure 1a, Table 1a–c), whereas only modest variations were observed in energy efficiencies (Figure 1b) comprising 10.5, 8.6, and $7.5 \text{ g}\cdot\text{kW}^{-1}\cdot\text{h}^{-1}$ at 50, 200, and 880 pps, respectively. At lower frequencies, the long-living ozone promotes, although quite moderately, toluene oxidation due to the longer periods of time between pulses and, thus, a longer overall treatment time. This indicates that ozone plays a minor role in toluene oxidation.

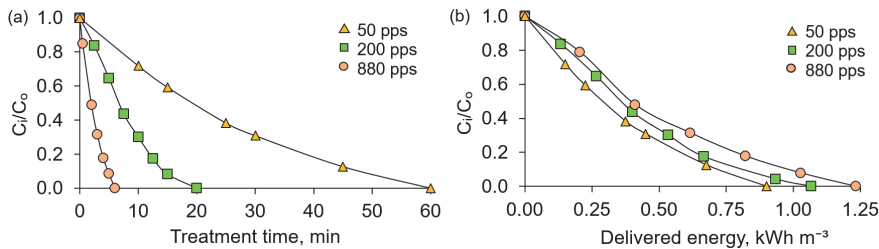


Figure 1. Degradation of aqueous toluene dependent on treatment time (a) and delivered energy (b) at pulse repetition frequencies of 50, 200, and 880 pps: $C_0 = 6.3 \text{ mg}\cdot\text{L}^{-1}$, initial pH 7.0, 20°C .

Table 1. The second-order kinetic constants and efficiency values of aqueous toluene PCD oxidation.

PCD Treatment Conditions		$k_2 \times 10^{-7}, \text{m}^3\cdot\text{J}^{-1}$	R^2	Efficiency of Toluene Oxidation for 40%, $\text{g}\cdot\text{kW}^{-1}\cdot\text{h}^{-1}$	
				Aqueous	Airborne
(a)	$C_0 = 6.3 \text{ mg}\cdot\text{L}^{-1}$, 880 pps, initial pH 7.0, 20°C	6.9	0.9981	7.5	22.3
(b)	$C_0 = 6.3 \text{ mg}\cdot\text{L}^{-1}$, 200 pps, initial pH 7.0, 20°C	8.3	0.9964	8.6	27.0
(c)	$C_0 = 6.3 \text{ mg}\cdot\text{L}^{-1}$, 50 pps, initial pH 7.0, 20°C	10.7	0.9905	10.5	29.3
(d)	$C_0 = 3.7 \text{ mg}\cdot\text{L}^{-1}$, 200 pps, initial pH 7.0, 20°C	12.4	0.9994	7.5	23.0
(e)	$C_0 = 1.0 \text{ mg}\cdot\text{L}^{-1}$, 200 pps, initial pH 7.0, 20°C	37.0	0.9938	6.4	13.7
(f)	$C_0 = 3.7 \text{ mg}\cdot\text{L}^{-1}$, 200 pps, pH 3.0, 20°C	12.5	0.9887	7.6	22.4
(g)	$C_0 = 3.7 \text{ mg}\cdot\text{L}^{-1}$, 200 pps, pH 12.0, 20°C	13.0	0.9943	7.6	24.9
(h)	$C_0 = 2.5 \text{ mg}\cdot\text{L}^{-1}$, 200 pps, initial pH 7.0, 30°C	12.2	0.9984	5.3	29.5

Further studies were carried out at a pulse repetition frequency of 200 pps, thus providing a treatment time long enough for accurate sampling at lower initial concentrations of toluene. The degradation of toluene in time of treatment in both the aqueous and air phases is shown in Figure 2, also illustrating the difference in oxidation rates depending on the initial aqueous toluene concentration. Gas-phase toluene degradation follows the pattern of the one in the aqueous phase, since the sampling method applied in the study (see Experimental Section) provided an equilibrium between phases that was achieved before sampling.

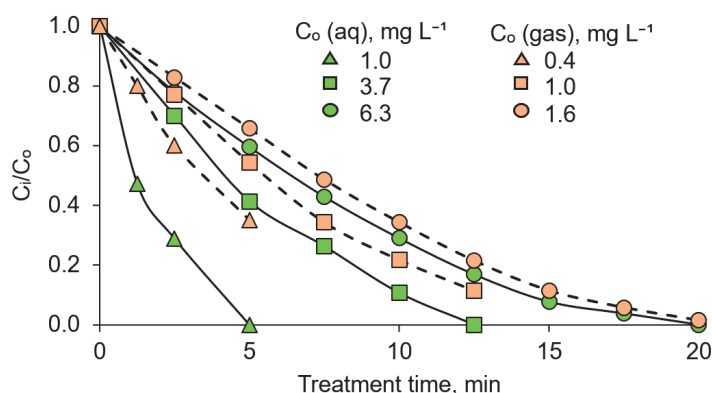


Figure 2. Simultaneous toluene PCD oxidation in aqueous and gaseous phases depending on treatment time at various concentrations: pulse repetition frequency of 200 pps, initial pH 7.0, 20 °C.

The dependence of toluene oxidation energy efficiency on its initial concentration is seen in Table 1b,d,e: the values of 6.4, 7.5, and 8.6 $\text{g}\cdot\text{kW}^{-1}\cdot\text{h}^{-1}$ correspond to the initial equilibrium aqueous toluene contents of 1.0, 3.7, and 6.3 $\text{mg}\cdot\text{L}^{-1}$, respectively. These values exceed the ones reported by Jose et al. by an order of magnitude [23], comprising 0.543 $\text{g}\cdot\text{kW}^{-1}\cdot\text{h}^{-1}$ in the needle-plate corona above water reactor at toluene concentrations as high as 200 $\text{mg}\cdot\text{L}^{-1}$.

Most of the earlier studies on airborne toluene oxidation reviewed by Preis et al. [24] were conducted using higher initial toluene concentrations, providing higher oxidation efficiency numbers as opposed to those presented here. Dou et al. [25] studied toluene oxidized in a 50-Hz AC dielectric barrier discharge (DBD) reactor with a starting concentration of 1200 ppm (4.6 $\text{mg}\cdot\text{L}^{-1}$), showing that the energy yield averaged around 5 $\text{g}\cdot\text{kW}^{-1}\cdot\text{h}^{-1}$, which is in accordance with the span given in the review by van Durme et al. [26], of 1 to 11 $\text{g}\cdot\text{kW}^{-1}\cdot\text{h}^{-1}$ for DBD combined with in situ or post-discharge catalysis. Schiorlin et al. [27] observed toluene degradation in pulsed DBD at a removal efficiency of about 7.2 $\text{g}\cdot\text{kW}^{-1}\cdot\text{h}^{-1}$ at a starting concentration in dry air as high as 500 ppm (1.9 $\text{mg}\cdot\text{L}^{-1}$). The air humidity rose to 40% at 20 °C, which resulted in the toluene oxidation efficiency increasing to about 8.4 $\text{g}\cdot\text{kW}^{-1}\cdot\text{h}^{-1}$. The energy efficiency of such treatment is inferior to the ones observed in this study for the air phase, taking into account that starting toluene concentrations are higher for an order of magnitude. Such an observation is expected for DBD, showing lower efficiencies [24]. The application of PCD, however, showed a dramatic growth in the oxidation energy yield: Malik et al. [28] reported a toluene oxidation efficiency as high as 30.1 $\text{g}\cdot\text{kW}^{-1}\cdot\text{h}^{-1}$ at the starting concentration of 300 ppm (1.1 $\text{mg}\cdot\text{L}^{-1}$) in dry air at a pulse repetition frequency of 2 pps, which is close to the numbers observed in the present study. We failed to find publications concerning the electric discharge application towards combined treatment of water and air polluted with VOCs.

The efficiency of airborne toluene oxidation also shown in Table 1 logically exceeds the ones of aqueous toluene by about three times in most of the cases, which is explained by the interface-borne HO-radicals at the gas-phase side shown earlier [19]. At higher

temperatures, the difference increased by about five times, which is also consistent with, on the one hand, the higher gas-phase equilibrium concentration and, on the other hand, lower oxidation rate of aqueous admixtures at elevated temperatures [29].

The measurement of gaseous ozone concentration showed its definitive involvement in the oxidation of toluene: the higher the toluene concentration, the slower the ozone concentration growth (Figure 3). The values of concentrations also indicate the ozone consumption by oxidation reactions being an order of magnitude lower than the ones observed in the reactor working with distilled water [20].

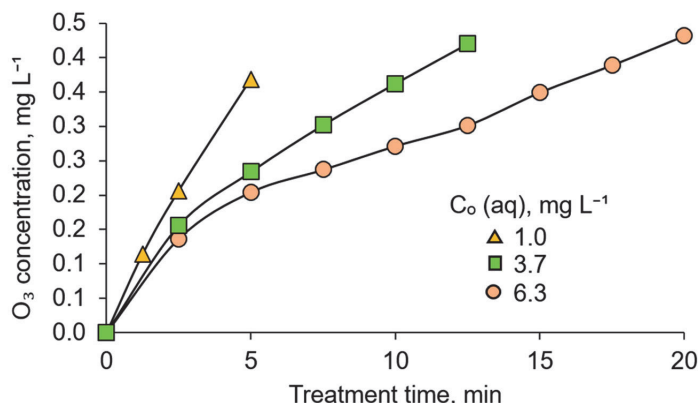


Figure 3. Gaseous ozone in PCD reactor at time of treatment dependent on the initial aqueous toluene concentration: pulse repetition frequency 200 pps, initial pH 7.0, 20 °C.

The impacts of the pH and of the temperature were studied at a toluene initial equilibrium concentration of 3.7 mg·L⁻¹. The pH of acidic and alkaline solutions remained unchanged throughout the treatment, while in neutral solutions the pH decreased from 7.0 ± 0.1 to 4.5 ± 0.2 within 12.5 min due to the formation of carboxylic acids [30] and nitrate [31]. Variations in pH had no effect on the aqueous toluene degradation Table 1d,f,g, regardless of the fact that basic pH conditions promote aqueous ozone decomposition, producing additional HO radicals [32]. The minor role of this reaction is explained by the low concentration of gaseous ozone. For example, within the first 5 min of treatment 0.22 mg·L⁻¹ of gaseous ozone in the reactor (Figure 3) may provide 0.07 mg·L⁻¹ of equilibrium aqueous ozone according to Henry's law [33]. This circumstance confirms the smaller role of ozone in toluene oxidation observed in experiments with various pulse repetition rates. Clearly, variations in pH from 3.0 to 12.0 did not alter the non-dissociating toluene molecule reactivity with discharge-generated HO-radicals in the PCD reactor.

The treated solution containing 3.7 mg·L⁻¹ of aqueous toluene in equilibrium with air in the reactor was adiabatically heated from 20 ± 2 °C to 30 ± 2 °C, providing a toluene aqueous concentration of 2.5 mg·L⁻¹. The increased temperature resulted in a noticeably lower energy efficiency of 5.9 g·kW⁻¹·h⁻¹ in toluene oxidation at a slightly lower reaction rate constant, as shown in Table 1d,h. This observation indirectly points to toluene oxidation at the gas–liquid interface [19], since the increased airborne toluene concentration resulted in a higher rate of oxidation at the gas-phase side.

The FTIR analysis of air outlet from the PCD reactor showed, in addition to toluene and ozone, the minor presence of the product of incomplete oxidation, carbon monoxide (CO). Compositions of gaseous exhaust originating from PCD at the end of the treatment are shown in Table 2.

Earlier, the authors noticed ozone increasing the yield of carbon monoxide in the photocatalytic oxidation of toluene [11]. In PCD experiments, both ozone and CO concentrations were found to be descending, with declining pulse repetition frequencies at low residual aqueous toluene concentrations being close to each other at the end of treatment,

as shown in Table 2a–c. This observation might point to the potential similarity in the roles of ozone in both photocatalytic and PCD oxidation: less ozone in the gas phase results in a lower yield of carbon monoxide. In addition, a smaller initial content of toluene also results in a smaller CO yield at approximately equal ozone concentrations, as shown in Table 2b,d,e. The reduced CO yield at lower ozone concentrations observed at elevated temperatures also fits into the association between CO production and gaseous ozone concentration, as shown in Table 2b,h. However, the PCD oxidation experiments at various pHs, as shown in Table 2d,f,g, show practically identical CO yields at ozone concentrations expectedly being an order of magnitude lower in alkaline medium as a result of fast decomposition and, thus, the chemisorption of ozone. From this, one can unequivocally conclude that CO is a product of toluene oxidation without a particular role of ozone, i.e., along the predominant mechanism with discharge-generated HO-radicals.

Table 2. Toluene, O₃, and CO concentrations in PCD outlet gas.

PCD Treatment Conditions		Sampling Time, min	Concentration, mg·L ^{−1}		
			Toluene	O ₃	CO
(a)	C ₀ = 6.3 mg·L ^{−1} (aq), C ₀ = 1.6 mg·L ^{−1} (gas), 880 pps, initial pH 7.0, 20 °C	6	0.057	0.61	0.051
(b)	C ₀ = 6.3 mg·L ^{−1} (aq), C ₀ = 1.6 mg·L ^{−1} (gas), 200 pps, initial pH 7.0, 20 °C	20	0.080	0.40	0.042
(c)	C ₀ = 6.3 mg·L ^{−1} (aq), C ₀ = 1.6 mg·L ^{−1} (gas), 50 pps, initial pH 7.0, 20 °C	60	0.10	0.22	0.033
(d)	C ₀ = 3.7 mg·L ^{−1} (aq), C ₀ = 1.0 mg·L ^{−1} (gas), 200 pps, initial pH 7.0, 20 °C	12.5	0.061	0.39	0.028
(e)	C ₀ = 1.0 mg·L ^{−1} (aq), C ₀ = 0.4 mg·L ^{−1} (gas), 200 pps, initial pH 7.0, 20 °C	5	0.065	0.34	0.016
(f)	C ₀ = 3.7 mg·L ^{−1} (aq), C ₀ = 1.0 mg·L ^{−1} (gas), 200 pps, pH 3.0, 20 °C	12.5	0.057	0.42	0.030
(g)	C ₀ = 3.7 mg·L ^{−1} (aq), C ₀ = 1.0 mg·L ^{−1} (gas), 200 pps, pH 12.0, 20 °C	12.5	0.065	0.044	0.030
(h)	C ₀ = 2.5 mg·L ^{−1} (aq), C ₀ = 1.2 mg·L ^{−1} (gas), 200 pps, initial pH 7.0, 30 °C	12.5	0.096	0.22	0.029

As shown in Table 2b,d,e, the trace concentrations of toluene remain at about 0.06–0.10 mg·L^{−1} after PCD treatment, regardless of its initial concentration. The complete PCD oxidation of toluene may prove to be a time-and energy-consuming task. Besides this, residual ozone is also considered an air pollutant. Under these circumstances, gaseous exhausts containing trace amounts of toluene and residual ozone treated photocatalytically present a reasonable approach.

2.2. Photocatalytic Treatment of Toluene and Ozone Residues in the PCD Exhaust

Residual toluene, O₃, and CO exiting the PCD reactor enter the photocatalytic reactor at the concentrations shown in Table 3.

Table 3. Contents of toluene, ozone, and carbon monoxide in PCD outlet gas entering photocatalytic reactor.

PCD Treatment Conditions	Sampling Time, min	Concentration, mg·L ^{−1}		
		Toluene	O ₃	CO
C ₀ = 6.3 mg·L ^{−1} (aq), C ₀ = 1.6 mg·L ^{−1} (gas), 200 pps, initial pH 7.0, 20 °C	20	0.034	0.29	0.038
C ₀ = 3.7 mg·L ^{−1} (aq), C ₀ = 1.0 mg·L ^{−1} (gas), 200 pps, initial pH 7.0, 20 °C	12.5	0.046	0.29	0.024
C ₀ = 1.0 mg·L ^{−1} (aq), C ₀ = 0.4 mg·L ^{−1} (gas), 200 pps, initial pH 7.0, 20 °C	5	0.042	0.24	0.014

Rather low inlet concentrations of toluene (Table 3) became undetectable over a TiO₂-coated area of 120 cm² within all tested residence times of 4, 8, and 16 s—i.e., at SRTs of 0.033, 0.065, and 0.13 s·cm^{−2}, respectively (Figure 4).

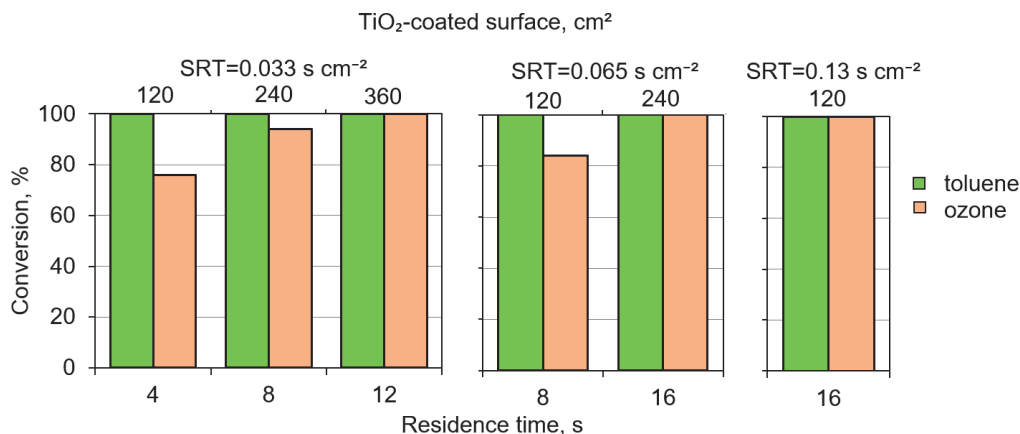
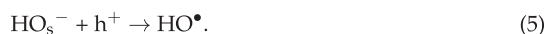
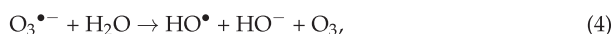
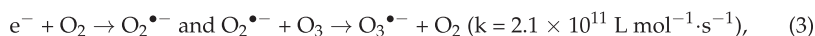
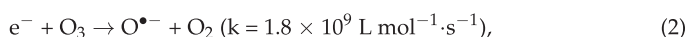


Figure 4. Conversion of airborne toluene and ozone in photocatalytic reactor dependent on residence time at the TiO₂-coated surface. PCD treatment conditions: C₀ = 3.7 mg·L^{−1} (aq), C₀ = 1.0 mg·L^{−1} (gas), 200 pps, initial pH 7.0, 20 °C.

The fast degradation of residual toluene is explained by the role of residual plentiful ozone: Pichat et al. [34] reported easier capture of electrons photolytically promoted to the TiO₂ conduction band by ozone, either directly (Equation (2)) or indirectly (Equation (3)). The radical-anion O₃^{•−} may react with water adsorbed on a TiO₂ surface, promoting the generation of HO[•] (Equation (4)). Additionally, the scavenging of photoproducted electrons with ozone obstructs the hole-electron recombination magnifying HO[•] formation from hydroxyl-anions at the photocatalyst surface (Equation (5)).



Since no significant difference in O₃ conversion was observed at variable residual toluene concentrations, Figure 4 only depicts the results obtained at an aqueous toluene starting equilibrium concentration of 3.7 mg·L^{−1}. At the longest SRT of 0.13 s·cm^{−2} provided by a residence time of 16 s over a TiO₂-covered photocatalytic surface of 120 cm², O₃ was fully degraded, although, at a SRT of 0.065 and 0.033 s·cm^{−2}, the O₃ depletion accordingly required 240 and 360 cm² with residence times of 16 and 12 s, respectively. At lower SRTs of 0.033 and 0.065 s·cm^{−2} provided by the respective residence times of 4 and 8 s over 120 cm² of TiO₂ coating, ozone did not decompose entirely, thus indicating the need for a greater area of the photocatalyst to ensure the time limit for O₃ degradation. The gradual depletion of O₃, within a time span longer than the one necessary for the complete oxidation of toluene residues confirms a deep oxidation of toluene degradation by-products under the experimental conditions; the accelerated depletion of O₃ in the presence of toluene degradation by-products adsorbed on TiO₂-coatings was reported earlier [11].

The photocatalytic treatment of the PCD exhaust air resulted in CO remaining intact, to which photocatalytic oxidation added slightly more of the CO produced from residual toluene in amounts of 0.002–0.007 mg·L^{−1}. Variations in the CO outlet concentrations are

determined by differences in the residual toluene concentrations in the air entering the photocatalytic reactor. The probable reason for the CO residues is the effect of water vapor hindering the oxidation of poorly adsorbed CO to CO₂, by blocking the active sites on the photocatalyst surface [35]. The resultant CO concentration, however, is lower than the maximum permissible concentration for an eight-hour exposure in a working zone comprising 0.058 mg·L⁻¹ [36].

3. Materials and Methods

3.1. Experimental Equipment and Procedure

The PCD reactor was combined with the photocatalytic one to treat the air exhaust containing residual toluene and ozone. A 3D illustration of the combination is shown in Supplementary Figure S1.

3.1.1. Pulsed Corona Discharge

Experiments with toluene aqueous solutions using 10 L samples were conducted using the PCD device described earlier [16], and shown in Figure 5 (Flowrox Oy, Lappeenranta, Finland). Toluene, as an easily fugitive compound, is rather difficult to use in precise dosing in a 154 L reactor. To avoid massive toluene evaporation in ambient air, toluene solutions were stored in hermetically closed vessels and transferred into the PCD reactor using a peristaltic pump (Masterflex, Vernon Hills, IL, USA). Solutions initially containing approximately 10 ± 0.5, 30 ± 1.5, and 50 ± 2.3 mg·L⁻¹ of toluene provided equilibrium to aqueous concentrations of 1.0 ± 0.05, 3.7 ± 0.15, and 6.3 ± 0.30 mg·L⁻¹ at 20 °C. These concentrations consistently provided equilibrium to airborne toluene concentrations in the air phase, 0.4 ± 0.02, 1.0 ± 0.04, and 1.6 ± 0.07 mg·L⁻¹, respectively, and in the overall free gaseous volume of the PCD reactor. In experiments at temperatures elevated to 30 °C, the equilibrium in solutions containing 30 mg·L⁻¹ was established at an aqueous concentration of 2.5 ± 0.10 mg·L⁻¹ and an airborne toluene content of 1.2 ± 0.05 mg·L⁻¹. An inbuilt spiral coil heater was used to obtain a higher temperature of the solution. The equilibrium state of toluene in a gas–liquid system verified implementing Henry’s law (Equation (6)) [37] showed the measured concentrations being close to the theoretically calculated ones:

$$H = H_0 \times \exp \left(\frac{d[\ln H]}{dT} \right) \left(\frac{1}{T} - \frac{1}{T_0} \right), \quad (6)$$

where H is Henry’s law solubility constant; H_0 is Henry’s law solubility constant at the reference temperature, mol·kg⁻¹·bar⁻¹ [38]; T is the treated solution temperature, K; T_0 is a reference temperature of 298.15 K.

The aqueous samples were treated in a recirculation regime and continuously sprayed into the electric discharge zone. High-voltage pulses were applied between horizontal high-voltage electrodes made of stainless steel wire 0.55 mm in diameter and a total length of 20 m, and two vertical grounded stainless steel plates with repetition frequencies of 50, 200, and 880 pps, corresponding to output powers of 9, 32, and 123 W, respectively. Water containing toluene was dispersed through a perforated plate with 51 perforations 1 mm in diameter with a flow rate of 1.0 m³·h⁻¹ using a circulation pump (Iwaki Co. Ltd., Tokyo, Japan). The PCD reactor was hermetically closed to prevent toluene vapor leaks to ambient air.

The delivered pulsed energy was calculated using the integrated waveforms of voltage and current, as described earlier [39]. Energy efficiency E , g·kW⁻¹·h⁻¹, was calculated at 40% of toluene oxidation using Equation (7):

$$E = \frac{\Delta C \cdot V}{W}, \quad (7)$$

where ΔC is the decrease in toluene concentration, g·m⁻³; V is the volume of treated sample, m³; and W is the consumption of energy, kWh.

Solution samples were recirculated for 10 min prior to the start of the experiment and for 5 min prior to the sampling after treatment in order to reach equilibrium concentrations of toluene in liquid and gas phases (Supplementary Figure S2). The gas samples from the PCD reactor were transferred to the FTIR gas cell by means of an air pump (KNF Neuberger S.A.S, France), and analyzed for the presence of VOCs and ozone (see below). After the PCD treatment, the gaseous exhaust was transferred to the photocatalytic reactor for post-treatment.

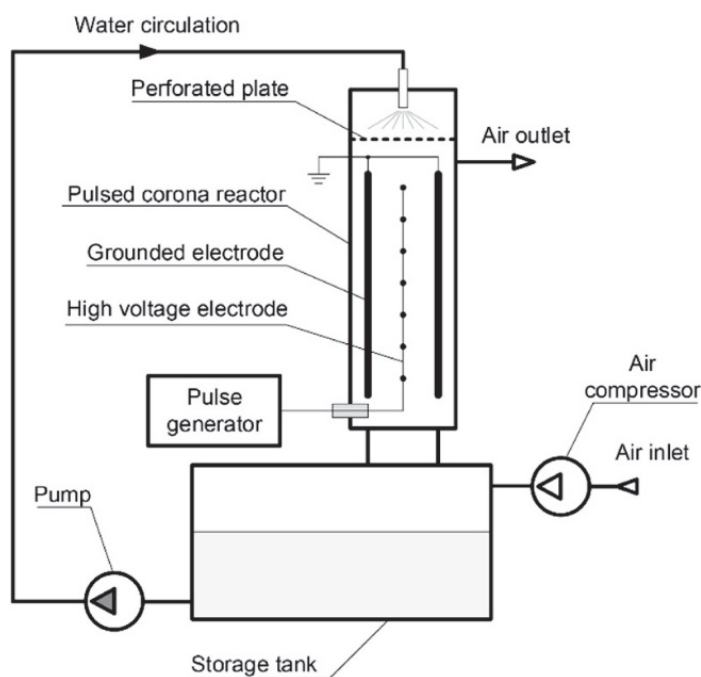


Figure 5. Schematic illustration of the PCD device.

3.1.2. Photocatalytic Oxidation

Air exhaust from the PCD reactor was treated photocatalytically using TiO₂-coated (P25, Evonik Industries, Essen, Germany) glass plates under UVA-emitting fluorescent lamps, Actinic T8, 15 W (Philips, Amsterdam, Netherlands) in a multi-section continuous reactor described earlier [11], consisting of five sequential sections with a volume of 130 mL each (0.9 × 4.9 × 29.5 cm) and a wall thickness of 0.2 cm (Figure 6). The catalyst-coated surface thus comprised 120 cm² per section, with a TiO₂ surface density of $1.4 \pm 0.2 \text{ mg} \cdot \text{cm}^{-2}$ and a coating thickness in the range of 1 μm .

Temperature in the reactor was measured with a temperature controller supplied with K-type thermocouple, CN9000A (Omega, Norwalk, CT, USA), comprising $38 \pm 1 \text{ }^{\circ}\text{C}$, maintained by the heat of the lamp. The gas flow rate was controlled using a flow metering valve SS-6MG-MM (Swagelok, Solon, OH, USA). The flow rates of 0.5, 1.0, and 2.0 L·min^{−1} were applied, providing residence times of 16, 8, and 4 s per section and specific residence times (SRT) of 0.13, 0.065, and 0.033 s·cm^{−2}, respectively.

3.2. Chemicals and Analyses

The concentration of aqueous toluene ($\geq 99\%$, Sigma-Aldrich, St. Louis, MO, USA) was measured using a 9300 HPLC System high-performance liquid chromatography (YL Instrument Co., Anyang, Korea) equipped with a UV/Vis detector and XBridge C18 column (130 Å pore size, 3.5 μm particle size, 150 mm in length, and 3.0 mm inner diameter) (Waters,

Milford, MA, USA). The flow rate was $0.2 \text{ mL} \cdot \text{min}^{-1}$ at the sample run time of 13 min. The isocratic elution was applied using 70% of 0.1% CH_3COOH in ultrapure water and 30% of acetonitrile.

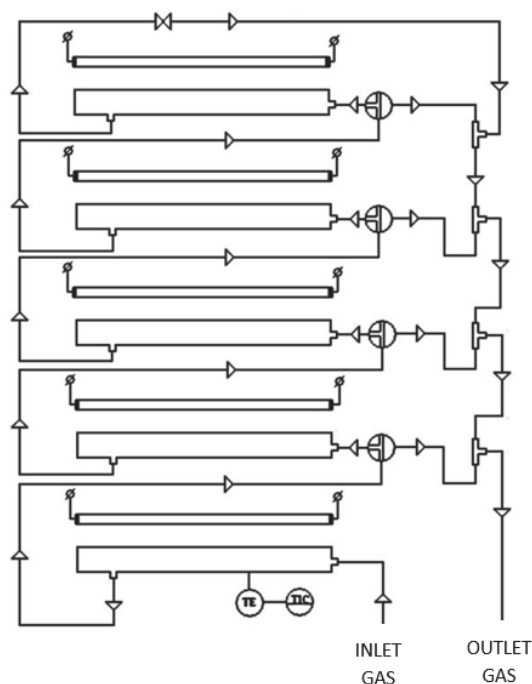


Figure 6. Schematic illustration of photocatalytic reactor: TIC: temperature indicator controller; TE: temperature element.

The pH was measured with a S220 digital pH-meter (Mettler Toledo, Greifensee, Switzerland) and adjusted with either 5 M H_2SO_4 (96%, LACH-NER, Neratovice, Czech Republic) or 5 M NaOH ($\geq 98\%$, Sigma-Aldrich, St. Luis, MO, USA). The concentrations of residual toluene and O_3 in the air were determined using Fourier transform infrared spectroscopy (FTIR, Interspec 200-X, Tõravere, Estonia). Gaseous samples were collected into the 8 m 1.33 L gas cell (Specac Tornado, Orpington, UK) and analyzed in the wavelength range of $500\text{--}4000 \text{ cm}^{-1}$. The spectrum was collected every 5 min for each reactor's section. Toluene peaks were integrated using the Essential FTIR software (Operant LLC, Houston, TX, USA) and a quantitative database (FDM, HiRes VPFTIR for Quant). The content of O_3 in the air was determined by FTIR spectroscopy, with calibration acquired using a MP-6060 ozone analyzer (Anseros Klaus Nonnenmacher GmbH, Tübingen, Germany). All the measurements were duplicated, indicating that the standard deviation was not higher than 5%.

4. Conclusions

The treatment of aqueous toluene in gas-phase pulsed corona discharge combined with the photocatalytic treatment of exhaust air eliminates residual toluene and ozone, thus producing carbon monoxide in minor amounts. The energy efficiency of both aqueous and airborne toluene PCD oxidation demonstrated unequalled levels of 6.4 to 10.5 and up to $29.6 \text{ g} \cdot \text{kW}^{-1} \cdot \text{h}^{-1}$, respectively, depending on the pulse repetition frequency and toluene concentration. A temperate difference in energy efficiencies at variable frequencies points to the moderate role of O_3 -induced oxidation of toluene. The increase of temperature in the treated toluene solution from 20 to 30°C resulted in the decreased oxidation efficiency of the

aqueous toluene of about 20%, showing higher oxidation rates in the gas phase. Indifference of toluene oxidation efficiency towards pH of treated solution indicates the predominant role of discharge-generated HO-radicals in oxidation: at pH 12.0, an order of magnitude lower gaseous ozone concentrations resulted in toluene oxidation efficiency attributable to other pH media with high ozone concentrations. Residual toluene, ozone, and CO₂ and minor amounts of CO were observed as the humid air PCD exhaust constituents. Properly selected conditions of photocatalytic oxidation over TiO₂ allow the complete elimination of toluene and ozone from the exhaust air, contributing, however, to a minor extent to CO formation from residual toluene.

Supplementary Materials: The following are available online at <https://www.mdpi.com/article/10.3390/catal11050549/s1>: Supplementary Figure S1: 3D illustration of combined PCD and photocatalytic reactor; Supplementary Figure S2: Equilibrium between liquid and gaseous phase of toluene in time: C₀ = 50 mg·L^{−1}, pH 7.0.

Author Contributions: Conceptualization, M.K. (Maarja Kask), M.K. (Marina Krichevskaya), S.P., and J.B.; data curation, M.K. (Maarja Kask); formal analysis, M.K. (Maarja Kask); funding acquisition, S.P.; investigation, M.K. (Maarja Kask); methodology, M.K. (Maarja Kask), M.K. (Marina Krichevskaya), and J.B.; project administration, S.P.; resources, S.P.; supervision, M.K. (Marina Krichevskaya) and J.B.; validation, M.K. (Maarja Kask); visualization, M.K. (Maarja Kask) and J.B.; writing—original draft, M.K. (Maarja Kask); Writing—review and editing, M.K. (Marina Krichevskaya), S.P., and J.B. All authors have read and agreed to the published version of the manuscript.

Funding: This research was funded by the Institutional Development Program of Tallinn University of Technology for 2016–2022, project 2014–2020.4.01.16–0032 from the EU Regional Development Fund, and the Research Group Support project PRG776 of Estonian Research Council.

Acknowledgments: The authors would like to acknowledge Arina Borissenko for her assistance with the experiments.

Conflicts of Interest: The authors declare no conflict of interest.

References

1. Anjum, H.; Johari, K.; Gnanasundaram, N.; Appusamy, A.; Thanabalana, M. Investigation of green functionalization of multiwall carbon nanotubes and its application in adsorption of benzene, toluene & p-xylene from aqueous solution. *J. Clean. Prod.* **2019**, *221*, 323–338. [\[CrossRef\]](#)
2. Cseri, L.; Razali, M.; Pogany, P.; Szekely, G. Chapter 3.15—Organic Solvents in Sustainable Synthesis and Engineering. In *Green Chemistry: An Inclusive Approach*, 1st ed.; Elsevier Inc.: Amsterdam, The Netherlands, 2018; pp. 513–553. [\[CrossRef\]](#)
3. Mrowiec, B. Toluene in sewage and sludge in wastewater treatment plants. *Water Sci. Technol.* **2014**, *69*, 128–134. [\[CrossRef\]](#) [\[PubMed\]](#)
4. World Health Organization (WHO). *Air Quality Guidelines for Europe*, 2nd ed.; Chapter 5.14—Toluene; WHO Regional Publications: Copenhagen, Denmark, 2000; p. 112.
5. Leusch, F.; Bartkow, M. *A Short Primer on Benzene, Toluene, Ethylbenzene and Xylenes (BTEX) in the Environment and in Hydraulic Fracturing Fluids*; Smart Water Research Centre, Griffith University: Queensland, Australia, 2010.
6. Toluene. Available online: <https://www.epa.gov/sites/production/files/2016-09/documents/toluene.pdf> (accessed on 30 March 2021).
7. Mo, J.; Zhang, Y.; Xu, Q.; Joaquin, J.; Zhao, R. Photocatalytic purification of volatile organic compounds in indoor air: A literature review. *Atmos. Environ.* **2009**, *43*, 2229–2246. [\[CrossRef\]](#)
8. Debono, O.; Thevenet, F.; Gravejat, P.; Hequet, V.; Raillard, C.; Lecoq, L.; Locoge, N. Toluene photocatalytic oxidation at ppbv levels: Kinetic investigation and carbon balance determination. *Appl. Catal. B Environ.* **2011**, *106*, 600–608. [\[CrossRef\]](#)
9. Bolobajev, J.; Bilgin Öncü, N.; Viisimaa, M.; Trapido, M.; Balcioglu, I.; Goi, A. Column experiment on activation aids and biosurfactant application to the persulphate treatment of chlorophene-contaminated soil. *Environ. Technol.* **2015**, *36*, 348–357. [\[CrossRef\]](#) [\[PubMed\]](#)
10. Kask, M.; Krichevskaya, M.; Bolobajev, J. Sonolytic degradation of pesticide metazachlor in water: The role of dissolved oxygen and ferric sludge in the process intensification. *J. Environ. Chem. Eng.* **2019**, *7*, 103095. [\[CrossRef\]](#)
11. Kask, M.; Bolobajev, J.; Krichevskaya, M. Gas-phase photocatalytic degradation of acetone and toluene, and their mixture in the presence of ozone in a continuous multi-section reactor as possible air post-treatment for exhaust from pulsed corona discharge. *Chem. Eng. J.* **2020**, *399*, 125815. [\[CrossRef\]](#)

12. Jose, J.; Philip, L. Continuous flow pulsed power plasma reactor for the treatment of aqueous solution containing volatile organic compounds and real pharmaceutical wastewater. *J. Environ. Manag.* **2021**, *286*, 112202. [CrossRef] [PubMed]
13. Zhu, F.; Li, X.; Zhang, H.; Wu, A.; Yan, J.; Ni, M.; Zhang, H.; Buekens, A. Destruction of toluene by rotating gliding arc discharge. *Fuel* **2016**, *176*, 78–85. [CrossRef]
14. Huang, H.; Ye, D.; Leung, Y.C.; Feng, F.; Guan, X. Byproducts and pathways of toluene destruction via plasma-catalysis. *J. Mol. Catal. A Chem.* **2011**, *336*, 87–93. [CrossRef]
15. Yao, X.; Jiang, N.; Li, J.; Lu, N.; Shang, K.; Wu, Y. An improved corona discharge ignited by oxide cathodes with high secondary electron emission for toluene degradation. *Chem. Eng. J.* **2019**, *362*, 339–348. [CrossRef]
16. Bolobajev, J.; Kornev, I.; Preis, S. Degradation of aqueous alachlor in pulsed corona discharge. *J. Electrostat.* **2021**, *109*, 103543. [CrossRef]
17. Kask, M.; Krichevskaya, M.; Preis, S.; Bolobajev, J. Oxidation of aqueous N-nitrosodiethylamine: Experimental comparison of pulsed corona discharge with H₂O₂-assisted ozonation. *J. Environ. Chem. Eng.* **2021**, *9*, 105102. [CrossRef]
18. Tikker, P.; Dulova, N.; Kornev, I.; Preis, S. Effects of persulfate and hydrogen peroxide on oxidation of oxalate by pulsed corona discharge. *Chem. Eng. J.* **2021**, *411*, 128586. [CrossRef]
19. Ajo, P.; Kornev, I.; Preis, S. Pulsed corona discharge induced hydroxyl radical transfer through the gas-liquid interface. *Sci. Rep.* **2017**, *7*, 16152. [CrossRef] [PubMed]
20. Preis, S.; Panorel, I.C.; Kornev, I.; Hatakka, H.; Kallas, J. Pulsed corona discharge: The role of ozone and hydroxyl radical in aqueous pollutants oxidation. *Water Sci. Technol.* **2013**, *68*, 1536–1542. [CrossRef] [PubMed]
21. Schneider, M.; Rataj, R.; Kolb, J.F.; Bláha, L. Cylindrospermopsin is effectively degraded in water by pulsed corona-like and dielectric barrier discharges. *Environ. Pollut.* **2020**, *266*, 115423. [CrossRef]
22. Scholtz, V.; Pazlarova, J.; Souskova, H.; Khun, J.; Julak, J. Nonthermal plasma—A tool for decontamination and disinfection. *Biotechnol. Adv.* **2015**, *33*, 1108–1119. [CrossRef] [PubMed]
23. Jose, J.; Philip, L. Comparative study of degradation of toluene and methyl isobutyl ketone (MIBK) in aqueous solution by pulsed corona discharge plasma. *J. Environ. Sci.* **2021**, *101*, 382–396. [CrossRef] [PubMed]
24. Preis, S.; Klauson, D.; Gregor, A. Potential of electric discharge plasma methods in abatement of volatile organic compounds originating from the food industry. *J. Environ. Manag.* **2013**, *114*, 125–138. [CrossRef] [PubMed]
25. Dou, B.; Li, J.; Liang, W.; Zhu, T.; Li, Y.; Jin, Y.; He, L. Volatile organic compounds (VOCs) removal by using dielectric barrier discharge. In Proceedings of the 2nd International Conference on Bioinformatics and Biomedical Engineering, Shanghai, China, 16–18 May 2008; IEEE: New York, NY, USA. [CrossRef]
26. van Durme, J.; Dewulf, J.; Leys, C.; van Langenhove, H. Combining non-thermal plasma with heterogeneous catalysis in waste gas treatment: A review. *Appl. Catal. B* **2008**, *78*, 324–333. [CrossRef]
27. Schiorlin, M.; Marotta, E.; Rea, M.; Paradisi, C. Comparison of toluene removal in air at atmospheric conditions by different corona discharges. *Environ. Sci. Technol.* **2009**, *43*, 9386–9392. [CrossRef] [PubMed]
28. Malik, M.A.; Minamitani, Y.; Schoenbach, K.H. Comparison of catalytic activity of aluminum oxide and silica gel for decomposition of volatile organic compounds (VOCs) in a plasmacatalytic reactor. *IEEE Trans. Plasma Sci.* **2005**, *33*, 50–56. [CrossRef]
29. Onga, L.; Kornev, I.; Preis, S. Oxidation of reactive azo-dyes with pulsed corona discharge: Surface reaction enhancement. *J. Electrostat.* **2020**, *103*, 103420. [CrossRef]
30. Panorel, I.C.; Preis, S.; Kornev, I.; Hatakka, H.; Louhi-Kultanen, M. Oxidation of aqueous paracetamol by pulsed corona discharge. *Ozone Sci. Eng.* **2013**, *35*, 116–124. [CrossRef]
31. Kornev, I.; Osokin, G.; Galanov, A.; Yavorovskiy, N.; Preis, S. Formation of nitrite- and nitrate-ions in aqueous solutions treated with pulsed electric discharges. *Ozone Sci. Eng.* **2013**, *35*, 22–30. [CrossRef]
32. Kasprzyk-Hordern, B.; Ziótek, M.; Nawrocki, J. Catalytic ozonation and methods of enhancing molecular ozone reactions in water treatment. *Appl. Catal. B Environ.* **2003**, *46*, 639–669. [CrossRef]
33. Gottschalk, C.; Libra, J.A.; Saupe, A. *Ozonation of Water and Waste Water: A Practical Guide to Understanding Ozone and Its Applications*, 2nd ed.; Wiley-VCH Verlag GmbH & Co. KGaA: Hoboken, NJ, USA, 2009; p. 109. [CrossRef]
34. Pichat, P.; Disdier, J.; Hoang-Van, C.; Mas, D.; Goutailler, G.; Gaysse, C. Purification/deodorization of indoor air and gaseous effluents by TiO₂ photocatalysis. *Catal. Today* **2000**, *63*, 363–369. [CrossRef]
35. Soliman, N.K. Factors affecting CO oxidation reaction over nanosized materials: A review. *J. Mater. Res. Technol.* **2019**, *8*, 2395–2407. [CrossRef]
36. Carbon Monoxide—Leading Cause of Poisoning Deaths. Available online: <https://www.creia.org/carbon-monoxide---leading-cause-of-poisoning-deaths> (accessed on 30 March 2021).
37. Sander, R. Compilation of Henry’s law constants (version 4.0) for water as solvent. *Atmos. Chem. Phys.* **2015**, *15*, 4399–4981. [CrossRef]
38. Leighton, D.T.; Calo, J.M. Distribution Coefficients of Chlorinated Hydrocarbons in Dilute Air-Water Systems for Groundwater Contamination Applications. *J. Chem. Eng. Data* **1981**, *26*, 382–385. [CrossRef]
39. Kornev, I.; Saprykin, F.; Preis, S. Stability and energy efficiency of pulsed corona discharge in treatment of dispersed high-conductivity aqueous solutions. *J. Electrostat.* **2017**, *89*, 42–50. [CrossRef]

Supplementary Materials

Oxidation of Aqueous Toluene by Gas-Phase Pulsed Corona Discharge in Air-Water Mixtures Followed by Photocatalytic Exhaust Air Cleaning

Maarja Kask *, Marina Krichevskaya, Sergei Preis and Juri Bolobajev *

Department of Materials and Environmental Technology, Tallinn University of Technology, Ehitajate Tee 5, 19086 Tallinn, Estonia; marina.kritsevskaja@taltech.ee (M.K.); sergei.preis@taltech.ee (S.P.)

* Correspondence: maarja.kask@taltech.ee (M.K.); juri.bolobajev@taltech.ee (J.B.)

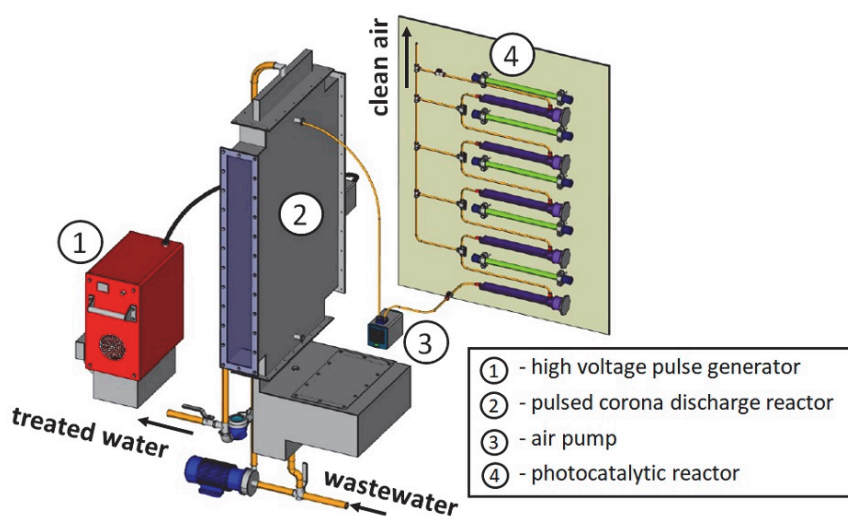


Figure S1. 3D illustration of combined PCD and photocatalytic reactor

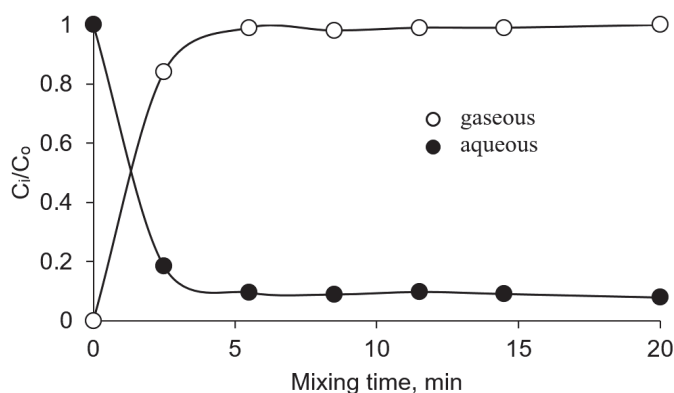


Figure S2. Equilibrium between liquid and gaseous phase of toluene in time: $C_0 = 50 \text{ mg} \cdot \text{L}^{-1}$, pH 7.0

Curriculum Vitae

Personal data

Name:	Maarja Kask
Date of birth:	19.09.1993
Place of birth:	Rakvere, Estonia
Citizenship:	Estonian

Contact data

E-mail:	maarja.kask@taltech.ee
---------	------------------------

Education

2017–2021	Tallinn University of Technology, Chemical and Materials Technology, PhD
2015–2017	Tallinn University of Technology, MSc in Engineering (cum laude)
2012–2015	Tallinn University of Technology, BSc in Engineering
2009–2012	Rakvere Realgymnasium

Language competence

Estonian	native speaker
English	fluent
Russian	beginner
Finnish	beginner

Professional employment

2017–2021	Tallinn University of Technology, School of Engineering, Department of Materials and Environmental Technology, Junior Researcher
-----------	--

Defended dissertations

Master's Degree, 2017, Photocatalytic effect of Metal-Doped Organic Aerogels on Trimethoprim Degradation, Tallinn University of Technology, School of Engineering, Department of Materials and Environmental Technology. Supervisors: Juri Bolobajev, Anna Goi.

Involvement in research projects

PRG776 Innovative energy-efficient abatement of aqueous and airborne hazardous pollutants combining pulsed corona discharge plasma with catalysis/photocatalysis

VEU17119 Toward a smart & integral treatment of natural radioactivity in water provision services

IUT1–7 Chemical engineering approach to removal of priority pollutants and emerging micropollutants from water/wastewater and soil: implementation and optimization of advanced oxidation technologies

Awards

2021	Tallinn city Rae scholarship
2019	TalTech Development Fund, Rickard Kruusberg "Adventure through studies!" scholarship
2019	European Cooperation in Science & Technology (COST) scholarship
2019	Baltic Sea region university consortium for Science and Technology (BALTECH) scholarship
2019	Dora Plus program (activity 1.1) scholarship

Attendance at conferences and training schools

2021	Attendance with an oral presentation at online conference "Athens Conference on Advances in Chemistry"; March 10–14, 2021, Athens, Greece
2020	Attendance with poster presentation at Graduate School of Functional Materials and Technologies (GSFMT) scientific conference; February 4–5, 2020, Tallinn, Estonia
2019	Attendance with an oral presentation at training school "Aerogels processing, modelling and environmental-driven applications"; October 21–23, 2019, Coimbra, Portugal (COST scholarship)
2019	Attendance at summer school "4th International PhD Summer School"; August 26–30, 2019, Trakai, Lithuania (BALTECH scholarship)
2019	Attendance with a poster presentation at conference "The 6th European Conference on Environmental Applications of Advanced Oxidation Processes"; June 26–30, 2019, Portorož, Slovenia (Dora Plus scholarship)
2019	Attendance at summer school "3rd European Summer School on Environmental Applications of Advanced Oxidation Processes" with poster presentation; June 3–7, 2019, Alcoy, Spain (GSFMT financial support)
2019	Attendance with poster presentation at Estonian Chemistry Days, April 18, 2019, Tallinn, Estonia
2019	Attendance with poster presentation at Graduate School of Functional Materials and Technologies (GSFMT) scientific conference; February 4–5, 2019, Tartu, Estonia
2018	Attendance at summer school "Wastewater and biosolids management (WWSS18)"; July 22–27, 2018, Patras, Greece (GSFMT financial support)

Supervised dissertations

Sofia Pereskoka, Master's Degree, 2021, (sup) Maarja Kask; Juri Bolobajev, Application of ferrocene aerogel and iron-doped organic aerogel in Fenton-like and photolytic processes for oxidation of N-nitrosodiethylamine and trimethoprim in water – a comparative study, Tallinn University of Technology School of Engineering, Department of Materials and Environmental Technology.

Marko Jaaksaar, Master's Degree, 2020, (sup) Juri Bolobajev; Maarja Kask, Application of ozonation, photolysis and O_3/H_2O_2 combination for the oxidation of N-nitrosodimethylamine and N-nitrosodiethylamine – a comparative study, Tallinn University of Technology School of Engineering, Department of Materials and Environmental Technology.

Irina Petrotšenko, Master's Degree, 2019, (sup) Marina Kritševskaja; Maarja Kask, Effect of ozone on photocatalytic degradation of acetone vapour on P25 TiO_2 coating, Tallinn University of Technology School of Engineering, Department of Materials and Environmental Technology.

Publications

Kask, M.; Krichevskaya, M.; Preis, S.; Bolobajev, J. (2021). Oxidation of Aqueous Toluene by Gas-Phase Pulsed Corona Discharge in Air-Water Mixtures Followed by Photocatalytic Exhaust Air Cleaning. *Catalysts*, 11 (5), #549. DOI: 10.3390/catal11050549.

Kask, M.; Krichevskaya, M.; Preis, S.; Bolobajev, J. (2021). Oxidation of Aqueous N-Nitrosodiethylamine: Experimental Comparison of Pulsed Corona Discharge with H_2O_2 -Assisted Ozonation. *Journal of Environmental Chemical Engineering*, #105102. DOI: 10.1016/j.jece.2021.105102.

Kask, M.; Bolobajev, J.; Krichevskaya, M. (2020). Gas-Phase Photocatalytic Degradation of Acetone and Toluene, and their Mixture in the Presence of Ozone in Continuous Multi-Section Reactor as Possible Air Post-Treatment for Exhaust from Pulsed Corona Discharge. *Chemical Engineering Journal*, 399, #125815. DOI: 10.1016/j.cej.2020.125815.

Kask, M.; Krichevskaya, M.; Bolobajev, J. (2019). Sonolytic Degradation of Pesticide Metazachlor in Water: The Role of Dissolved Oxygen and Ferric Sludge in the Process Intensification. *Journal of Environmental Chemical Engineering*, 7 (3), #103095. DOI: 10.1016/j.jece.2019.103095.

Bolobajev, J.; **Kask, M.**; Koel, M. (2019). Application of Metal-Doped Organic Aerogels for Photodegradation of Antibiotics in Water. *Chemical Industry Digest*, June, 92–95.

Bolobajev, J.; **Kask, M.**; Kreek, K.; Kulp, M.; Koel, M.; Goi, A. (2019). Metal-Doped Organic Aerogels for Photocatalytic Degradation of Trimethoprim. *Chemical Engineering Journal*, 357, 120–128. DOI: 10.1016/j.cej.2018.09.127.

Elulookirjeldus

Isikuandmed

Nimi:	Maarja Kask
Sünniaeg:	19.09.1993
Sünnikoht:	Rakvere, Eesti
Kodakondsus:	Eesti

Kontaktandmed

E-post:	maarja.kask@taltech.ee
---------	------------------------

Hariduskäik

2017–2021	Tallinna Tehnikaülikool, Chemical and Materials Technology, PhD
2015–2017	Tallinna Tehnikaülikool, tehnikateaduste magister (cum laude)
2012–2015	Tallinna Tehnikaülikool, tehnikateaduste bakalaureus
2009–2012	Rakvere Reaalgümnaasium

Keelteoskus

Eesti	emakeel
Inglise	kõrgtase
Vene	algtase
Soome	algtase

Teenistuskäik

2017–2021	Tallinna Tehnikaülikool, Inseneriteaduskond, Materjali- ja keskkonnatehnoloogia instituut, doktorant-nooremteadur
-----------	---

Kaitstud lõputööd

magistrikraad, 2017, Metalli sisaldavate orgaaniliste aerogeelide fotokatalüütiline mõju trimetoprimi lagundamisele, Tallinna Tehnikaülikool, Inseneriteaduskond, Materjali- ja keskkonnatehnoloogia instituut. Juhendajad: Juri Bolobajev, Anna Goi.

Osalemine uurimisprojektides

PRG776 Ohtlike vee ja õhu saasteainete lagundamine innovatiivse energiatõhusa kombineeritud impulss-koroona elektrilahenduse ja katalüüsi/fotokatalüüsiga

VEU17119 Parima veetöötlustehnoloogia rakendamine põhjavee kõrgeenenud loodusliku radioaktiivsuse korral

IUT1-7 Keemiatehnikapõhine lähenemisviis prioriteetsete saasteainete ja uute esilekerkivate mikrosaasteainete kõrvaldamisele veest/reoveest ja pinnasest: täiustatud oksüdatsioonitehnoloogiate kasutamine ja optimeerimine

Tunnustused

2021	Tallinna linna Raestipendium
2019	TalTech arengufond, Rickard Kruusbergi nimeline stipendium "Seikle õpingute läbi!"
2019	European Cooperation in Science & Technology (COST) stipendium
2019	Baltic Sea region university consortium for Science and Technology (BALTECH) stipendium
2019	Dora Pluss programmi (tegevus 1.1) stipendium

Konverentsidel ja treeningkoolides osalemine

2021	Suulise ettekandega esinemine online konverentsil "Athens Conference on Advances in Chemistry"; 10.–14.03.2021, Ateena, Kreeka
2020	Posterettekandega esinemine Funktsionaalsete materjalide ja tehnoloogiate doktorikooli (FMTDK) teaduskonverentsil; 4.–5.02.2020, Tallinn, Eesti
2019	Suulise ettekandega esinemine treeningkoolitusel "Aerogels processing, modelling and environmental-driven applications"; 21.–23.10.2019, Coimbra, Portugal (COST stipendium)
2019	Enesetäiendamine suvekoolis "4th International PhD Summer School"; 26.–30.08.2019, Trakai, Lithuania (BALTECH stipendium)
2019	Posterettekandega esinemine konverentsil "The 6th European Conference on Environmental Applications of Advanced Oxidation Processes"; 26.–30.06.2019, Portorož, Sloveenia (Dora Pluss stipendium)
2019	Posterettekandega esinemine suvekoolis "3rd European Summer School on Environmental Applications of Advanced Oxidation Processes"; 3.–7.06.2019, Alcoi, Hispaania (FMTDK poolne finantseerimine)
2019	Posterettekandega esinemine Eesti Keemiaseltsi 100. aastapäeva teaduskonverentsil, 18.04.2019, Tallinn, Eesti
2019	Posterettekandega esinemine Funktsionaalsete materjalide ja tehnoloogiate doktorikooli (FMTDK) teaduskonverentsil; 4.–5.02.2019, Tartu, Eesti
2018	Enesetäiendamine suvekoolis "Wastewater and biosolids management (WWSS18)"; 22.–27.07.2018, Patra, Kreeka (FMTDK poolne finantseerimine)

Juhendatud magistritööd

Sofia Pereskoka, magistrikraad, 2021, (juh) Maarja Kask; Juri Bolobajev, Ferrotseenaerogeeli ja rauaga legeritud orgaanilise aerogeeli rakendamine Fenton-tüüpi ja fotolüütilistes protsessides N-nitrosodietüülamiini ja trimetoprimi lagundamiseks vees – võrdlev uuring, Tallinna Tehnikaülikool, Inseneriteaduskond, Materjali- ja keskkonnatehnoloogia instituut.

Marko Jaaksaar, magistrikraad, 2020, (juh) Juri Bolobajev; Maarja Kask, Osoneerimise, fotolüüsi ja O_3/H_2O_2 kombinatsiooni kasutamine N-nitrosodimetüülamiini ja N-nitrosodietüülamiini oksüdeerimiseks vees – võrdlev uuring, Tallinna Tehnikaülikool, Inseneriteaduskond, Materjali- ja keskkonnatehnoloogia instituut.

Irina Petrotšenko, magistrikraad, 2019, (juh) Marina Kritševskaja; Maarja Kask, Osooni mõju atsetooniauru fotokatalüütilisele oksüdeerimisele P25 TiO₂ katetega, Tallinna Tehnikaülikool, Inseneriteaduskond, Materjali- ja keskkonnatehnoloogia instituut.

Publikatsioonid

Kask, M.; Krichevskaya, M.; Preis, S.; Bolobajev, J. (2021). Oxidation of Aqueous Toluene by Gas-Phase Pulsed Corona Discharge in Air-Water Mixtures Followed by Photocatalytic Exhaust Air Cleaning. *Catalysts*, 11 (5), #549. DOI: 10.3390/catal11050549.

Kask, M.; Krichevskaya, M.; Preis, S.; Bolobajev, J. (2021). Oxidation of Aqueous N-Nitrosodiethylamine: Experimental Comparison of Pulsed Corona Discharge with H₂O₂-Assisted Ozonation. *Journal of Environmental Chemical Engineering*, #105102. DOI: 10.1016/j.jece.2021.105102.

Kask, M.; Bolobajev, J.; Krichevskaya, M. (2020). Gas-Phase Photocatalytic Degradation of Acetone and Toluene, and their Mixture in the Presence of Ozone in Continuous Multi-Section Reactor as Possible Air Post-Treatment for Exhaust from Pulsed Corona Discharge. *Chemical Engineering Journal*, 399, #125815. DOI: 10.1016/j.cej.2020.125815.

Kask, M.; Krichevskaya, M.; Bolobajev, J. (2019). Sonolytic Degradation of Pesticide Metazachlor in Water: The Role of Dissolved Oxygen and Ferric Sludge in the Process Intensification. *Journal of Environmental Chemical Engineering*, 7 (3), #103095. DOI: 10.1016/j.jece.2019.103095.

Bolobajev, J.; **Kask, M.**; Koel, M. (2019). Application of Metal-Doped Organic Aerogels for Photodegradation of Antibiotics in Water. *Chemical Industry Digest*, June, 92–95.

Bolobajev, J.; **Kask, M.**; Kreek, K.; Kulp, M.; Koel, M.; Goi, A. (2019). Metal-Doped Organic Aerogels for Photocatalytic Degradation of Trimethoprim. *Chemical Engineering Journal*, 357, 120–128. DOI: 10.1016/j.cej.2018.09.127.

ISSN 2585-6901 (PDF)
ISBN 978-9949-83-725-0 (PDF)